

ROBUST ESTIMATION OF LIMIT LOADS
FOR CRACKED COMPONENTS

CENTRE FOR NEWFOUNDLAND STUDIES

**TOTAL OF 10 PAGES ONLY
MAY BE XEROXED**

(Without Author's Permission)

CHRISTOPHER G. FOWLER



INFORMATION TO USERS

This manuscript has been reproduced from the microfilm master. UMI films the text directly from the original or copy submitted. Thus, some thesis and dissertation copies are in typewriter face, while others may be from any type of computer printer.

The quality of this reproduction is dependent upon the quality of the copy submitted. Broken or indistinct print, colored or poor quality illustrations and photographs, print bleedthrough, substandard margins, and improper alignment can adversely affect reproduction.

In the unlikely event that the author did not send UMI a complete manuscript and there are missing pages, these will be noted. Also, if unauthorized copyright material had to be removed, a note will indicate the deletion.

Oversize materials (e.g., maps, drawings, charts) are reproduced by sectioning the original, beginning at the upper left-hand corner and continuing from left to right in equal sections with small overlaps.

Photographs included in the original manuscript have been reproduced xerographically in this copy. Higher quality 6" x 9" black and white photographic prints are available for any photographs or illustrations appearing in this copy for an additional charge. Contact UMI directly to order.

**Bell & Howell Information and Learning
300 North Zeeb Road, Ann Arbor, MI 48106-1346 USA**

UMI[®]
800-521-0600

NOTE TO USERS

This reproduction is the best copy available

UMI



**National Library
of Canada**

**Acquisitions and
Bibliographic Services**

395 Wellington Street
Ottawa ON K1A 0N4
Canada

**Bibliothèque nationale
du Canada**

**Acquisitions et
services bibliographiques**

395, rue Wellington
Ottawa ON K1A 0N4
Canada

Your file *Votre référence*

Our file *Notre référence*

The author has granted a non-exclusive licence allowing the National Library of Canada to reproduce, loan, distribute or sell copies of this thesis in microform, paper or electronic formats.

The author retains ownership of the copyright in this thesis. Neither the thesis nor substantial extracts from it may be printed or otherwise reproduced without the author's permission.

L'auteur a accordé une licence non exclusive permettant à la Bibliothèque nationale du Canada de reproduire, prêter, distribuer ou vendre des copies de cette thèse sous la forme de microfiche/film, de reproduction sur papier ou sur format électronique.

L'auteur conserve la propriété du droit d'auteur qui protège cette thèse. Ni la thèse ni des extraits substantiels de celle-ci ne doivent être imprimés ou autrement reproduits sans son autorisation.

0-612-42382-4

Canada

ROBUST ESTIMATION OF LIMIT LOADS FOR CRACKED COMPONENTS

BY

°CHRISTOPHER G. FOWLER, B. ENG.

**A THESIS SUBMITTED TO THE SCHOOL OF GRADUATE
STUDIES IN PARTIAL FULFILLMENT OF THE
REQUIREMENTS FOR THE DEGREE OF
MASTER OF ENGINEERING**

**FACULTY OF ENGINEERING AND APPLIED SCIENCE
MEMORIAL UNIVERSITY OF NEWFOUNDLAND**

JANUARY, 1998

ST. JOHN'S

NEWFOUNDLAND

CANADA

Abstract

The problem of stress corrosion cracking in natural gas pipelines in Central and Western Canada has led to a need for quick, efficient methods of evaluating pipeline integrity based on component geometry and operating parameters. The use of high toughness materials in modern engineering practice requires the application of elastic-plastic fracture mechanics, or limit type analysis, to evaluate defects. This thesis demonstrates the application of two robust finite element techniques, the Gloss R-node method and the m_{ϵ} -method, to finding limit loads for cracked components. Each of the methods relies on linear elastic finite element solutions in conjunction with a modulus adjustment scheme to provide a simple, systematic means for determining failure loads. The techniques are initially applied to standard fracture specimens to gage their effectiveness in analyzing crack geometries. The analysis is then directed to pipe geometries containing longitudinal defects (internal and external) of varying depths and culminates in the analysis of multiple defects typical of stress corrosion crack colonies. The robust limit load results are compared to traditional nonlinear finite element analysis results and analytical solutions, where applicable. The robust techniques consistently provide conservative results which compare well to both nonlinear finite element analysis and analytical solutions.

Acknowledgements

The author would like to thank Dr. R. Seshadri and Dr. C. Monahan for acting as supervisors for the duration of this degree program. The guidance and support provided are greatly appreciated. A special thanks to Dr. Sathya Prasad Mangalaramanan for all of his help in working through the many details and technical problems encountered during the course of this work. Thanks are extended to the Natural Sciences and Engineering Research Council of Canada, as well as the Faculty of Engineering and Applied Science at Memorial University of Newfoundland, through which funding was provided to carry out this research work. Many thanks to fellow graduate students, especially Mr. Rodney Hale, Mr. Paul Smith and Mr. Blair Carroll for helping to cope with the problems and frustrations encountered during this undertaking.

Contents

Abstract	ii
Acknowledgements	iii
List of Figures and Tables	vi
Nomenclature	viii
Chapter 1 Introduction	1
1.1 Background	1
1.2 Failure of Cracked Components	3
1.3 Organization of the Thesis	5
Chapter 2 Review Of Literature	6
2.1 Theoretical Limit Load Solutions for Axially Flawed Cylinders	6
2.2 Experimental Limit Load Solutions for Defected Cylinders	13
2.3 Numerical Limit Load Solutions for Defected Cylinders	20
Chapter 3 Robust Limit Load Estimation Techniques	25
3.1 Limit Load Predictions	25
3.2 GLOSS R-node Method	26
3.2.1 Determination of the r-node stress for cracked components	29
3.3 The m_r -Method	31
3.3.1 Theorem of nesting surfaces	31
3.3.2 Mura's variational formulation	33
3.3.3 Finite element implementation of Mura's formulation	37
3.3.4 Analysis of cracked components - Local plastic collapse	39
Chapter 4 Analysis of Standard Fracture Specimens	46
4.1 Finite Element Modeling Considerations	47
4.2 Compact Tension (CT) Specimen	49
4.3 Single Edge Notched Bend (SENB) Specimen	50
4.4 Single Edge Notched Tension (SENT) Panel	50
4.5 Limit Load Results Using The Gloss R-node Method	51
4.6 Limit Load Results Using The m_r -method	63

4.7	Summary and Discussion of Results	66
Chapter 5	Analysis of Axial Pipe Defects	69
5.1	Finite Element Modelling Considerations	69
5.2	Single Axial Defects	70
5.2.1	Gloss r-node limit load estimates	71
5.2.2	m_r -Method limit load estimates	79
5.3	Internal Axial Defects	80
5.4	Thick Walled Pipes Containing Defects	81
5.5	Multiple External Defects	83
5.5.1	Robust limit load estimates	86
5.6	Discussion of Results	91
Chapter 6	Conclusions	95
6.1	Contributions of the Thesis	95
6.2	Future Efforts	97
References		99
APPENDIX A	- ANSYS Input Files and Macro Code	102
APPENDIX B	- ANSYS Plots	152
APPENDIX C	- Full Stress Distributions and R-node Plots for Pipe Models	179
Bibliography		204

List of Figures and Tables

FIGURES

Figure 2.1 - Axial surface crack in a cylinder (Krasovskii, et al., 1990).	8
Figure 3.1 - R-node concepts (CT Specimen)	28
Figure 3.2 - Typical Stress Distributions	30
Figure 3.3 - Body with applied point loads.	31
Figure 3.4 - Two-bar structure with associated nesting surfaces (Boyle, 1982).	33
Figure 3.5 - Illustration of Total and Reference Volumes	40
Figure 3.6 - Variation of m° and m' with iterations.	41
Figure 4.1 - Standard fracture specimens.	47
Figure 4.2 - CT Specimen Stress Distribution Along Symmetry Plane	52
Figure 4.3 - SENB Specimen Stress Distribution Along Symmetry Plane	53
Figure 4.4 - SENT Specimen Stress Distribution Along Symmetry Plane	54
Figure 4.5 - Improved R-node Visualization Scheme	56
Figure 4.6 - CT Specimen R-node Plot	58
Figure 4.7 - SENB Specimen R-node Plot	59
Figure 4.8 - SENT Specimen R-node Plot	61
Figure 5.1 - Typical stress distributions for cracked and uncracked pipe.	72
Figure 5.2 - Stress distributions along the uncracked ligament.	74
Figure 5.3 - Stress distributions near the crack tip (2 mm defect).	75
Figure 5.4 - Stress distributions near the crack tip (3 mm defect).	77

Figure 5.5 - Stress distributions near the crack tip (4 mm defect).	78
Figure 5.6 - Stress distributions near the crack tip (2 mm internal defect).	80
Figure 5.7 - Stress distributions along uncracked ligament (thick wall pipe).	82
Figure 5.8 - 914 mm O.D. linepipe with multiple defects	84
Figure 5.9 - Detailed crack geometry - 914 mm O.D. linepipe	85
Figure 5.10 - Stress distributions near the crack tip (Model 1, Crack A).	86
Figure 5.11 - Stress distributions near the crack tip (Model 1, Crack B).	87
Figure 5.12 - Stress distributions near the crack tip (Model 1, Crack C).	88
Figure 5.13 - Stress distributions near the crack tip (Model 2, Crack A).	89
Figure 5.14 - Stress distributions near the crack tip (Model 2, Crack B).	90

TABLES

Table 4.1 - Standard Fracture Specimen Dimensions	47
Table 4.2 - Limit Load Estimation Results	67
Table 5.1 - Limit Load Results for Pipe Models	92

Nomenclature

Symbols

$\dot{\epsilon}$	strain rate
$(\sigma_e)_M$	maximum von Mises equivalent stress corresponding to an assumed statically admissible stress distribution
α	coefficient of strength reduction
α_1	modified coefficient of strength reduction
β	relative intensity of longitudinal force
δ_{ij}	Kronecker delta
ΔV_i	volume of i th element
ϵ_p	plastic strain
ζ	linear elastic iteration variable
λ	relative crack length
ν	Poisson's ratio
σ	hoop stress level at failure
σ_e	von Mises equivalent stress
σ_{arb}	arbitrary stress in the m_n modulus adjustment scheme
σ_{fail}	failure stress
σ_u	ultimate tensile stress
σ_y	yield stress
a	crack length
A	flaw area in the through thickness direction
A_o	flaw length x wall thickness
b	thickness of standard fracture specimens
B, n	creep parameters for second stage power law creep
c	flaw length

C_v	Charpy shelf energy
E	elastic modulus
E_s	modified elastic modulus
$f(s_{ij})$	von Mises yield function
$F(s_{ij}^o, \sigma^o, m^o, \mu^o, \phi^o)$	functional associated with Mura's formulation
$f_3(n)$	strain hardening factor
$\bar{\sigma}_{flow}$	flow stress
F_{sf}	free-surface factor
$H(t)$	Heaviside function
\bar{s}_{ij}^o	statically admissible deviatoric stress field corresponding to the traction P
J_{elp}	elastic-plastic J-integral
L	length of SENT specimen
m	safety factor corresponding to an applied load P
m_α	improved lower bound multiplier
m^o	upper bound multiplier corresponding to an applied load P
M_T	Folias correction factor
M_x	bending moment
m'	Mura's extended lower bound multiplier
n	strain hardening exponent
N	total number of elements in a discretized component or structure
N_ϕ	circumferential force acting in a cylinder subjected to internal pressure loading
N_x	longitudinal force acting in a cylinder subjected to internal pressure loading
P	applied load

P_{fail}	failure pressure
P_L	limit load
q	modulus adjustment index
Q_ϕ	transverse force acting in the circumferential direction for a cylinder subjected to internal pressure loading
Q_e	effective generalized stress
Q_f	elliptical shape factor
Q_x	transverse force acting in the longitudinal direction of a cylinder subjected to internal pressure loading
S	length of SENB specimen
s_{ij}^o	statically admissible deviatoric stress field corresponding to the traction $m^o P$
S_T	surface area of a structure over which a traction is applied
t	cylinder thickness
t_b	thickness of uncracked ligament
V	volume of a component or structure
V_R	reference volume of a component or structure
V_T	total volume of a component or structure
W	width of standard fracture specimens
z	optimization parameter

Subscripts

arb	arbitrary
e	von Mises equivalent
ij	tensorial indices
L	limit
y	yield

Acronyms

CT	compact tension
FEA	finite element analysis
IGSCC	intergranular stress corrosion cracking
LEFM	linear elastic fracture mechanics
O.D.	outside diameter
SCC	stress corrosion cracking
SENB	single edge notched bend
SENT	single edge notched tension
TCPL	TransCanada Pipelines Ltd.
TGSCC	transgranular stress corrosion cracking
TSB	Transportation Safety Board

CHAPTER 1

INTRODUCTION

1.1 Background

In recent years, buried pipelines in western and central Canada have been afflicted with stress corrosion cracking (SCC) problems which have led to failure in many instances. Several incidents in Ontario between January 1991 and July 1992 reported in a Transportation Safety Board of Canada (TSB), Commodity Pipeline Occurrence Report (Transportation, 1992) and more recently near Vermilion Bay, Ontario (Dec. 1996) are all examples of recent failures which, fortunately, have resulted in minimal damage to people and property. The incidents discussed in the TSB report have all been attributed to stress corrosion cracking and, in all likelihood, the Vermilion Bay failure will be determined to be SCC related as well.

The problem of stress corrosion cracking was first identified in the early twentieth century with the cracking of brass in ammonia environments. This problem also became apparent during both world wars with the failure of brass cartridge cases. In general, SCC requires three conditions to occur simultaneously: a critical environment, a susceptible alloy and some component of tensile stress (Jones, 1992).

Failures in natural gas pipelines in the United States have been attributed to inter-granular stress corrosion cracking (IGSCC) for more than twenty years. Extensive research has been carried out in the field and the crack mechanism for this process is reasonably well understood. In the mid 1980's, TransCanada Pipelines Ltd. (TCPL) experienced buried high pressure gas pipeline failures at three Ontario locations which were attributed to SCC. However, unlike the American case, these failures occurred as a result of transgranular stress corrosion cracking (TGSCC) for which the crack mechanism is not so well understood (Transportation, 1992). More recent failures, as mentioned earlier, have also been attributed to TGSCC.

The nature of these cracks is such that crack colonies form on the outside surface of the pipe and are oriented parallel to the pipes' longitudinal axis. Much work is being carried out in an attempt to determine the electrochemical mechanism responsible for the development of these cracks in order to mitigate the problem. However, until that goal is achieved there is an urgent need to:

- i.) Develop effective methods of crack detection and sizing.

- ii.) **Develop accurate methods for assessing fracture parameters based on crack dimensions.**

From this, reliable failure assessment models can be developed to improve the safety and integrity of problem pipelines. The focus of this thesis is in the second goal; the assessment of fracture parameters once the crack data has been obtained.

In particular, the assessment of robust finite element techniques are explored for their economy in preparation and computing time as compared to traditional nonlinear finite element analysis.

1.2 Failure of Cracked Components

Depending on material properties and loading conditions, cracked components will most likely fail in one of two ways:

1. **Toughness dependent fracture.**
2. **Failure due to unconstrained plastic flow across the uncracked ligament (net section collapse).**

Toughness dependent fracture falls into two domains; linear elastic fracture mechanics (LEFM) and nonlinear (elastic-plastic) fracture mechanics. LEFM is valid for materials

with low toughness for which brittle fracture is the governing failure mechanism. At higher toughness levels, the failure mechanism becomes ductile in nature and LEFM is no longer applicable and nonlinear (elastic-plastic) fracture mechanics is required to address the problem. Net section collapse of a component across the uncracked ligament is the failure mechanism prevalent in high toughness materials. If toughness is sufficiently high, fracture mechanics becomes irrelevant to the problem as the failure stress is insensitive to toughness. In this case, a limit load analysis is required to predict the failure stress.

The majority of engineering materials in use today are relatively high toughness steels and problems involving cracked components must be addressed using nonlinear fracture mechanics or a limit type analysis. In terms of developing a failure assessment model, each failure mechanism must be addressed in order to predict which type of failure is most likely to occur. Safe operating parameters and remaining life estimates may then be determined. The use of nonlinear finite element analysis is well suited to this application, but, at the cost of substantial preparation and processing time which can be quite expensive. In light of this, the development of accurate robust techniques, based on linear 2-D finite element techniques, can be very advantageous. Several robust techniques are in current use for calculating failure loads and J-integrals for various components. This thesis will examine the application of these techniques to the problem of cracked components; in particular, the case of linepipe containing measurable flaws.

1.3 Organization of the Thesis

A review of related literature is presented in Chapter 2. An examination of two robust linear elastic finite element techniques for determining limit loads is presented in Chapter 3. These are the Gloss R-node method and the m_x -method. Chapter 4 is a guideline for the practical application of these two techniques in order to obtain satisfactory results. Numerical examples that demonstrate the applicability of these techniques to cracked components are presented and compared with traditional analysis methods. Chapter 5 investigates the application of the robust techniques to the problem of longitudinal surface cracks in linepipe. Included in the analysis is the problem of multiple defects in the form of crack colonies, typical of TGSCC afflicted pipelines. The concluding chapter, Chapter 6, contains a summary of the thesis and a discussion on future research.

The key aspects of the research presented in this thesis are:

1. It applies robust limit load estimation techniques to cracked components.
2. It introduces an improved r-node identification scheme.
3. It outlines a practical guide for applying robust limit load determination techniques.
4. It advances the use of robust analysis to complex geometries including multiple defects in linepipe.

The following chapters elaborate on these aspects and provide the reader with some guidance on the use of robust analysis techniques.

CHAPTER 2

REVIEW OF LITERATURE

2.1 Theoretical Limit Load Solutions for Axially Flawed Cylinders

The classical theorems of limit analysis are the upper and lower bound theorems. The upper bound theorem states that if an estimate of plastic collapse load of a structure is made by equating the internal rate of energy dissipation to the rate at which the external forces do work in any kinematically admissible deformation field, then the estimate will be higher, or at best, equal to the actual collapse load (Calladine, 1969). The upper bound estimates are useful for metal forming or other processes where a higher than correct limit load prediction is appropriate for estimating power and drive requirements.

The lower bound theorem states that if an assumed stress distribution satisfies equilibrium with externally applied surface tractions, and is below yield everywhere

within the structure, then the limit load calculated using this stress field would be lower than the exact limit load. Lower bound limit loads are appropriate for use in safe design of mechanical components and structures. The classical lower bound limit load for an arbitrary load, P , given that the maximum equivalent stress corresponding to an assumed statically admissible stress distribution is $(\sigma_e^0)_M$, may be expressed as

$$P_L = P \frac{\sigma_y}{(\sigma_e^0)_M} \quad (2.1)$$

The classical limit load solution for a circular cylinder subjected to internal pressure for instance is given by the equation

$$P_L = \frac{2}{\sqrt{3}} \sigma_y \ln\left(\frac{b}{a}\right) \quad (2.2)$$

where σ_y is the material yield stress while b and a are the outer and inner diameters of the cylinder respectively. Inoue et al. (Inoue et al., 1977) derive this solution and use a linear combination of particular solutions to obtain a lower bound limit load for the case of a thick cylinder subjected to internal pressure loading and shear. The authors also show that the action of shear along the boundaries lowers the lower bounds to the collapse load of the cylinder. Equation 2.2 may be used for the case of part through axial cracks in pipes as a rough approximation of the limit load by omitting the cracked portion of the wall thickness when performing the calculation. This may then be used as a quick check on the results obtained by robust analysis.

Krasovskii et al. (Krasovskii et al., 1990) propose a limit load solution for an axially cracked pipe subjected to an internal pressure loading. The model is developed based on an analysis of the forces acting in the vicinity of the crack plane. The authors consider first the cause of ductile failure of a cylinder subjected to internal pressure with no defect. For this, the equilibrium of forces in the radial direction is considered for which the forces of interest are the circumferential force N_ϕ and the transverse forces Q_x and Q_ϕ

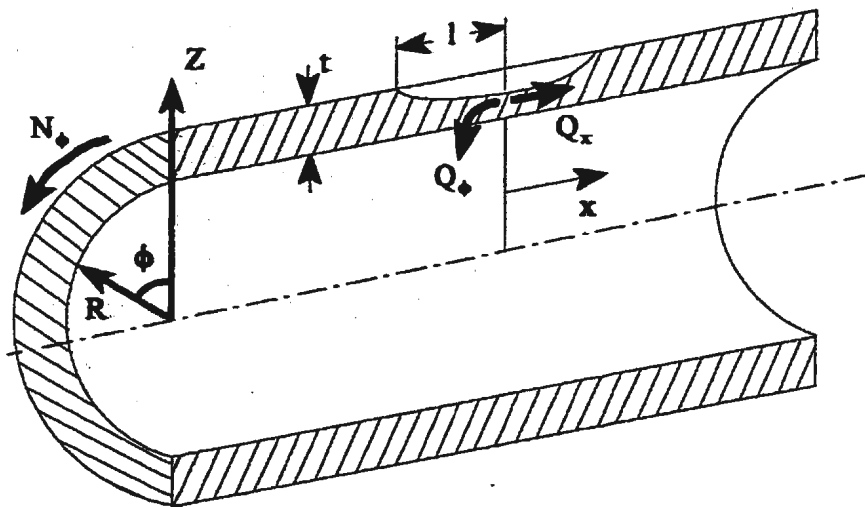


Figure 2.1 - Axial surface crack in a cylinder (Krasovskii, et al., 1990).

acting in their respective directions (Figure 2.1). With no flaws, the transverse forces are zero and the internal pressure is balanced by the hoop stress resulting from the circumferential force, N_ϕ . The presence of an axial flaw causes an imbalance between the circumferential stress and the internal pressure which must be balanced by the transverse forces to maintain equilibrium. The transverse forces induce bending moments. The cylinder passes into a limit state when the bending moments reach a critical value

corresponding to the chosen yield condition. Considering the case of an axial part-through crack (Figure 2.1) and the associated equilibrium equations the authors determined the forces of importance in this analysis to be the circumferential force N_ϕ , the transverse force Q_x , bending moment M_x and the longitudinal force N_x . The resulting solution of the differential equations of equilibrium gives an equation which essentially states that the bending moment induced due to the local discontinuity in the pipe must be balanced by the response of the pipe wall to maintain equilibrium. This leads to a limit state that is attained when M_x at the points $x = 0$ and $x = l_1$ assume the extreme negative and positive values respectively. The limit load, P_L , is then calculated from the following determinant equation

$$\Delta M_x = [M_x(x = 0)] - [M_x(x = l_1)] \quad (2.3)$$

where the extreme values of the bending moments are maximum.

The authors make use of the Tresca yield criterion for which the extreme values of the moment depend on the longitudinal force N_x and the thickness of the effective section to obtain the critical values of the bending moments at $x = 0$ and $x = l_1$. For the case where $x = 0$, the value of M_x is given as:

$$\left[M_x(x = 0) \right] = \frac{1}{8} \sigma_u t^2 \left[1 - (1 - 2\beta)^2 + 2 \left(1 - \beta - \frac{t_b(0)}{t} \right)^2 H \left(1 - \beta - \frac{t_b(0)}{t} \right) \right] \quad (2.4)$$

where: $\beta = N_x / \sigma_u t$ relative intensity of longitudinal force
 $t_b(x) = t - d(x)$ thickness of uncracked ligament

$$H(t) = \begin{cases} 0 & \text{for } t < 0 \\ 1 & \text{for } t \geq 0 \end{cases} \quad \text{Heaviside function}$$

At the point $x = l_1$, the critical value of M_x is given as:

$$\left[M_x(x = l_1) \right] = -\frac{1}{8} \sigma_u t^2 \left[1 - (1 - 2\beta)^2 \right] \quad (2.5)$$

Using these results, the authors derive the following implicit solution for P_L for the case of a cylinder with a part-through, rectangular shaped axial defect:

$$\frac{2 \lambda^2 \frac{d}{t} \left(\alpha - \frac{t_b}{t} \right)}{1 - \alpha} = 1 - (1 - 2\beta)^2 + \left(1 - \beta - \frac{t_b}{t} \right)^2 H \left(1 - \beta - \frac{t_b}{t} \right) \quad (2.6)$$

where: $\lambda = (l^2/Rt)^{1/2}$ relative crack length
 $\alpha = P_L/\sigma_u t$ coefficient of strength reduction

This formula was verified by comparison with published experimental results and found to give reasonable estimates for the failure load of cylinders having the particular crack geometry described above.

Orynyak and Borodii (Orynyak et al., 1994) extended the work of the previous authors by using the same analysis scheme to derive an expression for the limit load of a part-through, semi-elliptical shaped axial defect. Their solution may be expressed as:

$$\frac{2 \lambda^2 \left(\frac{\pi}{4} \right)^2 \frac{d}{t} \left[\frac{d}{t} - \left(\frac{4}{\pi} \right)^2 \frac{2}{3} (1 - \alpha) \right]}{1 - \alpha} = 1 - (1 - 2\beta)^2 + \left(1 - \beta - \frac{t_b}{t} \right)^2 \times H \left(1 - \beta - \frac{t_b}{t} \right) \quad (2.7)$$

The parameters λ and α are as previously defined. This solution, as well as that obtained by Krasovskii et al., are known to overestimate the limit load for increasing values of the relative wall thickness t/R (i.e. the solutions are conservative for thin-walled cylinders, but, the solutions become non-conservative for thicker walled structures). Orynyak and Borodii address this problem by proposing an empirical procedure for calculating the stress degradation factor, α , for thick-walled cylinders. The proposed solution makes use of the original calculation of α to give a new factor, α_1 , which may be expressed as:

$$\alpha_1 = \frac{\ln\left(1 + \frac{\alpha t}{R}\right)}{\frac{t}{R}} \quad (2.8)$$

This parameter may be used in place of α for thick-walled cylinders containing either rectangular or semi-elliptical shaped cracks. The difference in the solutions for thick and thin walled cylinders is due to the presence of radial stresses acting in the through-thickness direction. As the thickness increases, these stresses become increasingly important and tend to decrease the load bearing capacity of the defected cylinder. Hence, the overestimation of the limit load when using the thin-walled solution.

Orynyak (Orynyak, 1993) proposes a slightly different approach to the limit load solution for axially flawed cylinders which the author refers to as the optimization method. This approach allows for the presence of additional bending moments developed by positive and negative axial stresses. This solution was developed as a result of the author noting

that the solution by Krasovskii et al. underestimates the limit load for smaller values of the parameter β ($\beta = N_x/\sigma_x t$). Orynyak addresses this problem by considering the additional moments induced by the axial stresses $\pm\sigma_x$. The intensity of these stresses is defined as $z = \sigma_x/\sigma_x$. Using these results, the limit load solution for the rectangular shaped axial crack may be given as:

$$\frac{2\lambda^2\left(\frac{a}{t} - z\right)(\alpha - \tau)}{1 - \alpha - \tau} = 1 - \left(1 - 2\beta\right)^2 + \left(1 - \beta - \tau\right)H\left(1 - \beta - \tau\right) + \left(1 - \beta\right)^2 - \left(1 - \beta - 2z\right)^2 \quad (2.9)$$

where: $\tau = (t - a)/t$ (a is the crack depth)

$z =$ optimization parameter

This expression gives the maximum possible value for the limit load and, hence, may be taken as an upper bound estimate. This, however, is not useful for design or evaluation purposes.

A recent paper by Orynyak, Torop and Borodii (Orynyak et al., 1996) combines the results of the previously mentioned works to develop an algorithm that accounts for the three-dimensional state of stress as well as the three-dimensional geometry parameters (i.e. length, depth and breadth) describing the defect. The final algorithm makes direct use of the solutions previously discussed and combines this with further analysis to arrive at a limit load solution for part-through flaws of significant breadth. The aim of this approach is to develop a theoretical solution to compare with experimental results for

pipes with machined defects where the breadth of the machined notch may influence the predicted results of previous solutions for sharp, closed cracks.

The purpose of the aforementioned algorithm in relating theoretical solutions to experimental results is one which poses a continual problem for researchers. In this case, there are several assumptions and approximations made in determining the theoretical solution such that the result is really just an empirical estimate of the experimental results. In essence, the theoretical solution is derived based on the experimental results and as such cannot truly be used as an independent comparison of the experimental work.

2.2 Experimental Limit Load Solutions for Defected Cylinders

Much experimental work has been carried out to determine the burst or collapse pressures for various types of defects in circular cylinders. Kiefner et al. (Kiefner et al., 1973) conducted numerous tests on varying sizes of linepipe having both artificial and natural defects in which collapse pressures were determined. These collapse pressures are defined as the stress levels required to cause defect propagation through the remaining ligament for part-through defects. The failure results in leakage or rupture of the pipe. The work was performed at Battelle's Columbus Laboratories. A total of 140 experiments involving single, longitudinally-oriented defects (both through-wall and part-through) were performed. Analysis of the results and consideration of theoretical fracture mechanics have resulted in the development of semi-empirical equations for predicting

the failure stress of flawed linepipe.

For the case of part-through wall flaws, two modes of failure are considered: flow-stress dependent failure and toughness dependent failure. In either case, the equations account for both crack length and crack depth, as well as bulging of the crack flanks. For flow-stress dependent failures, the equation is expressed as:

$$\sigma = \bar{\sigma}_{flow} \left[\frac{1 - \frac{d}{t}}{1 - \frac{d}{M_T t}} \right] \quad (2.10)$$

where, σ = hoop stress level at failure (psi)
 $\bar{\sigma}_{flow}$ = flow stress (defined as $Y_s + 10000$ psi for typical linepipe steels)
 d = crack depth (in)
 t = pipe wall thickness (in)

and M_T is the Folias correction factor. The Folias correction accounts for stress amplification at the ends of the flaw resulting from the outward radial deflection along the flaw which is unique to pressurized pipe. This factor is calculated based on defect geometry factors which include the pipe thickness and diameter, as well as, defect length and depth.

For toughness dependent failures the derived equation is much more complex and is expressed as,

$$\left[\frac{\frac{12C_v}{A_c} E\pi}{8c\bar{\sigma}^2} \right] = \ln \sec \frac{\pi}{2} \left[\frac{M_p \sigma_p}{\bar{\sigma}} \right] \quad (2.11)$$

where C_v = Charpy shelf energy (ft·lb)

c = flaw length (in)

$\bar{\sigma}$ = flow stress (psi)

σ_p = collapse pressure (psi)

M_p = the inverse of equation (2.10) for flow-stress dependent failure

The basis of this equation is a combination of experimental results and earlier equation development for predicting collapse loads for brittle materials utilizing unstable crack propagation theory. The experimental results indicate that brittle fracture is not the predominant mode of failure. Therefore, the equations used to predict the failure pressures must in some way account for the ductility of the material. The use of the Folias correction factor in the above equation provides a means to predict collapse loads for ductile materials which undergo a toughness dependent mode of failure. In addition to the solutions presented above for part-through wall defects, the authors also provide solutions for through-wall axial defects.

The equations presented by Kiefner et al. account for internal pressure loading only. The presence of other loading behavior will make the use of these solutions invalid. In practice, loading conditions are rarely such that only internal pressure loading may be

considered. Even in the case of experimental work where conditions are controlled, it is extremely difficult to avoid the presence of axial stresses resulting from the use of capped pipes in the experimental setup. As a result, the solutions presented by Kiefner et al. may provide a reasonable comparison to the experimental data presented, but the solutions would be of little value in predicting failure loads for practical pipeline applications.

Lancaster and Palmer (Lancaster et al., 1996) have conducted research to determine the collapse pressure for pipes containing dents and gouges. The research looked at the effect on burst pressure of three different situations; a dent only on the pipe surface, a gouge only on the pipe surface, and a combined dent and gouge. For the dent only case, the authors found that the presence of a dent, even of considerable size, has little effect on the collapse pressure. This is true for cases where the dent does not significantly alter the curvature of the pipe resulting in a stress concentration. The size of the pipe relative to the shape and orientation of the dent will determine the extent to which the defect affects the failure pressure. However, dents in the vicinity of welds or which induce sharp changes in curvature require a detailed assessment as the presence of high localized stresses may significantly reduce the load bearing capacity of the pipe. The research has shown that the collapse pressure for the case of gouges only (local loss in pipe wall thickness without change in the shape of the pipe) is dependent on the axial length of the gouge, the loss in wall thickness and the material properties of the pipe. Failure pressures estimated using the solutions of Kiefner et al. are in good agreement with the experimental results obtained by the authors. The combination of a dent and gouge

showed the most serious reduction in collapse pressure. Gouges located near the high strain regions of the dent (typically at the ends of the long axis) fail at much lower pressure levels than gouges located within the dent area but remote from the high strain regions. This is due to the very high localized stresses arising from the combined effect of a sharp curvature change due to the dent and the inherent stress concentration resulting from the local loss in wall thickness. For gouges in areas other than the high strain region, the failure pressure is well predicted using the Battelle model of Kiefner et al.

Jaske, Beavers and Harle (Jaske et al., 1996) of Cortest Columbus Technologies Inc., have developed empirical equations derived from experimental results, in a manner similar to that of the Battelle model. Unlike the Battelle model, which considers only hoop stresses, the Cortest Columbus model accounts for both axial and hoop stress in flaw evaluation. The Cortest Columbus and Battelle models both consider that failure may occur in either a flow-stress dependent mode or a fracture-toughness dependent mode. An effective-flaw approach is used to predict flow-stress dependent failure stresses. The equation for flow-stress dependent failure is similar to that of the Battelle model and is given by:

$$\sigma_{fail} = \sigma_{flow} \left[\frac{1 - \frac{A}{A_o}}{1 - \frac{A}{MA_o}} \right] \quad (2.12)$$

where: σ_{flow} = flow strength of material ($\sigma_{flow} = \sigma_y + 68.95$ MPa for typical pipe steels)

A = area of the flaw in the through thickness direction (m^2)

A_o = flaw length x wall thickness (m^2)

M = Folias correction factor

The failure pressure, P_{fail} , for the pipe is computed by equating the failure stress, σ_{fail} , to the hoop stress, σ_h . This accounts for hoop stresses only. The expression for the failure pressure is given as:

$$P_{fail} = \sigma_{flow} \left[\frac{1 - \frac{A}{A_o}}{\left(1 - \frac{A}{MA_o}\right) \left(\frac{D}{2t} - y\right)} \right] \quad (2.13)$$

The parameters D and t are defined as the pipe outside diameter and the pipe wall thickness respectively. The parameter, y , is taken as either 0.4 for temperatures below the creep range or 0 for $D/2t > 10$. The latter is typically used for linepipe steels. To account for the presence of axial stresses, the factor $\left[\left(1 - A/A_o\right) / \left(1 - A/MA_o\right) \right]$ in equation (2.12) is computed for both the length and the width of the axial defect. The lowest of the two values is then used in the calculation of the failure pressure. For the case of both axial and hoop stresses, the stresses are combined using the von Mises equivalent stress (σ_{eq}) for plane stress conditions and compared with the failure stress calculated using equation (2.12) to see if failure is predicted for the combination of stresses. Calculation of the failure pressure for the combined stresses requires an iterative calculation until $\sigma_{eq} = \sigma_{fail}$.

For toughness-dependent failure, the Cortest Columbus model uses an inelastic fracture mechanics approach to predict failure stresses. An empirical equation for the elastic-

plastic J-integral is given as:

$$J_{ep} = Q_f F_{sf} \left[\frac{\sigma^2 \pi a}{E} + f_3(n) a \epsilon_p \sigma \right] \quad (2.14)$$

where: Q_f = elliptical shape factor (assumes elliptical shaped defect)

F_{sf} = free-surface factor

σ = local stress

a = crack depth

E = elastic modulus

$f_3(n)$ = strain hardening factor

n = strain hardening exponent

ϵ_p = plastic strain

Expressions for the parameters Q_f , F_{sf} and $f_3(n)$ are found in (Jaske et al., 1996). The values for E and n are material dependent and readily available while the plastic strain, ϵ_p , is computed from the local stress, σ , using a power law σ - ϵ_p relationship. The local stress includes the Folias correction and is obtained by multiplying the nominal stress by the Folias correction factor. The toughness-dependent failure stress is taken as the nominal stress value that corresponds to the computed value of the elastic-plastic J-integral that equals the critical J-integral for the material. Calculation of the J-integral values requires an iterative approach. The actual failure stress for a pipe containing a defect is the lower of the two failure stresses predicted using both the flow-stress dependent and the fracture-toughness dependent failure models. Cortest Columbus Technologies Inc. have

developed a computer program called CorLAS (Corrosion Life Assessment Software) based on the two models described.

The methodology and results obtained by Jaske et al. are much improved over that obtained by Kiefner et al. Jaske has included the presence of axial stresses in his equations and uses an elastic-plastic fracture mechanics approach when dealing with toughness dependent modes of failure. However, the solutions provided are still based on controlled experimental results which in most cases do not give an accurate representation of in service operating conditions. Having said this, the approach adopted by Jaske et al. does provide one of the better failure estimation procedures currently available.

2.3 Numerical Limit Load Solutions for Defected Cylinders

The use of finite element analysis techniques in determining limit load solutions is common in the stress analysis field. Typical approaches utilize non-linear finite element analysis which usually requires more complex models and extensive computing time.

Zarrabi (Zarrabi, 1994) used non-linear finite element analysis to determine the collapse pressure of a cylindrical pressure vessel containing a part-through thickness defect. The analysis assumes elastic-perfectly plastic material behavior and obeys the von Mises yield criterion. The material was also assumed to be homogenous and isotropic and to remain

so during plastic deformation. The vessel loading was uniform internal pressure with the vessel ends experiencing uniformly distributed pressure. The defect type chosen for the analysis was a part-through rectangular slot extending around the circumference of the cylinder. The model results were conservative when compared to experimental collapse pressures, which indicate that the numerical results are acceptable for design or integrity analysis. The processing time required for a simple model is quite extensive with 3000 s on a SUN 3 platform needed for a model having only 163 elements and a maximum wavefront of 150. The use of elaborate numerical methods provides a powerful tool for designers in terms of design optimization and analysis. The ability to create a numerical model of a proposed design and subject it to various loading conditions enables the designer to see how a particular component or structure will behave under simulated conditions before being entered into service. As a result, many possible problems can be addressed in the design office before they arise in operation thereby increasing safety and reliability while reducing costs.

Cheung and Wu (Cheung et al., 1993) propose the use of an incompatible axisymmetric element to replace the isoparametric axisymmetric elements normally used in fracture analysis. The authors argue that the isoparametric elements have large deformation constraints induced at the onset of plasticity such that the stress/strain fields in the vicinity of the crack tip are not accurately approximated. That is, the isoparametric elastic elements become incompressible plastic elements after reaching the yield stress. Since the elements allow no compressive deformation, the complex stress/strain field

near the crack tip is unable to be accurately modeled due to the rigid constraint imposed by the plastic elements. Refining the element mesh in the crack tip region is not a solution as it tends to further increase the constraints. The incompatible element suggested by the authors avoids the plastic deformation constraints of the isoparametric element by adding a set of incompatible displacements to the existing element. The mathematical theory is covered in the paper. The end result is an element which may be used in both the elastic and plastic regions surrounding the crack tip without the strong constraints inherent in existing isoparametric elements. However, there is a danger that the incompatible displacements may destroy the convergence of discrete solutions. The element has been used to model a circular cylinder with a circumferential defect loaded in tension and has provided good limit load predictions as well as accurate mode I stress intensity factor solutions.

The use of the incompatible axisymmetric element leads to improved accuracy in determining elastic-plastic parameters and limit load results for the given problem. However, existing isoparametric elements provide limit load results that while not quite as accurate as the proposed element provide consistently conservative results which are ideal for design and evaluation purposes. Therefore, the use of standard isoparametric elements in determining plastic collapse loads for cracked components will provide acceptable results with an inherent factor of safety.

Attempts are being made to develop robust numerical techniques for determining limit

loads that will significantly reduce model complexity and computer processing time. As shown in the work of Zarrabi, significant processing time was required for a very simple model when performing a non-linear analysis. Seshadri (Seshadri, 1991) proposed a robust method known as Generalized Local Stress Strain (GLOSS) analysis. GLOSS analysis is a simple and systematic method for carrying out inelastic evaluations of mechanical components and structures on the basis of two linear elastic finite element analysis. This technique has been used for a wide range of analyses including the determination of multiaxial stress relaxation, follow-up, creep damage, inelastic strain concentrations, low-cycle fatigue estimates, limit analysis and stress-classification issues. With regard to limit analysis, GLOSS analysis can be used in conjunction with the concept of redistribution nodes to determine limit loads. The technique requires the use of no more than two linear elastic finite element analysis to determine limit load estimates. This technique is one of two robust finite element analysis techniques used in this thesis and is discussed in detail in the following chapter.

Mackenzie and Boyle (Mackenzie et al., 1993) have developed a limit load estimation technique along lines similar to that of Seshadri using an iterative elastic analysis which they refer to as the elastic compensation technique. This method utilizes a sequence of elastic finite element analyses and the lower bound theorem. The aim is to generate an admissible stress field, corresponding to the highest possible load such that derived stresses are in equilibrium and do not violate the yield condition. For a given load, the admissible stress field is obtained by a sequence of elastic calculations where the elastic

moduli of selected elements are modified to reduce stress levels below yield. The elastic modulus of the elements are modified using the equation,

$$E_i = E_{i-1} \frac{\sigma_n}{\sigma_{i-1}} \quad (2.15)$$

for the i^{th} iteration where σ_{i-1} is the maximum nodal equivalent stress in the element based on the previous finite element solution. The value of σ_n is arbitrary, but the authors generally take the value as one half or two-thirds of the yield stress. After several iterations, the maximum stress level decreases until a limit value is reached. This provides an admissible stress field for the given load which may then be scaled to obtain a limit load estimate, P_L , using the following equation:

$$P_L = P_D \frac{\sigma_y}{\sigma_R} \quad (2.16)$$

The parameters P_D and σ_R are defined as the applied load and the limit stress value respectively. This procedure may be extended to account for combined loadings. The authors have used the elastic compensation method with slight improvements to obtain limit load estimates for such pressure components as flush nozzles (Nadarajah, Mackenzie and Boyle, 1993) and torispherical heads (Shi, Mackenzie and Boyle, 1993).

CHAPTER 3

ROBUST LIMIT LOAD ESTIMATION TECHNIQUES

3.1 Limit Load Predictions

As discussed in Chapter 2, many different approximations are available in the literature for the estimation of upper and lower bound limit loads based on particular geometries and loading conditions. In this thesis, two robust limit load prediction techniques have been chosen to estimate limit loads for several crack geometries. Both the Gloss R-node method and the m_z -method predict limit load solutions based on no more than two linear elastic finite element analyses. The application of these methods to uncracked geometries has provided excellent predictions when compared to nonlinear finite element results. The application of these methods to cracked geometries would significantly reduce the time required for analysis. Each of the two methods is discussed in the following sections

of this chapter. Their implementation into a finite element analysis scheme is also addressed.

3.2 GLOSS R-node Method

The ASME Codes explicitly recognize load and deformation controlled effects.

Deformation controlled stresses arise in a structure as a result of statically indeterminate actions. Load controlled stresses, however, are statically determinate in that they are induced within a structure to maintain equilibrium with externally applied loads (Seshadri et al., 1992). With the onset of inelastic action such as creep or plasticity, the statically indeterminate stresses and strains undergo a redistribution throughout the structure.

However, no redistribution occurs at the statically determinate locations which are essentially load-controlled. These locations are known as redistribution nodes (r-nodes).

Given the load controlled nature of the stresses at the r-nodes, equilibrium requirements dictate that these stresses be linearly proportional to the externally applied load, P , or load combination, $\langle P, M \rangle$. This may be expressed as

$$\begin{aligned}\sigma_{r-node} &= C_1 P \\ \sigma_{r-node} &= C_2 \langle P, M \rangle\end{aligned}\tag{3.1}$$

The constants C_1 and C_2 are scaling parameters that are dependent on the loading conditions, geometry of the structure and material properties. Taking the simplified case

of elastic-perfectly plastic material behaviour, when the equivalent r-node effective stress, $(\sigma_e)_{r-node}$ approaches the yield stress as given by the von Mises yield criterion, the externally applied load will correspond to the limit load. The von Mises equivalent stress is given by,

$$\sigma_e = \frac{1}{\sqrt{2}} \left[(\sigma_1 - \sigma_2)^2 + (\sigma_2 - \sigma_3)^2 + (\sigma_3 - \sigma_1)^2 \right]^{1/2} \quad (3.2)$$

where σ_1 , σ_2 and σ_3 are principal stresses. When $(\sigma_e)_{r-node}$ approaches yield, P corresponds to P_L . Therefore, equation (3.1) may be written as

$$\begin{aligned} \sigma_y &= C_1 P_L \\ \sigma_y &= C_2 \langle P, M \rangle_L \end{aligned} \quad (3.3)$$

Combining equations (3.1) and (3.3) gives an expression for the limit load as

$$\begin{aligned} P_L &= \left[\frac{\sigma_y}{(\sigma_e)_{r-node}} \right] P \\ \langle P, M \rangle_L &= \left[\frac{\sigma_y}{(\sigma_e)_{r-node}} \right] \langle P, M \rangle \end{aligned} \quad (3.4)$$

The equivalent r-node effective stress, $(\sigma_e)_{r-node}$, is load controlled. Therefore, the equivalent stresses at these points are directly proportional to the external loads irrespective of the material constitutive relations. As a result, any two stress distributions satisfying equilibrium with the externally applied tractions will intersect at the r-nodes.

Given the load controlled nature of these points and assuming an elastic-perfectly plastic

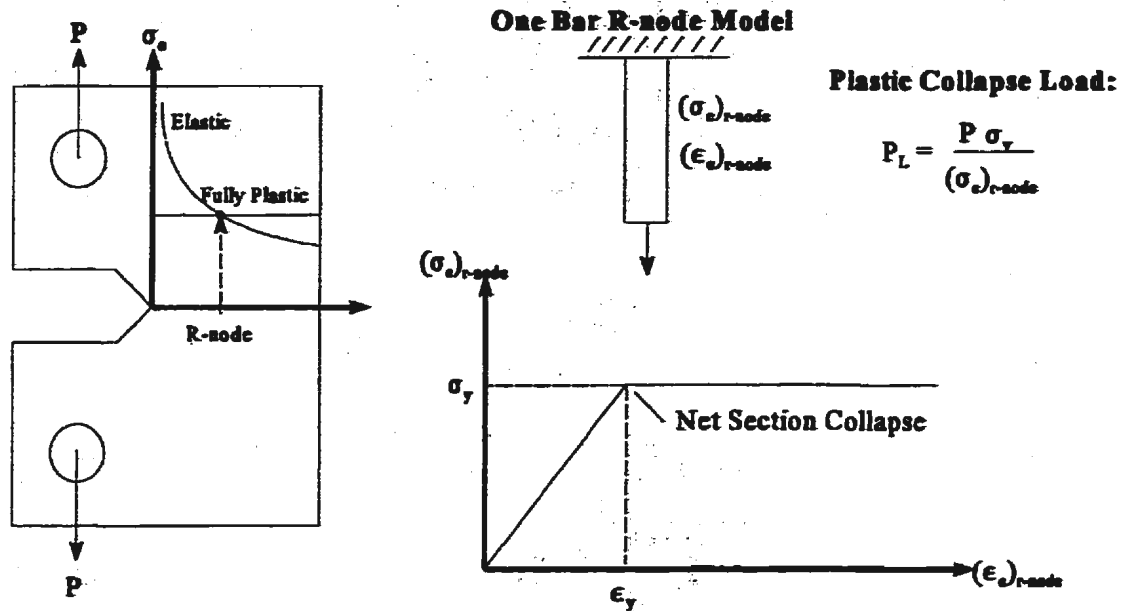


Figure 3.1 - R-node concepts (CT Specimen)

material, when the r-node stress reaches yield, uncontrolled plastic flow occurs resulting in the formation of a plastic hinge and collapse of the structure. The occurrence of a single r-node across the thickness of a component or structure is indicative of a load controlled membrane mode of collapse and may be represented by a one bar model as shown in Figure 3.1 (Seshadri, 1992). In the case of a cracked component, failure will generally occur as a net section collapse of the uncracked ligament rather than an overall plastic collapse of the structure. This usually results in the formation of a single r-node along this ligament. Multiple r-nodes are also possible and are discussed later. Seshadri and Fernando, 1992 and Seshadri, 1995 give models for multiple r-node cases.

3.2.1 Determination of the r-node stress for cracked components

GLOSS analysis can be used to determine the r-node stress in the following manner:

- i.) A linear elastic finite element analysis is performed.
- ii.) The elastic moduli of all elements are modified by the equation

$$E_s = \left[\frac{(\sigma_e)_f}{(\sigma_e)} \right] E_0 \quad (3.5)$$

where $(\sigma_e)_f$ is the equivalent stress at a particular location within the structure (Seshadri, 1995) and σ_e is the elemental equivalent stress. For cracked components, this location is commonly chosen along the uncracked ligament. The choice of location is arbitrary provided that $(\sigma_e)_f$ is nonzero and the resulting stress distribution satisfies equilibrium with externally applied loads.

The modification of elemental stiffness is used to force the stress distribution to that of a limit type distribution. Examination of equation (3.5) indicates that the elemental stiffness values are changed in such a manner that elements with equivalent stress values greater than $(\sigma_e)_f$ are softened while those with equivalent stress values less than $(\sigma_e)_f$ are stiffened.

- iii.) A second linear elastic analysis is performed and the equivalent stress distribution along the symmetry plane (uncracked ligament for cracked components) is plotted for each analysis.

Figure 3.2 shows a typical stress distribution for a cylinder loaded by internal pressure and the resulting stress distribution that can be expected using the stiffness modification

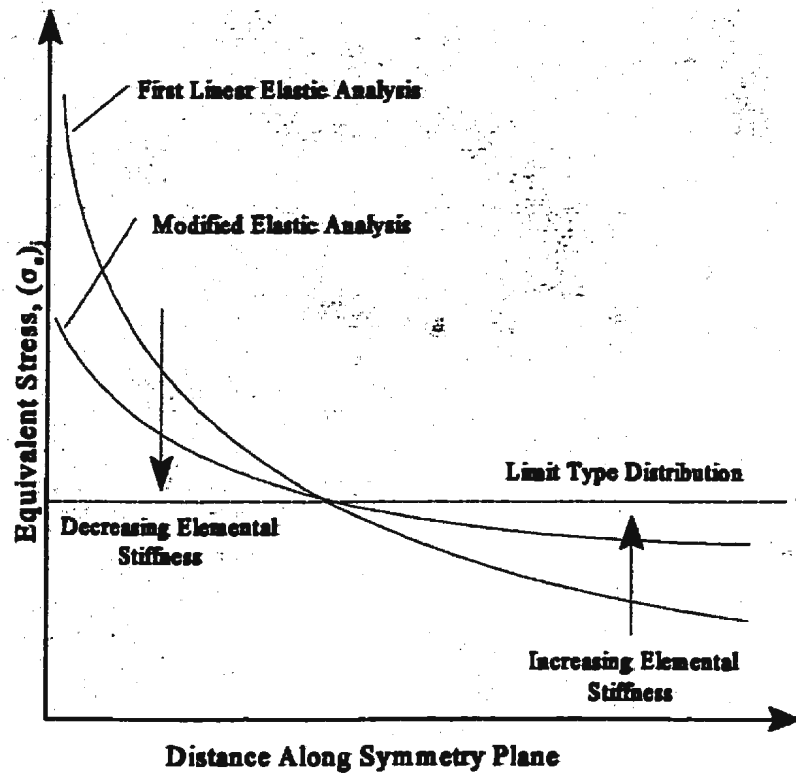


Figure 3.2 - Typical Stress Distributions

equation (3.5). The intersection of the two plots gives the r-node stress. Since the r-node stress is load-controlled, it is linearly proportional to the externally applied tractions.

Plastic collapse occurs when the r-node stress reaches yield. Therefore the limit load can be expressed as

$$P_L = P \frac{\sigma_y}{\sigma_{r-n}} \quad (3.6)$$

This value gives a lower bound estimate of the limit load for the given component or structure if certain criteria are satisfied. The GLOSS R-node method has also been used to provide a robust estimate of inelastic fracture parameters for standard fracture specimens such as the compact tension specimen. The estimates are made by scaling the load point displacements, based upon the results of the two linear elastic finite element analyses, to obtain a strain parameter from which the elastic-plastic J-integral is calculated (Seshadri et al., 1995).

3.3 The m_e -Method

3.3.1 Theorem of nesting surfaces

Consider a structure of volume, V , bounded by the surface, S , and acted upon by a system of generalized loads Q_k ($k = 1, 2, \dots$) as shown in Figure 3.3. Within the structure, there

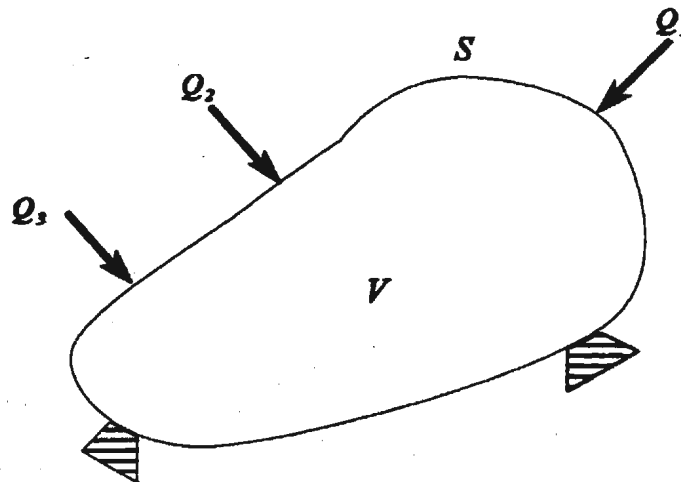


Figure 3.3 - Body with applied point loads.

is a stress field σ_{ij} and a corresponding steady strain-rate field $\dot{\epsilon}_{ij}$. The problem is restricted to that of steady isothermal creep in which the material behavior of the structure is governed by the constitutive equation

$$\dot{\epsilon} = B\sigma^n \quad (3.7)$$

The "generalized effective stress" for this structure is given by

$$Q_E = \left[\frac{1}{V} \int_V \sigma_e^{n+1} dV \right]^{\frac{1}{n+1}} \quad (3.8)$$

where, σ_e , is the effective stress associated with the actual stress field inside the structure.

Based on the work of Calladine and Drucker (Calladine et al., 1962), the theorem of nesting surfaces may be stated as follows:

If the hypersurfaces $Q_E(\sigma_{ij}) = \text{constant}$ in a stress space is considered and Q_E is strictly monotonic, then for increasing values of n these hypersurfaces must "nest" inside each other. That is to say, $Q_E|_{n=1} \leq Q_E \leq \lim_{n \rightarrow \infty} Q_E$. They are bounded on the outside by the surface $n = 1$ which is analogous to linear elasticity and on the inside by the limit surface for $n \rightarrow \infty$, which is the yield surface in terms of the generalized forces constructed on the assumption that the condition of plasticity is given by $Q_E = \text{constant}$.

The nesting surfaces for a pin-jointed two-bar structure are illustrated in Figure 3.4.

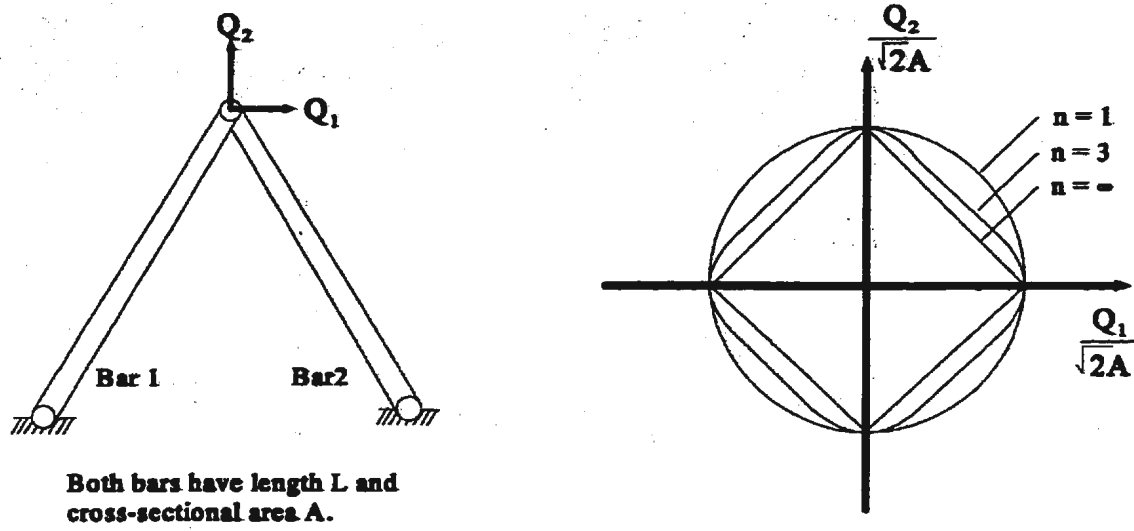


Figure 3.4 - Two-bar structure with associated nesting surfaces (Boyle, 1982).

3.3.2 Mura's variational formulation

In a limit analysis, it is well established that a statically admissible stress field cannot lie outside the hypersurface defined by the yield criterion. As well, the stress field obtained from a kinematically acceptable strain-rate field should lie on the hypersurface. The introduction of the "integral mean of yield" concept by Mura and associates (Mura et al., 1963) into a variational formulation has made it possible to bypass the previously mentioned requirements.

Mura and Lee (Mura et al., 1963) showed that for a state of impending plastic flow, the functional, F , becomes stationary with the safety factor being the stationary value of the

functional. The functional is expressed as follows:

$$\begin{aligned}
 F = & \int_V s_{ij} \frac{1}{2} (v_{ij} + v_{ji}) dV + \int_V \sigma \delta_{ij} v_{ij} dV - \int_{S_v} R_i v_i dS \\
 & - m \left(\int_{S_T} T_i v_i dS - 1 \right) - \int_V \mu [f(s_{ij}) + \phi^2] dV
 \end{aligned} \tag{3.9}$$

with the constraint condition $\mu \geq 0$. The arguments of the functional are the independent variables; velocity v_i , the deviatoric stress tensor s_{ij} , as well as the Lagrangian multipliers. The Lagrangian multipliers include the mean stress σ , the surface reaction R_i , the safety factor m , the positive scalar of proportionality μ , and the yield parameter ϕ . Other parameters include the given surface traction, T_i , defined on a part of the boundary surface denoted by S_T (the remaining boundary is denoted S_v), the Kronecker delta δ_{ij} and the function $f(s_{ij})$, which is the yield criterion. The yield criterion is expressed as

$$f(s_{ij}) = \frac{1}{2} s_{ij} s_{ij} - k^2 = \frac{1}{2} s_{ij} s_{ij} - \frac{\sigma_y^2}{3} \tag{3.10}$$

The variables s_{ij} , σ , m , μ , and ϕ all correspond to a state of impending plastic flow.

Taking the variation of (3.9) and equating it to zero yields several natural conditions, one of which includes the plastic potential flow law given by

$$\dot{\epsilon}_{ij} = \frac{1}{2} (v_{ij} + v_{ji}) = \mu \frac{\partial f}{\partial s_{ij}} \tag{3.11}$$

Other important conditions yielded are the equilibrium conditions, which may be

expressed as

$$\begin{aligned}
 (s_{ij} + \delta_{ij}\sigma)_{,j} &= 0 && \text{in } V \\
 (s_{ij} + \delta_{ij}\sigma)n_j &= mT_i && \text{on } S_T \\
 (s_{ij} + \delta_{ij}\sigma)n_j &= R_i && \text{on } S_V
 \end{aligned} \tag{3.12}$$

We now introduce the arbitrary arguments

$$\begin{aligned}
 v_i^o &= v_i + \delta v_i \\
 s_{ij}^o &= s_{ij} + \delta s_{ij} \\
 \sigma^o &= \sigma + \delta\sigma \\
 R_i^o &= R_i + \delta R_i \\
 m^o &= m + \delta m \\
 \mu^o &= \mu + \delta\mu \\
 \phi^o &= \phi + \delta\phi
 \end{aligned} \tag{3.13}$$

in which $v_i, s_{ij}, \sigma, \dots$ denote the stationary set of arguments of equation (3.9) and $\delta v_i, \delta s_{ij},$ etc., denote the variations. In the above set of equations, s_{ij}^o is the statically admissible deviatoric stress tensor corresponding to impending plastic collapse, where $s_{ij}^o = \sigma_{ij}^o - \delta_{ij}\sigma^o$. The parameter σ_{ij}^o represents a statically admissible stress field, $\sigma^o = \sigma_{kk}^o/3$ and δ_{ij} is the Kronecker delta.

Substituting the arguments of (3.13) into equation (3.9) using the equilibrium conditions (3.12) and the additional conditions

$$\begin{aligned}
 (s_{ij}^o + \delta_{ij}\sigma^o)_{,j} &= 0 && \text{in } V \\
 (s_{ij}^o + \delta_{ij}\sigma^o)n_j &= m^o T_i && \text{on } S_T \\
 (s_{ij}^o + \delta_{ij}\sigma^o)n_j &= R_i^o && \text{on } S_V
 \end{aligned} \tag{3.14}$$

expression (3.9) can be manipulated to give

$$F = m - \int_V \mu \left\{ \frac{1}{2} \delta s_{ij} \delta s_{ij} + (\delta \phi)^2 \right\} dV - \int_V \delta \mu \left\{ f(s_{ij}^o) + (\phi^o)^2 \right\} dV \quad (3.15)$$

Mura and Lee also showed that integrating equation (3.9) with arbitrary arguments (3.13) and using the constraint conditions (3.14), the functional, F , can be expressed as

$$F = m^o - \int_V \mu^o \left\{ f(s_{ij}^o) + (\phi^o)^2 \right\} dV \quad (3.16)$$

Furthermore, the parameters m^o , μ^o and ϕ^o may be determined by rendering the above functional, F , stationary which leads to the following set of equations

$$\frac{\partial F}{\partial m^o} = 0; \quad \frac{\partial F}{\partial \mu^o} = 0; \quad \frac{\partial F}{\partial \phi^o} = 0; \quad (3.17)$$

Using equations (3.15) and (3.16) along with the additional condition, $f(s_{ij}^o) + (\phi^o)^2 = 0$ in V , yields the extended lower bound theorem.

Mura's extended lower bound theorem (Mura et al., 1965) may be expressed as

$$\frac{m^o}{1 + \frac{\max \left\{ f(s_{ij}^o) + (\phi^o)^2 \right\}}{2k^2}} \leq m \quad (3.18)$$

for any set of s_{ij}^o , σ^o , m^o , μ^o and ϕ^o which satisfy the conditions,

$$\begin{aligned} (s_{ij}^o + \delta_{ij}\sigma^o)_{,j} &= 0 && \text{in } V \\ (s_{ij}^o + \delta_{ij}\sigma^o)n_j &= m^o T_i && \text{on } S_T \end{aligned} \quad (3.19)$$

and the integral mean of yield criterion given by

$$\int_V \mu^o \{f(s_{ij}^o + (\phi^o)^2)\} dV = 0 \quad (3.20)$$

Since the right side of equation (3.18) is the safety factor, the left side gives the lower bound for the safety factor.

3.3.3 Finite element implementation of Mura's formulation

Seshadri and Mangalaramanan (Seshadri et al., 1996) implement Mura's formulation into a finite element scheme, whereby the improved lower bound multiplier may be determined from the results of a linear elastic finite element analysis. The linear elastic stress distribution, s_{ij}^o , corresponds to the applied traction, $m^o P$. Given a second statically admissible stress distribution, \tilde{s}_{ij}^o , corresponding to an applied traction P , then $m^o \tilde{s}_{ij}^o$ would correspond to $m^o P$. Therefore, the following relationship holds

$$s_{ij}^o = m^o \tilde{s}_{ij}^o \quad (3.21)$$

Substituting equation (3.21) into (3.16) yields the following expression for the functional, F ,

$$F = m^o - \int_V \mu^o \left[\frac{1}{2} (m^o)^2 \bar{s}_{ij}^o \bar{s}_{ij}^o - k^2 + (\phi^o)^2 \right] dV \quad (3.22)$$

The von Mises equivalent stress for the case of a uniaxial state of stress can be expressed as

$$\frac{1}{2} \bar{s}_{ij}^o \bar{s}_{ij}^o = \frac{(\sigma^o)^2}{3} \quad (3.23)$$

Substituting equation (3.23) into (3.22) gives

$$F = m^o - \int_V \frac{\mu^o}{3} \left[\left\{ (m^o)^2 (\sigma^o)^2 - \sigma_y^2 \right\} + 3(\phi^o)^2 \right] dV \quad (3.24)$$

If we now apply equations (3.17) to the above result, we arrive at the following expressions for ϕ^o and m^o

$$\begin{aligned} \phi^o &= 0 \\ m^o &= \frac{\sigma_y \sqrt{V_T}}{\sqrt{\sum_{k=1}^N (\sigma_{ek}^o)^2 \Delta V_k}} \end{aligned} \quad (3.25)$$

The parameter σ_{ek}^o is the equivalent von Mises stress and ΔV_k is the volume of respective elements in the FEA discretization scheme. If we now consider Mura's extended lower bound theorem, we can use equation (3.25) to simplify (3.18) to give (Seshadri et al., 1996),

$$m' = \frac{2m^o \sigma_y^2}{\sigma_y^2 + (m^o)^2 (\sigma_e^o)_M^2} \leq m \quad (3.26)$$

where m' is the lower bound multiplier. Equations (3.25) and (3.26) are easily obtained from a linear elastic finite element analysis. The quantity $(\sigma_e^o)_M$ is the maximum equivalent stress in the structure for a given load P . Therefore, the lower bound limit load may be expressed as

$$P_L = m' P \quad (3.27)$$

Calladine and Drucker (Calladine et al., 1962) and Boyle (Boyle, 1982) have developed an equation based on the average surfaces of dissipation that is similar to equation (3.25). Therefore, the parameter m^o may be regarded as a multiplier for an upper bound limit load. It follows that the exact limit load for a given structure is bounded by the upper and lower multipliers, i.e. $m' \leq m \leq m^o$. The challenge is to reduce the range between these values in order to focus on the actual limit load value. For the purpose of design and failure analysis, the lower bound value introduces a conservative estimate of the limit load with an inherent factor of safety that is desirable for this type of work.

3.3.4 Analysis of cracked components - Local plastic collapse

Based on Mura's formulation, the parameter m^o corresponds to the upper bound multiplier and is found from equation (3.25). The quantities σ_{ek}^o and ΔV_k represent the

Von Mises equivalent stress and the volume of individual elements in the FEA discretization scheme. The quantity V_T represents the total volume of the component. However, in the case of cracked components which undergo failure by localized plastic collapse, the use of the total volume would greatly overestimate the upper bound limit load which, in turn, would result in a poor estimate of the lower bound limit. In order to account for this behaviour, Seshadri and Mangalaramanan (Seshadri et al., 1996) make use of a reference volume, V_R , corresponding to the volume of the plastic region which is used to calculate m^o .

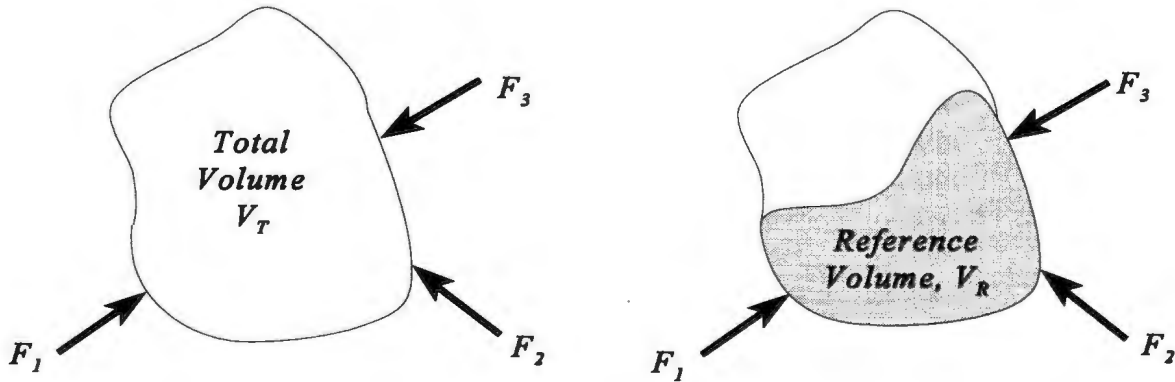


Figure 3.5 - Illustration of Total and Reference Volumes

The reference volume identifies the active portion of the structure that participates in any plastic action. Since the reference volume consists of a localized region of the structure, the inequality $V_R \leq V_T$ must hold (Figure 3.5). For cracked components, plastic action is limited to a sub-region of V_T . Therefore, the magnitude of the upper bound multiplier, m^o , is dependent on the size of the sub-volume, which may be written as

$$V_\beta = \sum_{k=1}^{\beta} (\Delta V_k) \quad (3.28)$$

For the case when $\beta = 1$, equation (3.28) degenerates to the classical lower bound value given by $m^o = \sigma_y / \sigma_{e1}$.

Next, consider an iterative linear elastic FEA process, similar to that of the GLOSS R-node approach, where the element stiffness values of the individual elements are altered

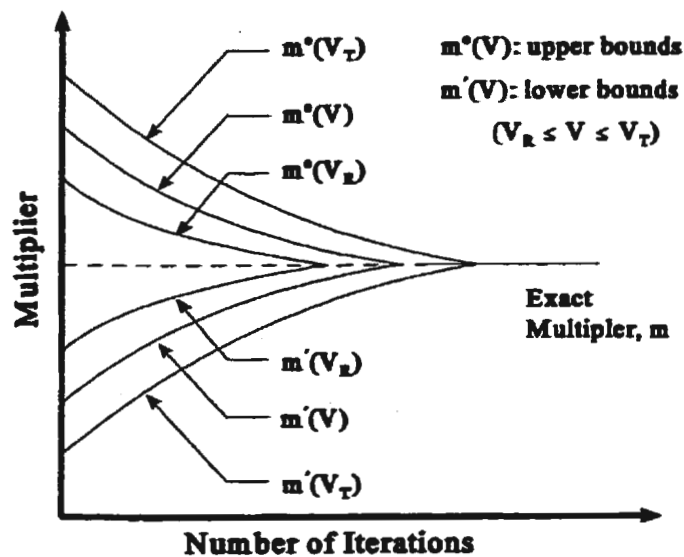


Figure 3.6 - Variation of m^o and m' with iterations.

in the second and subsequent iterations to obtain a flatter stress distribution which approaches a limit type distribution. If m^o is evaluated on the basis of the total volume V_T , then it will decrease with increasing iterations, giving a flatter distribution of stress with increasing iterations. Of course, if m^o increases with increasing iterations, the theorem of nesting surfaces will be violated. If m^o is evaluated on the basis of the reference volume V_R , and the various summations are carried out in the following sequence,

$$(\sigma_{e1}^o)^2 \Delta V_1 > (\sigma_{e2}^o)^2 \Delta V_2 > \dots > (\sigma_{eN}^o)^2 \Delta V_N \quad (3.29)$$

then for some reference volume, where $\Delta V_1 < V_R < V_D$, the multiplier m^o obtained from the first and second linear elastic FEA will be equal, i.e. ($m_1^o = m_2^o$). That is to say that the theorem of nesting surfaces is just satisfied. A schematic of the variation of the upper and lower bound multipliers with the number of iterations is shown in Figure 3.6.

Seshadri and Mangalaramanan (Seshadri et al.,1996) use the concept of reference volume in conjunction with Mura's variational approach to develop an improved lower bound limit load estimate known as the m_e -method. This method makes use of a stiffness adjustment scheme similar to that of the GLOSS R-node method in which two linear elastic FEA are performed. The first is a conventional analysis, while the second analysis is based on a modification of the elemental stiffness values using the following equation:

$$(E_s)_k = \left[\frac{\sigma_{arb}}{(\sigma_e^o)_k} \right]^q E_o \quad (3.30)$$

where σ_{arb} is any arbitrary, nonzero stress value, σ_e^o is the elemental centroidal equivalent stress, E_s is the modified element elastic modulus and E_o is the original elastic modulus. The subscript k refers to the element numbers and varies from $k = 1$ to $k = N$. The parameter q is the stiffness adjustment index and is used to moderate the degree of modification for "sensitive" structures. For the majority of analyses, the value of q is set to unity.

Based on the results of the two linear elastic FEA, and making use of the expression for Mura's upper bound multiplier, m^o (equation 3.25), the values m_1^o and m_2^o may be determined. The theorem of nesting surfaces asserts that $m_1^o \geq m_2^o \geq m$, which is shown in Figure 3.6. The variation of m^o with volume is also shown in Figure 3.6.

Seshadri and Mangalaramanan introduce an iteration variable ζ , such that infinitesimal variations in the elemental stiffness in the second linear elastic FEA result in a corresponding change $\Delta\zeta$, the magnitude of which depends on the nature of the stiffness adjustment. Therefore, as ζ increases with successive linear elastic iterations beyond two, the upper and lower multipliers converge to the actual safety factor (Figure 3.6). Mura's lower bound multiplier may now be expressed in terms of the iteration variable, as:

$$m^i(\zeta) = \frac{2m^o(\zeta)\sigma_y^2}{\sigma_y^2 + [m^o(\zeta)]^2 [\sigma_M^o(\zeta)]^2} \quad (3.31)$$

where $\sigma_M^o(\zeta)$ is the maximum equivalent stress for a given iteration " i ". The quantities m^i , m^o and σ_M are all functions of the iteration variable. Differentiating both sides of equation 3.31 with respect to ζ , gives

$$\frac{dm^i}{d\zeta} = \frac{\partial m^i}{\partial m^o} \frac{dm^o}{d\zeta} + \frac{\partial m^i}{\partial \sigma_M^o} \frac{d\sigma_M^o}{d\zeta} \quad (3.32)$$

Equation (3.32) is valid for any given iteration, however, only two are required for the m_u -method. This equation may also be written in terms of finite differences, as follows:

$$\Delta m^f = \left. \frac{\partial m^f}{\partial m^o} \right|_{\zeta = \zeta_i} (\Delta m^o) + \left. \frac{\partial m^f}{\partial \sigma_M^o} \right|_{\zeta = \zeta_i} (\Delta \sigma_M^o) \quad (3.33)$$

Using equations (3.31), (3.33) and the following defined quantities

$$\begin{aligned} \Delta m^f &= m_\alpha - m_i^f \\ \Delta m^o &= m_\alpha - m_i^o \\ \Delta \sigma_M^o &= \frac{\sigma_y}{m_\alpha} - \sigma_{Mi}^o \end{aligned} \quad (3.34)$$

Seshadri and Mangalaraman arrived at a quadratic equation for m_α , which may be expressed as:

$$Am_\alpha^2 + Bm_\alpha + C = 0 \quad (3.35)$$

where the coefficients A , B and C are given by

$$\begin{aligned} A &= (m_i^o)^4 (\sigma_{Mi}^o)^4 + 4 (m_i^o)^2 (\sigma_{Mi}^o)^2 - 1 \\ B &= -8 (m_i^o)^3 (\sigma_{Mi}^o)^2 \\ C &= 4 (m_i^o)^3 (\sigma_{Mi}^o) \end{aligned} \quad (3.36)$$

These coefficients can be obtained from the results of any linear elastic FEA. Real roots are ensured for equation (3.35) by insisting that the discriminant be greater than zero, i.e. $(m_i^o)(\sigma_{Mi}^o) \leq (1 + \sqrt{2})$. Although it is possible to calculate m_α based on a single linear elastic FEA, provided the given condition is met, the use of the reference volume along with two linear elastic FEA's gives improved estimates of m_α . In addition, the use of the

reference volume serves to reduce the spread between the upper and lower bound multipliers, thereby focusing much more closely on the actual multiplier, m , which is bounded by m^o and m_u .

CHAPTER 4

ANALYSIS OF STANDARD FRACTURE SPECIMENS

In the following chapter, three standard fracture specimens are used as a benchmark for application of both the Gloss R-node and m_x -methods of robust analysis to determine limit loads for cracked components. The three specimens included in the analysis include the compact tension (CT), single edge notched bend (SENB) and the single edge notched tension (SENT) specimens which are shown in Figure 4.1. The figure outlines the important geometry parameters for each specimen and indicates the applied loading condition. Four independent limit load solutions will be calculated for each specimen for the purpose of comparison. These solutions will include both the Gloss R-node and m_x solutions as well as a nonlinear finite element solution and analytical solutions which are available for these particular geometries. The robust limit load results will be compared to the nonlinear finite element analysis and the analytical solution to gauge the accuracy of the robust estimates.

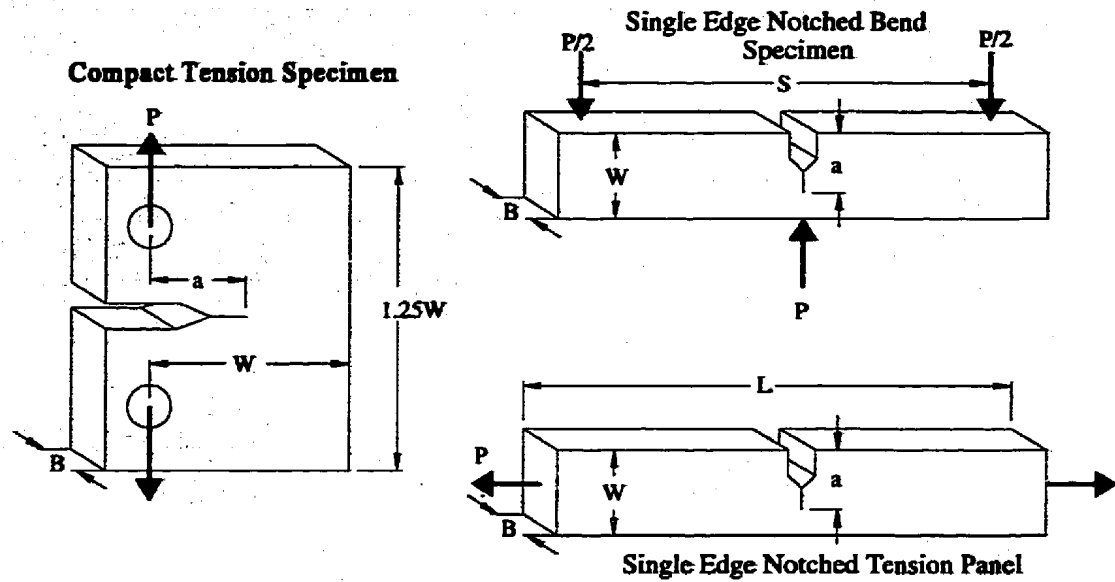


Figure 4.1 - Standard fracture specimens.

Table 4.1 - Standard Fracture Specimen Dimensions

Dimension (mm)	Fracture Specimen		
	CT	SENB	SENT
a	46.6	50	30
B	3	3	3
W	100	100	50
L	-	-	200
S	-	400	-

4.1 Finite Element Modeling Considerations

All of the finite element analyses discussed in this thesis have been performed using the ANSYS Version 5.2 software package from Swanson Analysis Systems. This program has been used for both linear and non-linear analysis.

For the two dimensional linear elastic analyses, it is necessary to model the $1/\sqrt{r}$ singularity of the strain field at the crack tip. Based on work by Barsoum, this is most effectively achieved by using an isoparametric six-noded triangular element with the midside nodes moved to the quarter point (Barsoum, 1976). This element exhibits strain singularity along the element boundaries as well as in the interior, and has a finite strain energy and stiffness at all points within the element. The singular elements are used only around the crack tip and allow a coarser mesh in this region than would be possible with ordinary elements. In the ANSYS software the recommended element for two dimensional fracture models is known as the PLANE2 element and is used exclusively in modeling the three specimens. In all cases the crack tip is modeled using nine elements with the radius of the first array of crack elements at the crack tip equal to 1 mm (see Appendix B). The ratio of the size of the second row of elements to the first row is 0.5.

Material behavior is assumed to be elastic perfectly-plastic for simplicity. However, modeling of strain-hardening behavior may be easily approximated using a flow stress approach in the analysis. The flow stress for typical pipe steels is defined in the literature in one of two ways; i) $\sigma_{flow} = \sigma_y + 69 \text{ MPa}$ or ii) $\sigma_{flow} = (\sigma_y + \sigma_t)/2$ where σ_t is the ultimate tensile strength of the particular material. In either case, the yield stress value of the material is extended to account for the effect of strain-hardening in the analysis. For elastic perfectly-plastic material behavior, Rice and Rosengren have shown the crack tip strain singularity to be of the order $1/r$ (Rice et al., 1968). This is achieved using isoparametric eight-noded quadrilateral elements that are degenerated to triangles with the

mid-side nodes moved to the quarter point. Again, these elements are only used around the crack tip to effectively model the strain singularity. Material properties are isotropic with the following values of material constants used; Young's Modulus = 211 GPa, Poisson's ratio = 0.3 and yield stress = 488 MPa. Each of the three problems are modelled as plane stress with specified thickness. ANSYS code necessary to generate and solve these and subsequent models may be found in Appendix A as is all macro code used in postprocessing. Typical mesh plots are illustrated in Appendix B.

4.2 Compact Tension (CT) Specimen

An illustration of the CT specimen is shown in Figure 4.1, along with the applicable geometry parameters. A half model is used to avail of symmetry in the geometry and loading conditions, which allows for faster model generation and shorter solution times. The relevant dimensions of the specimen are given in Table 4.1. For the linear elastic analyses an arbitrary tensile load of 1300 N was applied to the specimen which is modelled as a plane stress problem with a specified thickness.

An analytical limit load solution is available for the CT geometry and is given as (Anderson, 1991) :

$$P_L = 1.072\eta Bb\sigma_y$$
$$\eta = \sqrt{\left(\frac{2a}{b}\right)^2 + \frac{4a}{b} + 2} - \left(\frac{2a}{b} + 1\right) \quad (4.1)$$

The parameters B , b and σ_y are the thickness, uncracked ligament length and the yield stress respectively. The results of the robust methods will be compared to the analytical and nonlinear finite element solutions.

4.3 Single Edge Notched Bend (SENB) Specimen

The SENB specimen is shown in Figure 4.1 with pertinent dimensions listed in Table 4.1. As in the case of the CT specimen, a half-model is used to avail of symmetry. An arbitrary load of 600 N is applied to the model for the linear elastic analyses. The problem is modeled as plane stress with specified thickness. The analytical solution for the SENB specimen may be expressed as (Anderson, 1991):

$$P_L = \frac{1.072 B b^2 \sigma_y}{S} \quad (4.2)$$

where B is the thickness, b is the uncracked ligament length, S is the length and σ_y is the yield strength. The results are discussed in section 4.5.

4.4 Single Edge Notched Tension (SENT) Panel

As in the previous two cases, the SENT panel is such that the half-model may be used on the basis of symmetry. The relevant model dimensions are found in Table 4.1. The arbitrary applied tensile load for the linear elastic analyses was 500 N. The specimen is,

again, modeled as a plane stress problem with specified thickness. The analytical limit load solution for the SENT specimen is given as (Anderson, 1991):

$$\begin{aligned} P_L &= 1.072 \eta B b \sigma_y \\ \eta &= \sqrt{1 + \left(\frac{a}{b}\right)^2} - \frac{a}{b} \end{aligned} \quad (4.3)$$

where, B , b and σ_y are the thickness, uncracked ligament length and the yield stress respectively. Limit load estimation results are given in the following section.

4.5 Limit Load Results Using The Gloss R-node Method

The Gloss R-node analysis requires the determination of the r-node stress based on two elastic finite element analyses. For the three fracture specimens under consideration, failure occurs as a result of net section yielding along the uncracked ligament. Therefore, the most likely locations for r-nodes will be located along this ligament. R-nodes are identified as locations in the structure where the equivalent stress distributions for the first and second linear analyses intersect. For the two dimensional fracture models considered, this is most easily obtained by plotting the distributions along the remaining ligament, as collapse will occur along this section. Using the ANSYS software, the path is defined by specifying nodes at the beginning and the end of the desired path. Intermediate nodes may also be used in the definition of the path to increase the number of data points in the distribution. The FEA software calculates fifty data points between each two nodes defined in the path, with the data points obtained by interpolation

between known nodal values as necessary. The stress distributions are based on nodal stress values for elements located along the symmetry plane, with stress values averaged across the elements. Plots of the equivalent stress distributions along the ligament are

R-Node Stress Determination CT Specimen

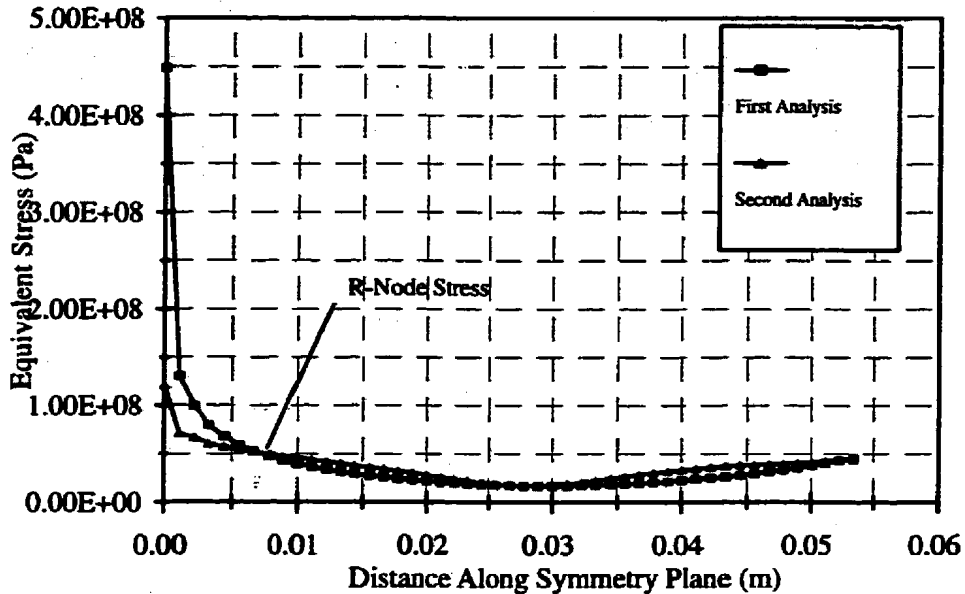


Figure 4.2 - CT Specimen Stress Distribution Along Symmetry Plane

given for each specimen and the relevant R-node stresses are determined. Plots illustrating the finite element mesh and other model data are located in Appendix B. Figure 4.2 shows the equivalent stress distribution for the CT specimen after the first and second linear elastic analyses. The distributions are plotted from the crack tip (position of 0 m) to the end of the uncracked ligament. Although difficult to see, there is only one intersection of the two distributions at a location near the crack tip. This indicates the

presence of one r-node for this problem and the r-node stress is the equivalent stress value corresponding to the intersection point. At a position of 0.03 m, there appears to be an

R-Node Stress Determination SENB Specimen

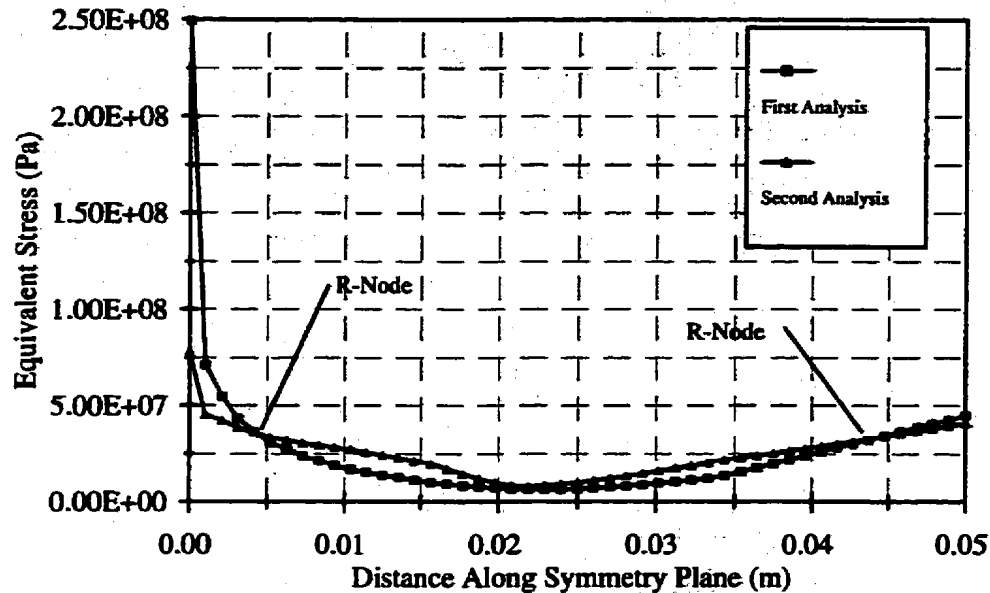


Figure 4.3 - SENB Specimen Stress Distribution Along Symmetry Plane

overlap in the two stress distributions. However, there is no clear intersection. As a result, this cannot be taken as an r-node. In all likelihood, the apparent intersection is the result of interpolation errors in calculating the element centroidal stresses. The same may be said for the apparent intersection at the far end of the plot (position of 0.052 m). It can be shown that these apparent intersections progressively vanish as the modified elastic stress distribution approaches limit type (Seshadri, 1996). However, this would require multiple elastic iterations, which would defeat the purpose of attaining good limit load

estimates using only two elastic iterations. The actual r-node equivalent stress value taken from the plot is 52 MPa which corresponds to a limit load value for the CT specimen of 12 182 N.

R-Node Stress Determination SENT Specimen

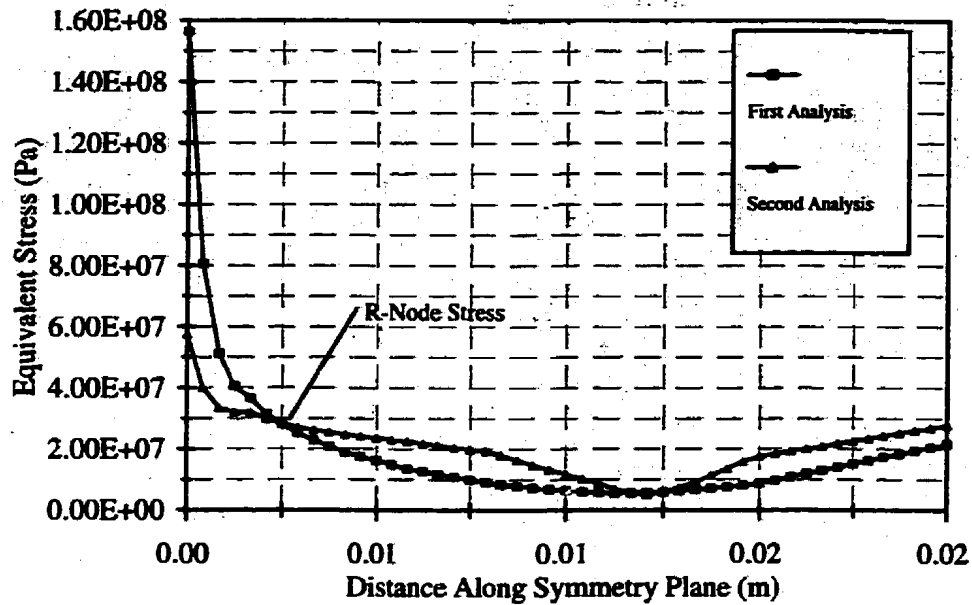


Figure 4.4 - SENT Specimen Stress Distribution Along Symmetry Plane

Similar stress distribution plots for the first and second linear analyses along the uncracked ligaments are given in Figures 4.3 and 4.4 for the SENB and SENT specimens respectively. In each case, the distribution is plotted from the crack tip along the extent of the uncracked ligament. The plot for the bend specimen shows two possible intersections at either end of the plot, with an overlapping region at the center. The first intersection at the left hand side of the plot is a clear distinct intersection in the vicinity of the crack tip

and as such must be considered an r-node. The overlapping section at the center of the plot does not show a clear, distinct intersection between the two distributions. Therefore, this is a virtual r-node. The intersection at the right hand side of the plot also appears to be clear and distinct which indicates an r-node location. The loading configuration of the SENB specimen is such that tensile and compressive stresses are present along the remaining ligament due to the bending moment. Plotting the von Mises equivalent stresses, the resulting stress distribution across the ligament is u-shaped. As a result, it is possible for this distribution to yield two r-node locations with similar stress values. This is the case for the SENB specimen. Since there are two r-nodes indicated in Figure 4.3, the r-node equivalent stress used in the evaluation of the limit load is the arithmetic mean of the two r-node stresses shown in the figure. If unsure about the validity of multiple r-nodes for more complex structures, use the highest r-node equivalent stress value to calculate the limit load to ensure a conservative estimate. The equivalent stress value in this case is 34 MPa which gives a limit load for the SENB specimen of 8508 N.

The stress distribution plot for the SENT specimen is similar to that of the CT specimen, as the loading conditions are similar. In this case, the plot shows a single, well defined intersection at a position of approximately 0.005 m along the symmetry plane.

As well, there is an apparent overlap towards the center of the plot characteristic of the previous two specimens. This overlap is again considered a virtual r-node and therefore does not play a role in the collapse mechanism. Based on the plot, the r-node equivalent stress for this geometry is 28 MPa which corresponds to a limit load of 8 589 N.

There are several problems associated with determining r-nodes using the stress distribution along the uncracked ligament. The previous discussion outlines the difficulties in determining what criteria constitute an r-node based on the plots shown. This method is satisfactory for the simple, two-dimensional fracture models given. However, for more complex geometries and crack configurations the method outlined needs development. Cases involving complex cracks and three-dimensional geometries make this approach a challenge.

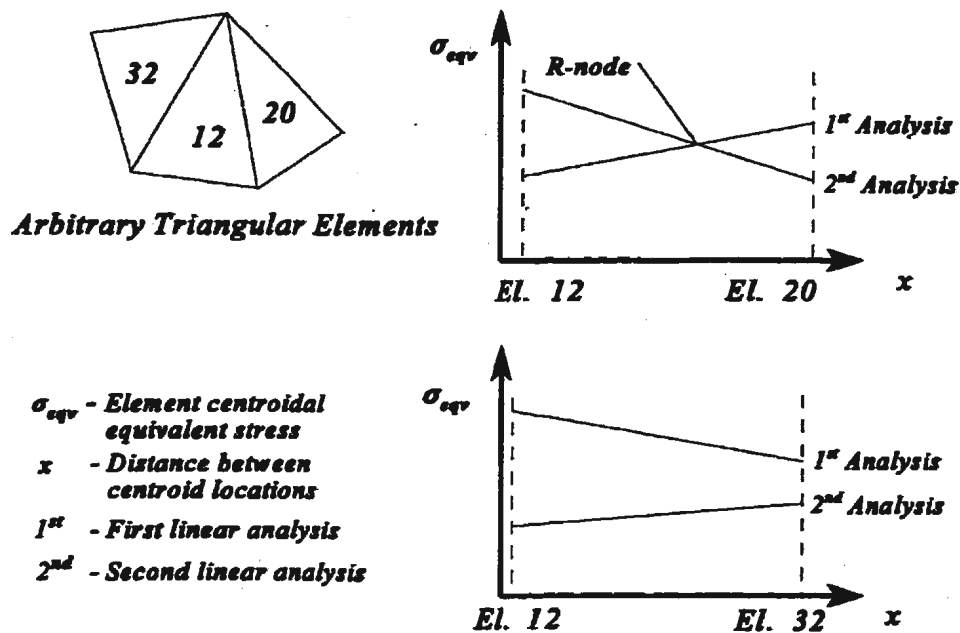


Figure 4.5 - Improved R-node Visualization Scheme

An improved method of visualizing r-node locations and stress values has recently been used with good success. The improved method involves calculating r-nodes for every combination of adjacent elements in the entire model (Mangalaramanan, 1997). The

method may be used for both two and three dimensional models and provides a visual representation of all the r-nodes within a structure. The r-nodes are determined by plotting the element centroidal equivalent stress values of adjacent elements from both the first and second linear analyses. A linear relationship is assumed between the values of the first and second analyses and the lines plotted for each element. An r-node is identified if the lines intersect and the r-node stress value is taken as the intersection value. Figure 4.5 illustrates this method. Three triangular elements are depicted in the figure with element centroidal equivalent stresses plotted for the two pairs of adjacent elements. The plot in the upper right corner shows two intersecting lines which indicates an r-node at this location. The r-node equivalent stress is taken as the stress value at which the lines intersect. The lower plot shows the stress values for both the first and second linear analyses which do not intersect. In this case, there is no r-node present. This calculation is performed for all adjacent elements within the model to determine r-node locations and their associated stress values.

Having identified all the r-nodes within the structure, the next task is to identify the peaks. If we consider all the r-nodes within the structure and plot them based on their equivalent stress values, an r-node stress contour can be depicted within the structure. Plastic collapse will occur in the area where the r-node stress values are highest (as these areas will reach the yield stress sooner) which may be easily identified from the r-node stress contour. A recent paper by Seshadri lists several basic rules for identifying legitimate r-node peaks which may be used for this approach (Seshadri, 1996). The r-

node diagrams referred to in Seshadri's paper are two dimensional plots of r-nodes along a path consistent with the model geometry. However, the same peak visualization and identification rules may be applied to the prescribed method and extended into three dimensions. It is important to note that proper identification of r-node peaks requires substantial experience and that the rules which are given should only be used as guidelines.

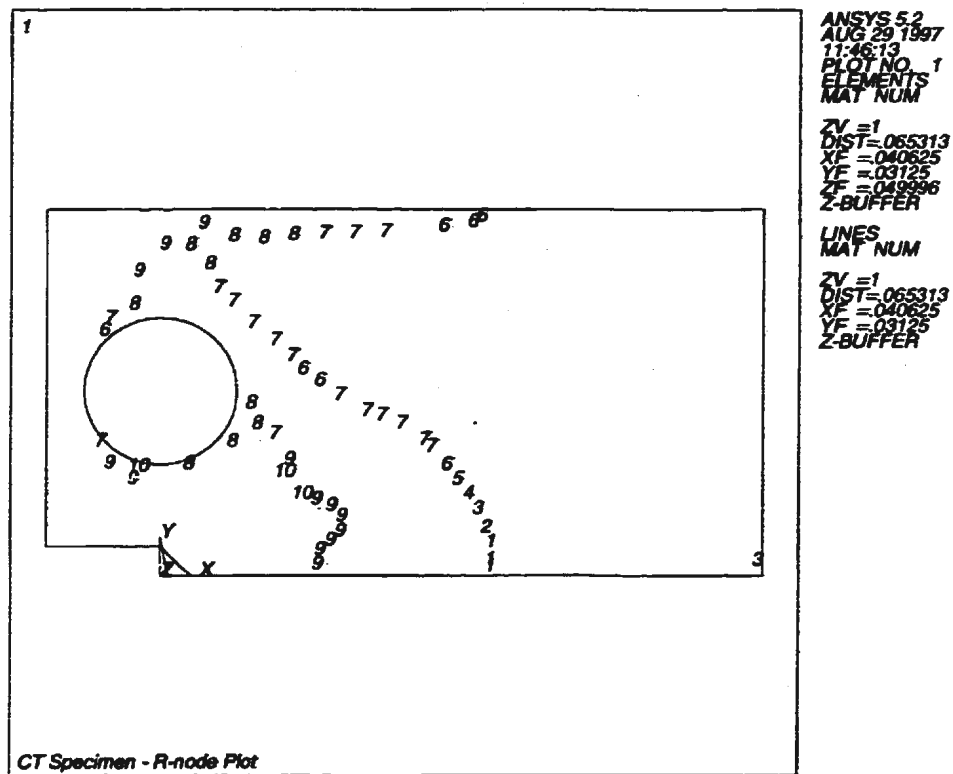


Figure 4.6 - CT Specimen R-node Plot

The improved r-node visualization scheme is used to determine the r-node peaks for the three standard fracture specimens discussed previously and the results are compared to those obtained earlier. The r-node plot for the CT specimen is shown in Figure 4.6. The

numbered values inside the model outline indicate ranges of stress values for the r-nodes and are given in descending order of stress (i.e. one represents the highest stress value while ten indicates the lowest stress value). The range of r-node equivalent stress values

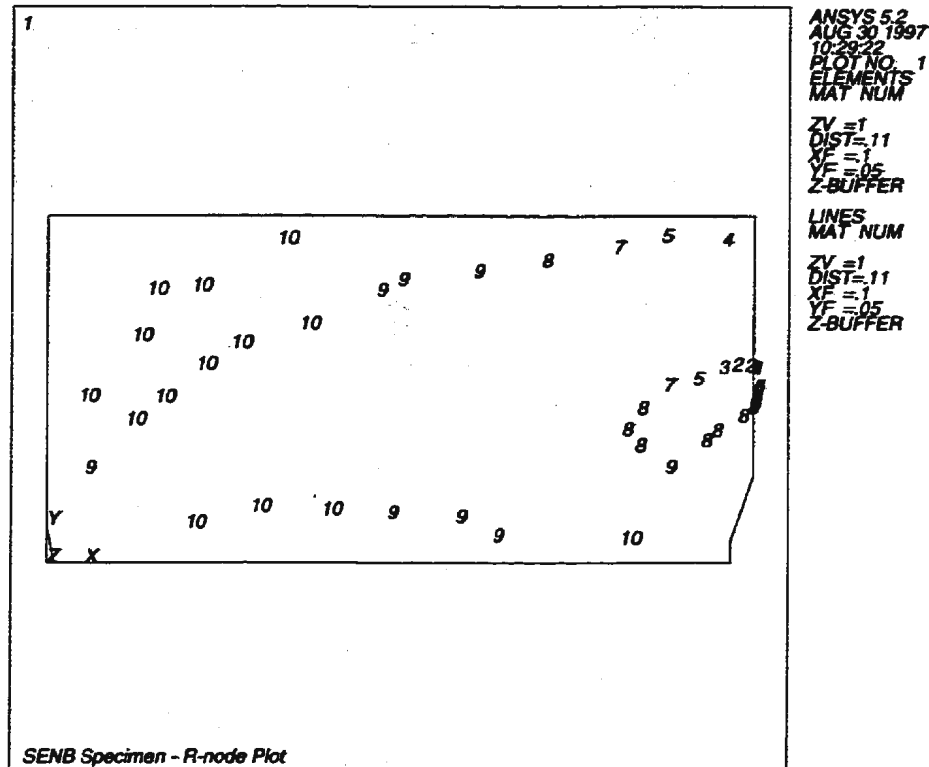


Figure 4.7 - SENB Specimen R-node Plot

is broken into ten contour divisions for this particular model, as well as the others discussed here. The number of contour divisions may be increased or decreased as desired. The r-node contours shown in Figure 4.6 clearly indicate the presence of one significant r-node peak for this model. The peak is located along the uncracked ligament near the crack tip and is indicated by the contour value of one as shown in the plot. All the r-nodes surrounding these have contour values less than one indicating a decreasing

contour. A second peak may be considered at the top of the figure where there is a cluster of r-nodes with the contour value of six with all surrounding r-nodes having lesser values. However, based on the rules outlined by Seshadri, this is identified as a virtual peak as it is not distinct and is located away from a critical region of the structure. The real peak is consistent with the r-node peak identified in Figure 4.2, based on the stress distribution plot along the ligament. The equivalent stress value at the peak location for the CT model is 103 MPa which corresponds to a limit load value of 12 341 N.

The r-node plot for the SENB specimen is shown in Figure 4.7. This plot is similar to that of the CT specimen in that there is only one clear r-node peak present. This differs significantly from the result obtained from the equivalent stress plot along the uncracked ligament, shown in Figure 4.3. Based on the results of Figure 4.3, two r-node peaks were identified, whereas the full r-node plot of the structure indicates only one relevant peak. It is difficult to see the contour numbers near the crack tip in the r-node plot above due to the fine mesh in this area and a significant number of r-nodes. The contour numbers overlap in this region. However, this is indeed the location of the r-node peak which occurs near the crack tip, as was the case with the CT specimen described previously. The peak r-node equivalent stress value for this geometry is 35 MPa which corresponds to a limit load value for the SENB specimen of 8 336 N.

The method in which r-nodes are determined by the improved r-node visualization scheme is dependent on element size. Element centroidal equivalent stress values, which

are computed based on the nodal stress values for a particular element, are used in this method. If the element size is relatively large, a significant difference in nodal stress values could occur over the extent of the element. This is particularly true for smaller regions in a structure having stress concentrations or other localized behaviour. As a

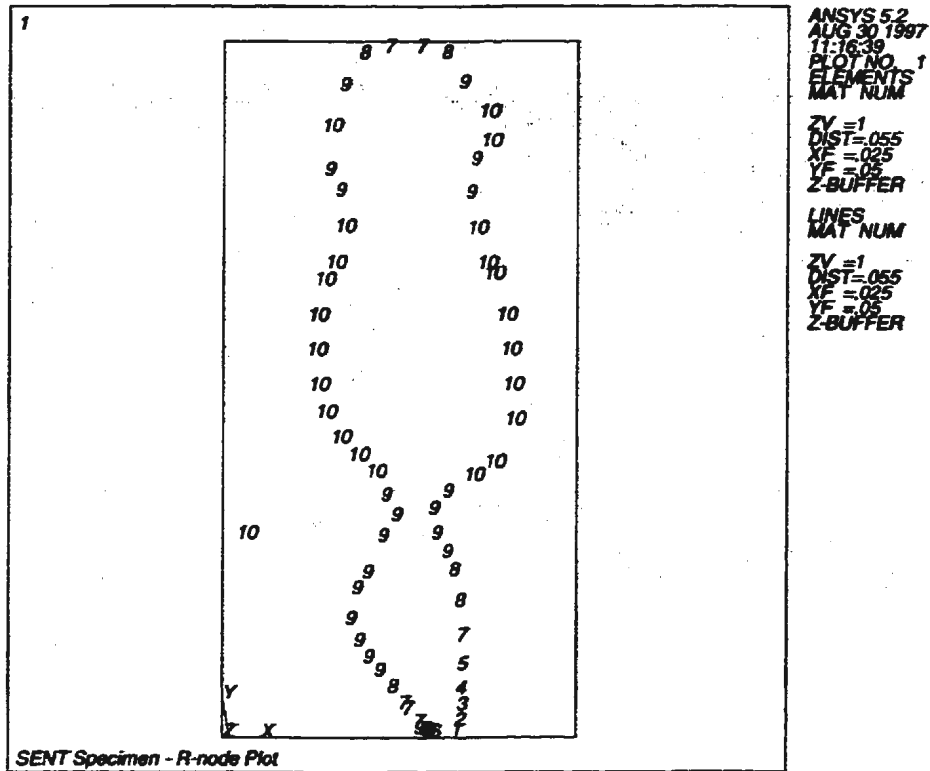


Figure 4.8 - SENT Specimen R-node Plot

result, the important activity in a localized region may be shadowed by the limitations imposed by using only the centroidal stress value for a large element. This is likely the case for the SENB specimen for which the improved identification scheme does not identify the second r-node as did the plot of the stress distributions across the uncracked ligament (Figure 4.3). The stress plot along a particular path obtained from the ANSYS

software averages stress values across the elements and will always give fifty data points between every pair of nodes used in the path definition. Depending on the mesh density along the path (element size), several data points are interpolated across an element, based on the nodal values, leading to a more accurate distribution of stress across an element. Using element centroidal stress values does not give a clear representation of how stress values are changing across the element. Therefore, there may be inaccuracies in identifying all the r-nodes when using the improved r-node visualization scheme. This inaccuracy is clearly seen in the SENB model. The improved scheme gives a clear representation of what occurs in the entire structure, as opposed to one particular region. In addition, the improved scheme eliminates the need to identify an appropriate path along which to plot the stress distribution. Although this is not a problem for the examples given, it would create a significant problem for more complex geometries. In any case, if there is some doubt as to the identification of legitimate r-node peaks always choose the highest equivalent stress value in determining the limit load in order to ensure a conservative estimate.

The results of the r-node plot for the SENT specimen (Figure 4.8) are similar to those of the CT specimen. One relevant r-node peak is identified and corresponds quite well to the stress plot along the ligament shown in Figure 4.4. Again, the r-node peak is located in the vicinity of the crack tip. A lesser peak appears to exist at the top of the model. However, this is due to the manner in which the load is applied along the upper surface. Applying the rules for r-node peak identification given by Seshadri, the second peak

would be considered a virtual peak and would not be used when determining the limit load. The r-node peak stress value for the SENT specimen is 29 MPa which corresponds to a limit load value of 8 477 N.

4.6 Limit Load Results Using The m_e -method

The m_e - method for determining limit loads was applied to the three standard specimens. The results from this approach provide for both upper and lower bound values of the actual limit load. The lower bound estimate is the one of primary concern for failure analysis. However, the upper bound result has practical applications in the areas of metal forming and cutting. A detailed explanation of the theoretical foundation for this method is found in Chapter 3. A practical guide for obtaining m_e results is given below, in a step by step approach.

- 1.) Create model geometry and perform the first linear elastic analysis.
- 2.) Adjust the elastic moduli of the elements and perform the second linear elastic analysis. The moduli are modified as per equation (3.30), with any arbitrary stress value used for σ_{arb} .
- 3.) Obtain the equivalent stress and volume from the first analysis for each element in the model and perform the calculation: $\sigma_{e1}^2 \Delta V_1$; $\sigma_{e2}^2 \Delta V_2$; ... $\sigma_{en}^2 \Delta V_n$ for all n elements.
- 4.) Arrange the data in descending order, based on the results of the calculation performed in step 3.

5.) Sort the stress and volume listing from the second analysis, corresponding to the ordered listing of the first analysis. Next, perform the calculation described in step 3 using the results obtained from the second analysis. The final data listing should contain a list of matching element numbers with corresponding elemental equivalent stress values, element volumes and step 3 calculation results for each analysis as shown below:

First Linear Elastic Analysis				Second Linear Analysis			
Elem No.	Stress	Volume	$\sigma^2\Delta V$	Elem No.	Stress	Volume	$\sigma^2\Delta V$
89	1.2e+06	1.2e-03	1440	89	1.1e+06	1.2e-03	1320
5	1.0e+06	1.4e-03	1400	5	9.2e+05	1.4e-03	1288
67	9.7e+05	9.0e-04	873	67	9.9e+04	9.0e-04	89.1
⋮	⋮	⋮	⋮	⋮	⋮	⋮	⋮

6.) Based on the element order established in the previous step calculate the energy dissipation summation as follows:

First Linear Elastic Analysis		Second Linear Elastic Analysis	
Element	Dissipation	Element	Dissipation
89	$\sigma_{e89}^2\Delta V_{89}$	89	$\sigma_{e89}^2\Delta V_{89}$
5	$\sigma_{e89}^2\Delta V_{89} + \sigma_{e5}^2\Delta V_5$	5	$\sigma_{e89}^2\Delta V_{89} + \sigma_{e5}^2\Delta V_5$
67	$\sigma_{e89}^2\Delta V_{89} + \sigma_{e5}^2\Delta V_5 + \sigma_{e67}^2\Delta V_{67}$	67	$\sigma_{e89}^2\Delta V_{89} + \sigma_{e5}^2\Delta V_5 + \sigma_{e67}^2\Delta V_{67}$
⋮	⋮	⋮	⋮

7.) To satisfy the theorem of nesting surfaces, the condition $m_1^o \geq m_2^o \geq \dots \geq m_n^o$ must be met. Here, m_i^o is based on the summation of the first linear finite element

analysis and m_2^o is based on the summation of the second linear finite element analysis (refer to sections 3.2.3 and 3.2.4 for further explanation). Therefore, based on the energy dissipation summation (step 6), the reference volume may be determined by identifying the point at which the summation for the first analysis becomes less than that of the second analysis. The upper bound multiplier, based on the reference volume, is then calculated using equation (3.25).

8.) Finally, the improved lower bound multiplier, m_{σ} , may be calculated using equations (3.35) and (3.36).

When following this procedure to determine limit loads, three important checks are necessary to ensure a valid limit load estimate. These are:

- i.) Following modulus modification, the maximum equivalent stress value for both the first and second analysis should occur in the same element. For the case of cracked components with requirements for modeling the crack tip singularity, this check may be relaxed if the maximum stress occurs in different elements. However, this may only be considered if the elements in question are in close proximity to one another in the model.
- ii.) The maximum equivalent stress for the first analysis must be greater than that of the second analysis. If this is not true then $m_1^o \leq m_2^o$ and the theorem of nesting surfaces will be violated.
- iii.) To ensure real roots, the discriminant for the quadratic equation (3.35) must be greater than zero (i.e. the value for m_{σ} must not be imaginary).

If any of the three checks are negative, the analysis must be repeated with a slightly different modulus adjustment. For the three fracture specimens discussed, at least three different modulus adjustment values were used in each case to ensure a valid pair of results with which to calculate a limit load. It is important to note that while only two linear analysis are required to calculate the m_a multiplier, more than one modulus adjustment may be required to obtain a valid distribution to satisfy the three checks given above. The macros required to perform the modulus modification, as well as the m_a calculation, are included in Appendix A.

The limit load results obtained for the three fracture specimens using the m_a method are as follows: CT specimen, $P_L = 13\,910\text{ N}$, SENB specimen, $P_L = 8\,591\text{ N}$ and SENT specimen, $P_L = 9\,085\text{ N}$. The following section discusses and compares the robust limit load estimates with those of the nonlinear finite element analysis and the analytical limit load equations given previously.

4.7 Summary and Discussion of Results

Robust limit load estimations for the three standard fracture specimens were given in the two preceding sections. These results are now compared to results obtained through nonlinear finite element analysis as well as to results obtained from analytical limit load solutions available for these geometries. Table 4.1 lists all limit load results for the three specimens. A percentage error calculation for each robust limit load estimate based on

the nonlinear finite element analysis result is also given in Table 4.1. The error calculation is based on the nonlinear FEA solution to provide a consistent basis of comparison with components for which analytical solutions are unavailable.

Table 4.2 - Limit Load Estimation Results

Specimen	Gloss R-Node		m_z -method		Nonlinear FEA	Analytical
	P_L	% Error	P_L	% Error		
CT	12182 N 12341 N	19.7%	13910 N	8.3%	15170 N	14801 N
SENB	8508 N 8336 N	19.1%	8591 N	18.4%	10523 N	9817 N
SENT	8589 N 8477 N	14.5%	9085 N	9.6%	10049 N	9512 N

Note: The lower value in the Gloss R-node columns is the result obtained using the improved r-node identification scheme.

For the most part, the robust estimates compare quite well to the nonlinear FEA and analytical solutions. Both robust techniques provided reasonably good results for the CT and SENB specimens. Calculation of a limit load for the SENT specimen using the m_z -method posed problems when using a modulus modification index, $q = 1$. This can be attributed to the extreme depth of the crack used in this model. The crack depth in this case is 60% of the total specimen width, leaving a small ligament to support the applied load. The stress redistribution in this area is extensive and provides quite a wide range of stress values in a limited reference volume for this specimen. As a result, one of the three criterion required for a satisfactory solution was violated. The modulus modification index was reduced to a value of 0.5 which provided the necessary conditions to obtain a

satisfactory solution. In cases involving very deep cracks, the modulus adjustment index for the m_s approach should be taken as 0.5 and reduced as necessary.

CHAPTER 5

ANALYSIS OF AXIAL PIPE DEFECTS

The following chapter extends the use of robust finite element analysis to the practical problem of axial pipe defects typical of stress corrosion cracking (SCC). The analysis of these geometries is simplified to that of loading by internal pressure only in order to gauge the effectiveness of the robust techniques in limit load determination. The analysis includes single defects of varying depths as well as multiple defect geometries typical of crack colonies prevalent in SCC cases. Furthermore, all cracks are assumed to be infinitely long with uniform depth.

5.1 Finite Element Modelling Considerations

The pipe models used in the analysis are based on typical, Class 1 grade, natural gas transmission pipelines. Class 1 lines are those that are laid in regions with little or no

human population as outlined in existing industry standards. The finite element models developed here are based on a 914 mm O.D. linepipe having a wall thickness of 10 mm. The maximum allowable operating pressure for this particular linepipe is in the vicinity of 7 MPa (Transportation, 1992). These parameters are typical of the common American Petroleum Institute (API) pipe grade, X-65.

The finite element modeling is performed with the ANSYS Version 5.2 software package developed by Swanson Analysis Systems. ANSYS is used for both the linear and non-linear analyses. The pipe is modeled in two dimensions with defects running in the axial direction. Both the pipe and the defect are assumed to be infinitely long with internal pressure loading only. Therefore, the pipe is modeled using PLANE2 elements with the plane strain option, the details of which are given in Chapter 4. The crack tip singularity is simulated by moving the midside nodes of the triangular PLANE2 elements to the quarter point (Barsoum, 1976). Material behaviour in the non-linear case is assumed to be elastic, perfectly-plastic. The analysis is based on the incremental theory of plasticity for which the total load is applied in gradual increments. Newton-Raphson iterations are performed for each substep in order to obtain a converged solution.

5.2 Single Axial Defects

In this study, a 914 mm O.D. pipe model having a single axial defect is considered. The analysis is performed for various crack depths in the radial direction, with all defects

being continuous and breaking on the external surface of the pipe. Three different crack geometries are considered (i.e. single axial defects having depths of 2, 3 and 4 mm). The finite element model for each geometry is generated using the ANSYS software, with only the symmetric half of the component being considered. Six-noded isoparametric elements are used for the bulk of the mesh, with the singularity at the crack tip being modeled using nine crack tip elements. The radius of the first array of crack tip elements is 0.5 mm, with the ratio of the second row of elements to the first row being one. Material properties used for modelling purposes include an elastic modulus of 211 GPa and a yield stress of 488.43 MPa.

The limit loads for each of the three models is evaluated using the Gloss r-node and m_x robust methods, as well as traditional non-linear finite element analysis. The non-linear analysis is used as a benchmark for comparison with the robust estimates. The loading for all robust analysis runs is uniform internal pressure of magnitude, $P = 2$ MPa.

5.2.1 Gloss r-node limit load estimates

The r-node stress for each model is obtained by plotting the stress distributions of the first and second linear elastic analyses along the uncracked ligament and determining the points of intersection, as detailed in Chapter 4. The through thickness stress distribution for a defect-free pipe is compared with that of a pipe containing an external axial defect in Figure 5.1. The defect-free distribution shows the maximum stress developing at the

inside surface of the pipe and decreasing towards the outside surface. When an external defect is introduced, the distribution changes considerably. The maximum stress now occurs at the crack tip, where there is a singularity in the resulting stress field. The presence of a stress field singularity in combination with a thin pipe wall thickness introduces a number of problems when determining effective r-node stress values for these models.

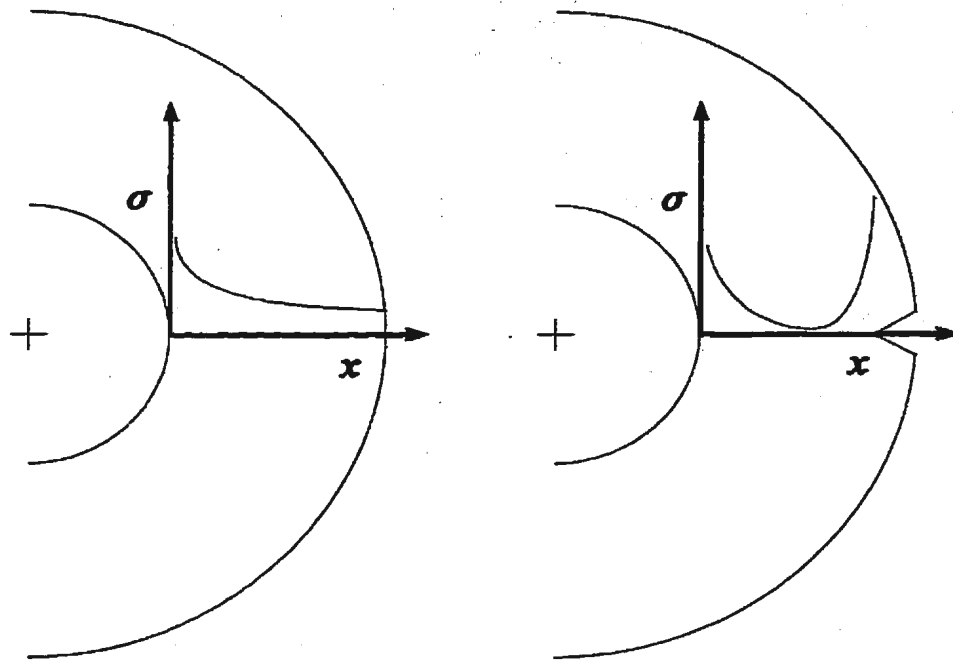


Figure 5.1 - Typical stress distributions for uncracked and cracked pipe.

Figure 5.1 indicates a U-shaped stress distribution for the defective pipe and a corresponding peak stress at the crack tip. The singularity caused by the presence of the defect results in a wider range of stress values over the remaining ligament and, as a result, stress redistribution over this region is more extensive. For the pipe models here,

the uncracked ligament is relatively small and the redistribution of stress must occur over a very small region. A typical modulus modification creates a relatively large change in the resulting stress field. This change is too drastic for structures which have small regions in which stress redistribution can occur. As a result, several iterations are required to achieve a proper stress redistribution. Thus, it is necessary to manipulate the modulus modification scheme used for the Gloss r-node technique such that the redistribution of stress may occur properly in the limited region available. This is accomplished by introducing a modulus-softening index, q , to equation (3.5) to give the following modulus modification equation,

$$E_s = \left[\frac{(\sigma_e)_f}{(\sigma_e)} \right]^q E_0 \quad (5.1)$$

The modulus-softening index serves the same purpose in the Gloss r-node scheme as it does in the m_e scheme. It moderates the change in the resulting stress field brought about by the elemental moduli modification, so redistribution can properly occur within the space available. To achieve this, the value of q is reduced from one to a value of 0.25, or lower, as necessary.

The pipe models considered in this section are the three described earlier, having crack depths of 2, 3 and 4 mm. In each case, the modulus-softening index, q , was reduced to a value of 0.10 to give reasonable results for the Gloss r-node analysis. The stress distributions obtained from the first and second linear analyses for the pipe containing the

2 mm defect are presented in Figure 5.2. As shown, the two distributions appear to be almost coincident over the length of the ligament. This indicates that modification of the original stress distribution due to changes in the elemental moduli has been slight. This is

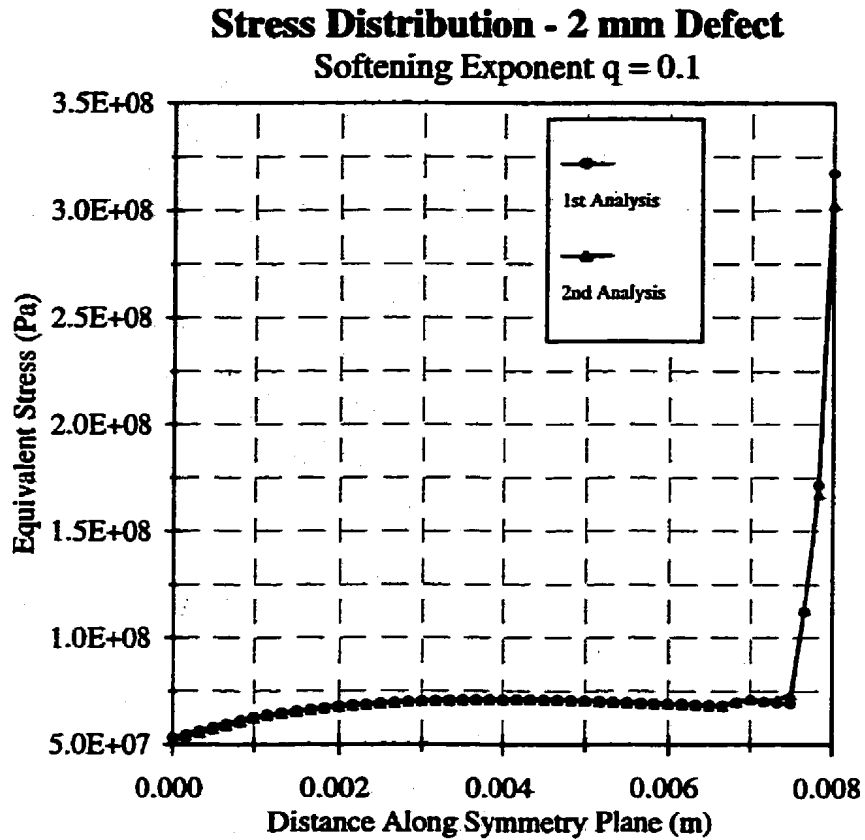


Figure 5.2 - Stress distributions along the uncracked ligament.

the behaviour intended by introducing a modulus-softening index, $q < 1$. As shown, Figure 5.2 is of little help in determining r-node locations or stress values. Therefore, the next step is to focus on the area of the plot where one would expect to find a clear intersection of the two distributions, which indicates the presence of an r-node. A point of interest in Figure 5.2 is the shape of the stress distribution curve. The expected U-shape is not evident in this particular model and in fact, the lowest equivalent stress

occurs at the inside wall of the pipe. This result is due to the very thin wall thickness and the presence of a stress singularity at the crack tip. The influence of the crack is extending along the entire ligament in such a way as to reduce the stress level at the inner surface of the pipe. In uncracked regions of the pipe, remote from the defect, the stress distribution is typical of an uncracked cylinder with maximum stress occurring at the inner surface and reducing to a minimum at the outer surface.

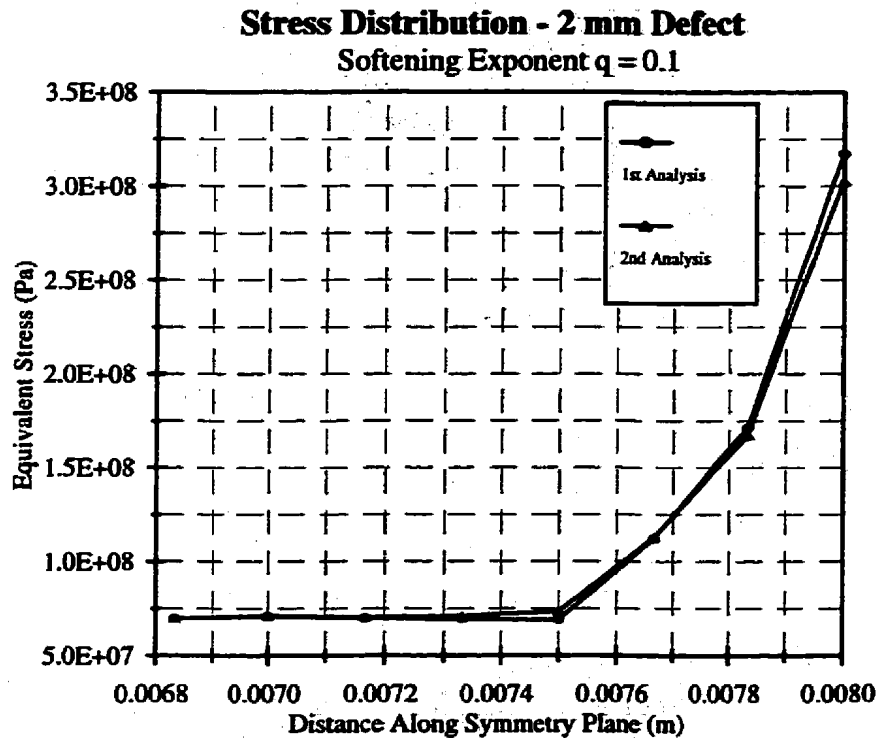


Figure 5.3 - Stress distributions near the crack tip (2 mm defect).

Intuitively, the origin of plasticity leading to plastic collapse of the structure will occur at or near the crack tip, where stress levels are highest. Therefore, a closer look at the stress distributions in this area is likely to reveal the location of an r-node. Figure 5.3 shows a plot of the stress distributions from the first and second linear analyses in the region of

the ligament adjacent to the crack tip. It is apparent from this figure that the slight perturbation in the stress field due to the modification of the elemental moduli has made very little change to the stress distribution along the uncracked ligament. However, the change is enough to identify an intersection of the two distributions at a distance of approximately 7.7 mm. The r-node stress corresponding to this intersection is approximately 120 MPa, which corresponds to a limit pressure of 8.14 MPa. There appears to be a region at the left side of Figure 5.3 where the two distributions are coincident, however, closer examination reveals this to be untrue. Although not visible in Figure 5.2, closer examination of the stress distributions over the entire ligament shows an intersection in the vicinity of the inner surface of the pipe (left side of plot). This point of intersection corresponds to an effective r-node stress of approximately 65 MPa. If this r-node is considered together with the r-node near the crack tip, the resulting limit load prediction would be approximately 10.56 MPa, which is greater than the nonlinear FEA result of 9.72 MPa. Considering the most probable origin of plasticity leading to collapse to be in the area adjacent to the crack, it is more reasonable, in this case, to consider only the r-node near the crack tip. In any case, choosing the larger value of r-node stress will always give the most conservative limit load estimate when using this method.

Figure 5.4 shows the stress distributions from the first and second linear elastic analyses for a similar pipe containing a 3 mm deep external axial defect. The stress plot, in this case, is shown for the portion of the ligament adjacent to the crack tip. The stress distribution plots for the entire uncracked ligament may be found in Appendix C. The

distributions in this case are very similar to that shown in Figure 5.3 for the 2 mm defect.

The modulus softening index, q , was set to 0.10 to moderate the redistribution effect on the stress field and is again evident in the stress plot. As expected, the intersection of the

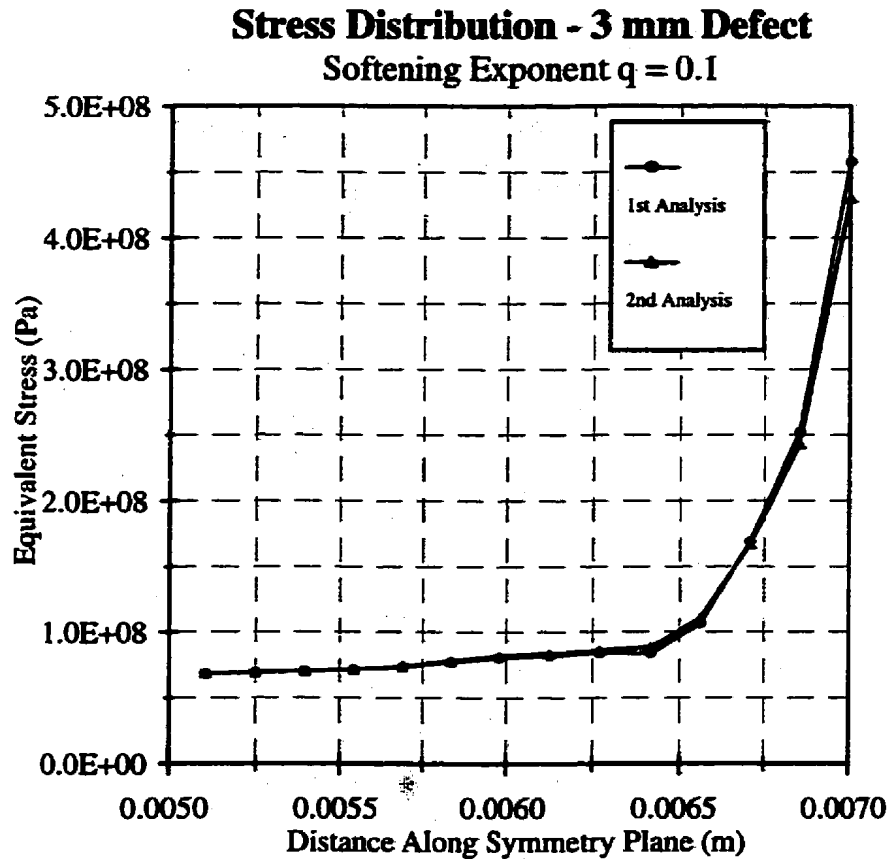


Figure 5.4 - Stress distributions near the crack tip (3 mm defect).

two plots occurs very near the crack tip and gives an r-node stress value of approximately 145 MPa. This gives a limit load value of 6.74 MPa for the structure, which compares well with the nonlinear FEA result of 8.06 MPa. The higher r-node stress value observed for the 3 mm defect (as compared to that observed for the 2 mm defect) is expected, as the limit load is inversely proportional to the r-node stress. As the depth of the defect

increases the load bearing capacity of the uncracked ligament decreases, leading to a decline in the limit load value.

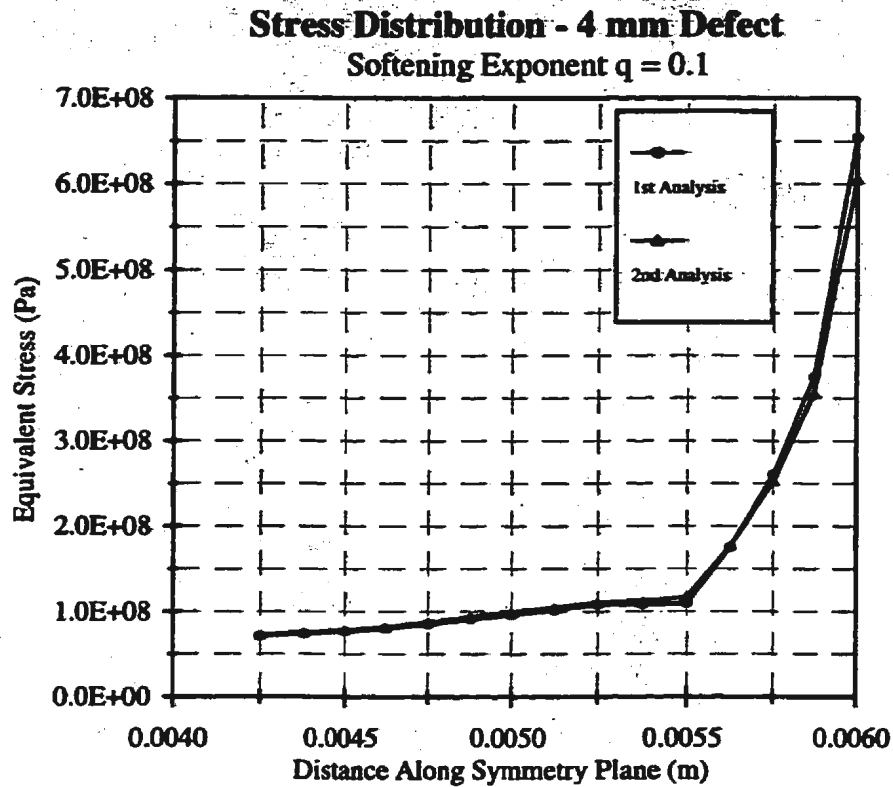


Figure 5.5 - Stress distributions near the crack tip (4 mm defect).

The last of the three models is that of a pipe containing a 4 mm defect. This defect is quite deep, as it penetrates 40% of the wall thickness. A defect of this particular depth would rarely be encountered in natural gas transmission pipelines, as it would be detected and mitigative action taken before growing to this depth. However, in assessing the ability of the robust methods to determine limit loads for cracked components, it is necessary to proceed beyond the range of defect sizes normally encountered. The stress distributions near the crack tip for this model are given in Figure 5.5. Once again, the plots look very similar to those of the previous two models. In this case, the intersection

occurs at a position of approximately 5.6 mm, relative to the inner pipe surface, which gives an r-node stress value of approximately 190 MPa. This corresponds to a limit load value of 5.14 MPa, which compares reasonably well with the nonlinear FEA result of $P_L = 6.31$ MPa.

5.2.2 m_q -Method limit load estimates

The results of the m_q -method limit load estimate for the three pipe models discussed previously are summarized in Table 5.1. The results for each of the three models are conservative estimates when compared to the nonlinear FEA results. The results for the 2 and 3 mm defects are obtained using a modulus modification index of $q = 1$. Initial attempts to use the m_q -method for the model containing a 4 mm deep defect failed to yield any useful results while using this value for q . As in the case of the Gloss r-node method, the change in the stress field due to modulus modification is too drastic for the small region in which stress redistribution can occur. This problem was also encountered in the SENT specimen discussed in Chapter 4. Reducing the modulus modification index to 0.5 gives a good limit load estimate for the deeper defect. The m_q limit load result for this crack geometry is given in Table 5.1.

5.3 Internal Axial Defects

The previous section considered examples of external axial defects and the characteristic stress distributions which result. This section will examine a single model of a pipe containing an internal axial defect to illustrate the versatility of the robust techniques in predicting limit loads for various crack geometries. The defect-free stress distribution for

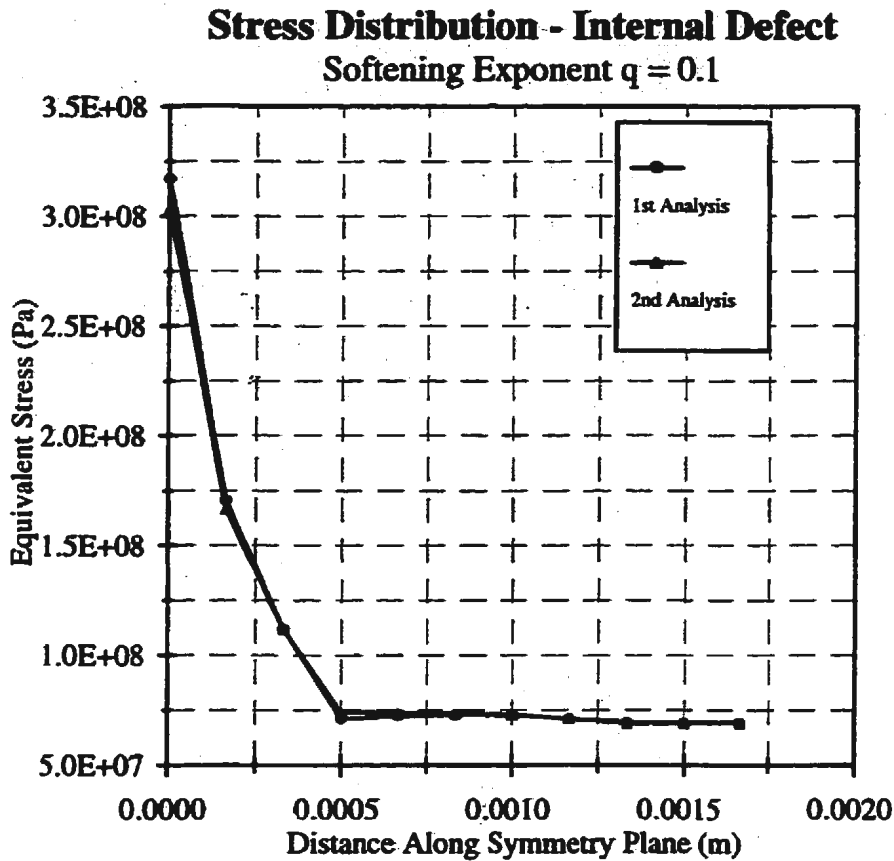


Figure 5.6 - Stress distributions near the crack tip (2 mm internal defect).

this case is similar to that shown in Figure 5.1 for the uncracked pipe. The highest stress will occur at the crack tip and reduce to a minimum at the outside surface of the pipe.

The peak stress will be significantly higher than that of the same model without a defect.

The pipe characteristics and properties are the same as those of the pipe models discussed previously with the only difference being the location of the defect. The internal pressure load is not applied to the crack face for this model and the crack is assumed to be infinitely long with a constant depth of 2 mm. The stress distributions along the uncracked ligament for the first and second linear analyses are given in Figure 5.6, for the region adjacent to the crack tip. The intersection of the first and second linear elastic stress distributions occurs at a location of approximately 0.75 mm from the crack tip and yields an r-node equivalent stress value of 110 MPa. This corresponds to a limit load estimate of 8.88 MPa, which compares quite well to the nonlinear FEA result of 9.81 MPa. The m_e -method yields a limit load estimate of 8.11 MPa, which is also quite satisfactory as a conservative estimate of the collapse load.

5.4 Thick Walled Pipes Containing Defects

The use of the Gloss r-node and m_e -methods of robust limit load estimation for predicting collapse loads of defect-free thick walled cylinders is well documented (Seshadri, 1996). The following example is that of a thick walled pipe containing a shallow external axial defect. The material properties for the pipe are the same as those discussed previously and outlined in section 5.2. The pipe dimensions for the thick walled model include an outer radius of 0.457 m, an internal radius of 0.357 m, a wall thickness of 100 mm and a crack depth of 2 mm. As with the other external defects discussed, the crack is assumed to be infinitely long with a constant depth.

Figure 5.7 shows the stress distributions along the entire remaining ligament for the thick walled pipe model. The distributions shown here are similar to those depicted in Figure

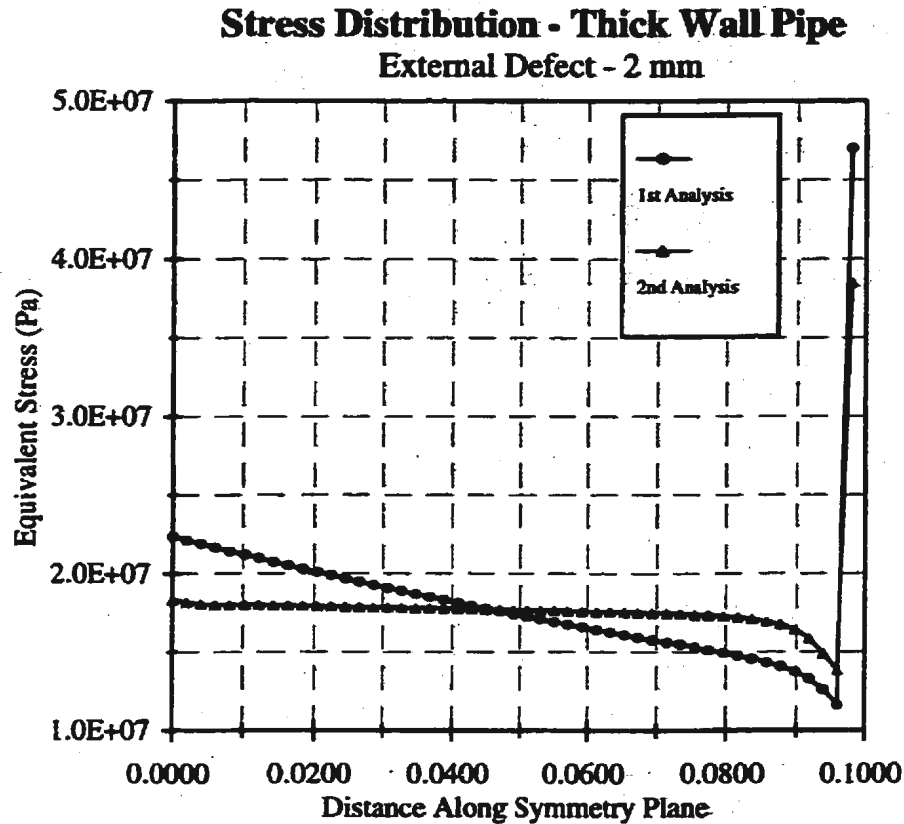


Figure 5.7 - Stress distributions along uncracked ligament (thick wall pipe).

5.1 for a pipe with an external axial defect. The distributions show a high stress level at the inside surface with a decreasing stress level towards the outer surface. A peak in the stress distribution occurs near the crack tip to give the U-shaped distribution expected.

This was not seen for the thin wall structures discussed earlier. The softening exponent used in the modulus modification equation for this model was taken as unity. The thick walled pipe model does not exhibit the sensitivity typical of the thin walled structures.

The cross section for this model is sufficiently large to handle the stress redistribution that

occurs with a standard modification of the elemental moduli. The plot shows a clear and distinct intersection of the two distributions at a location of approximately 45 mm from the inner surface of the pipe. This intersection is quite remote from the crack tip where an r-node location would be expected. However, closer inspection of the region near the crack tip does indeed indicate the presence of an intersection. A comparison of the two r-nodes gives a value of approximately 17.7 MPa for the r-node located remote from the crack tip and a value of approximately 18.5 MPa for the r-node located near the crack tip. Given the closeness of the two values, it would appear that the crack has little influence on the r-node stress. Taking the higher of the two r-node stresses we arrive at a limit load value for the pipe of 132.00 MPa. The m_{α} -method limit load result for the pipe is 124.01 MPa. Both robust limit load estimates compare very well to the nonlinear FEA result of 136.09 MPa.

5.5 Multiple External Defects

Stress corrosion cracks typically appear in colonies with several parallel defects in close proximity constituting a crack colony. In this section, two cases of pipes with multiple defects are examined. In each case, the pipe contains three parallel defects with two of the three having the same depth and the third having a slightly different depth. Figure 5.8 illustrates the orientation and location of the defects as used in the finite element models. The cracks project radially into the pipe material, from the outer surface, and are separated by a one degree spacing. Each of the models maintains the physical dimensions

of the single defect models discussed in section 5.3, which include an outer radius of 0.457 m, an inner radius of 0.447 m and a wall thickness of 10 mm. All material properties remain as before.

The first model considered is shown in Figure 5.9 and consists of three parallel defects of depths 2 mm, 3 mm and 2 mm. The three cracks are labeled A through C, with the

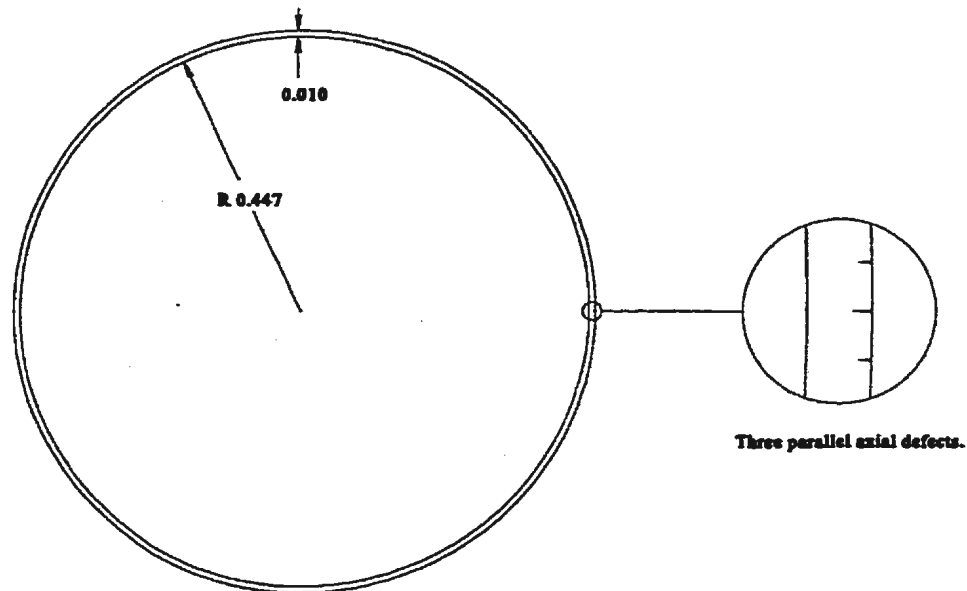


Figure 5.8 - 914 mm O.D. linepipe with multiple defects

top crack being A as shown. The crack spacings used in the models are quite wide compared to actual crack colony spacings. The larger crack spacing was chosen to simplify model creation and reduce the number of elements required. As shown, the crack geometries are symmetrical, allowing for half models to be used to advantage. However, if the cracks are such that each has a different depth, or spacings are not regular, then a full model must be used to obtain accurate results. The geometry shown

was modeled using a full pipe model and required approximately 3500 elements. The more complex the crack geometry, the more elements required for accurate modelling. This becomes an important issue with regards to processing time for nonlinear vs linear analysis.

The second multiple defect model has the same crack locations as those shown in Figure 5.9, but has different crack depths. The crack depths are 3 mm for Crack A, 1 mm for Crack B and 3 mm for Crack C. A half model is used for this case to avail of symmetry conditions.

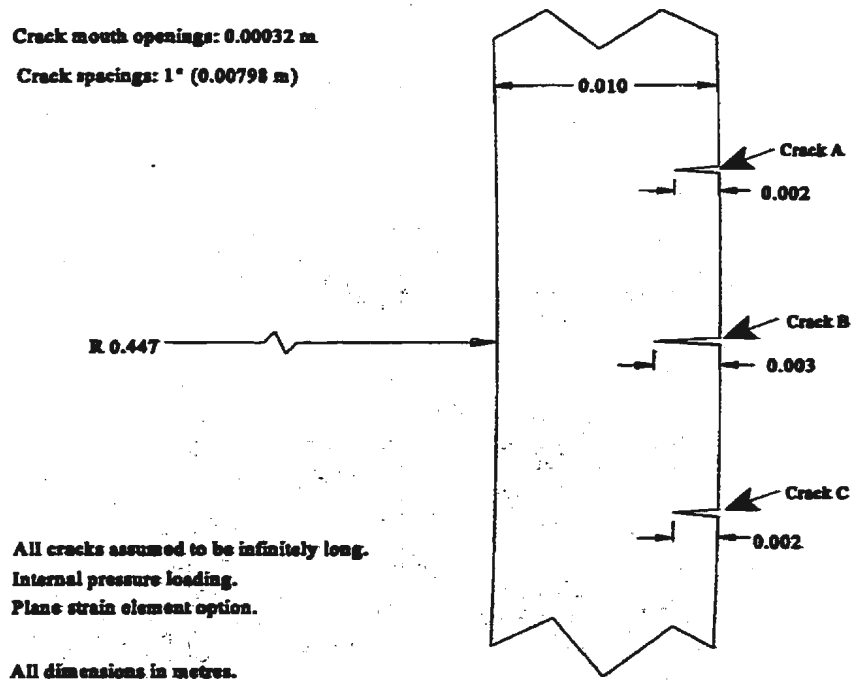


Figure 5.9 - Detailed crack geometry - 914 mm O.D. linepipe

5.5.1 Robust limit load estimates

Models containing multiple defects require plotting stress distributions for the first and second linear elastic analyses along the remaining ligament, for each defect present. As there will be one or more r-nodes identified for each defect, the question arises as to which r-nodes will be considered in calculating the limit load. The most conservative approach is to identify all the r-nodes and use the highest r-node stress value in the limit

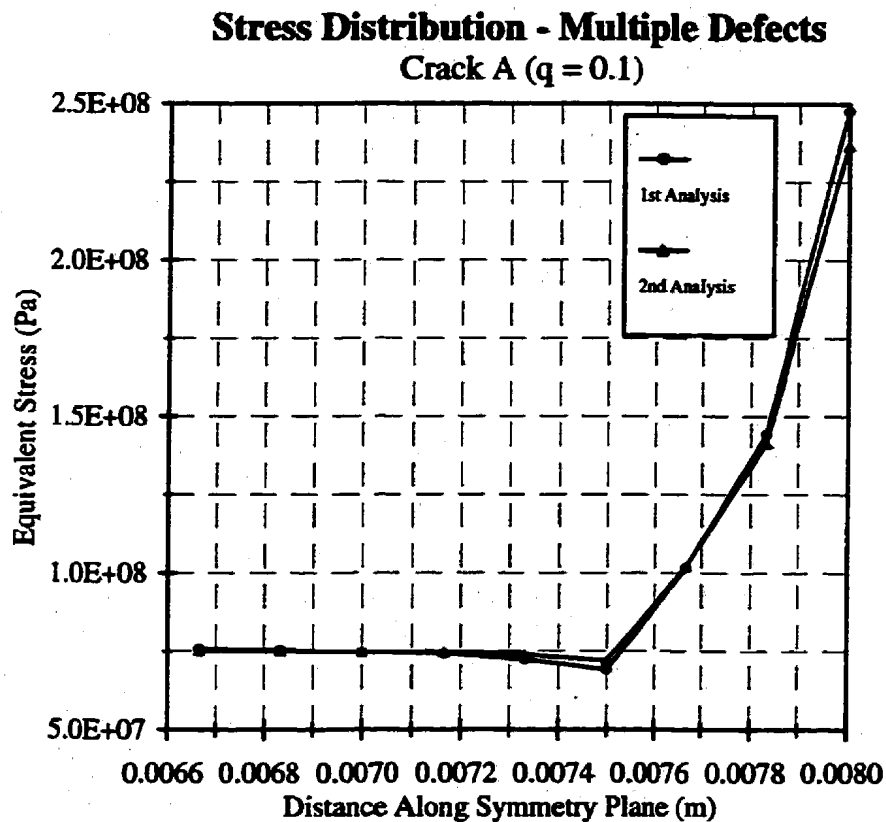


Figure 5.10 - Stress distributions near the crack tip (Model 1, Crack A).

load calculation. This is the approach taken in the analysis of the multiple defects discussed here. This approach may provide limit load estimates that are well below the

actual limit load. However, the problem of crack interaction and coalescence is one that is not well understood. As a result, taking the most conservative means in determining the limit load may well be the most prudent action.

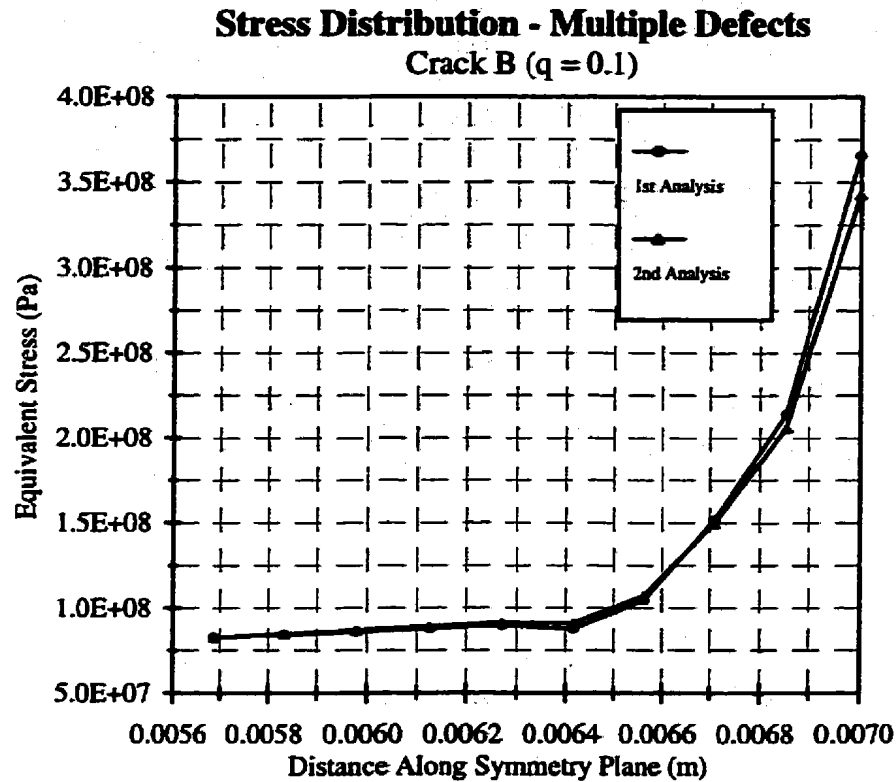


Figure 5.11 - Stress distributions near the crack tip (Model 1, Crack B).

Figures 5.10, 5.11 and 5.12 show the stress distributions near the crack tip for Cracks A, B and C, respectively, for the multiple crack model illustrated in Figure 5.9. The plots for Cracks A and C are, for the most part, identical which supports the idea that a half model may be used to model symmetric crack colonies. The stress distributions for Crack A show an intersection at a location of approximately 7.7 mm from the inner surface of the pipe. This gives an r-node equivalent stress in the order of 110 MPa. The distributions for Crack C gives the same result. Crack B is slightly deeper than A or C and the

corresponding stress distributions (Figure 5.11) show the same shape as the other two, but produce a higher r-node stress. The higher stress value is expected here as the spread of plasticity is anticipated to occur at the location of the deepest crack and highest stress concentration. The intersection of the stress distributions for Crack B occurs at a location

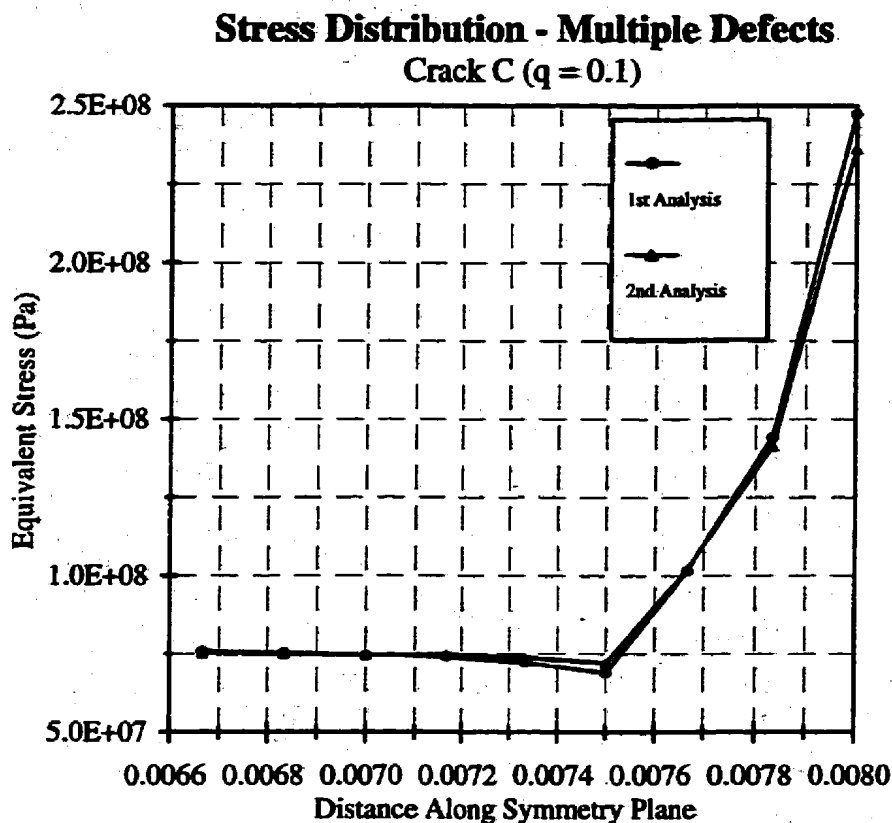


Figure 5.12 - Stress distributions near the crack tip (Model 1, Crack C).

of 6.65 mm from the inner surface of the pipe and gives an r-node stress of 140 MPa. Calculation of the corresponding limit load is based on the highest r-node equivalent stress, which occurs near the tip of Crack B. The resulting limit load for this model is 6.98 MPa.

The m_x -method is also applied to the multiple crack problem and gives a limit load estimate that is close to that of the Gloss r-node result. The limit load calculated for the m_x -method is 6.54 MPa, which compares quite well to the nonlinear FEA result of 8.26 MPa.

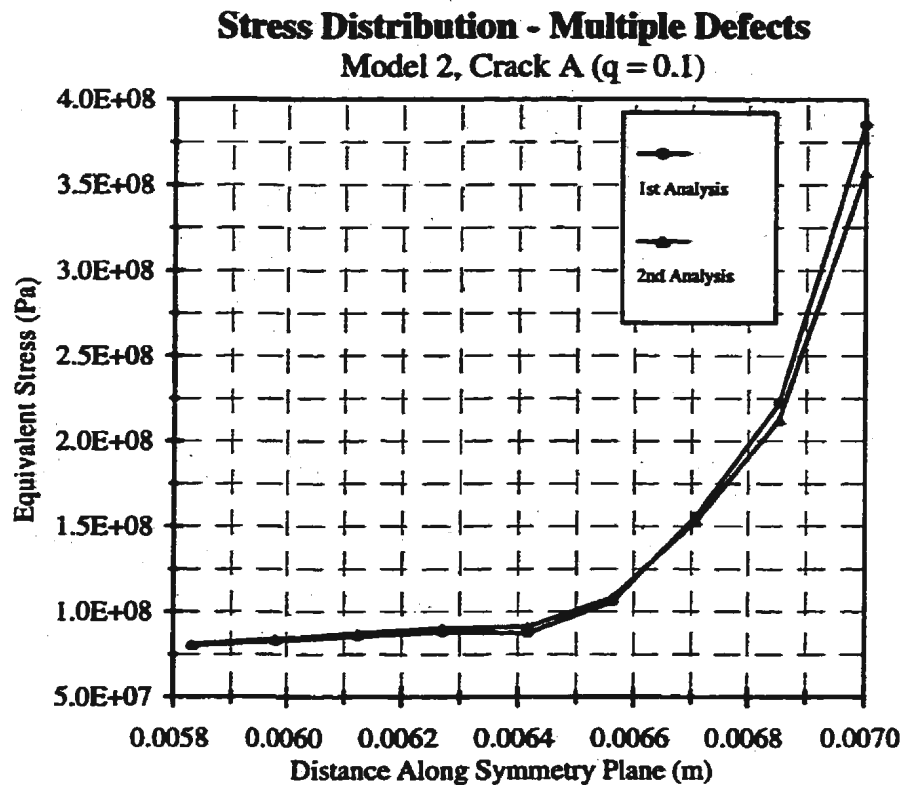


Figure 5.13 - Stress distributions near the crack tip (Model 2, Crack A).

A second model containing multiple defects is also considered in this section. The crack geometry is changed such that a shallow central defect (1 mm deep) is flanked on either side by two deeper defects (3 mm deep). The crack spacing and other parameters are unchanged. The geometry is symmetrical, therefore, a half model is used to simplify the analysis. The half model approach requires the plotting of stress distributions for Cracks

A and B only, as the distributions for Crack C will be the same as those of Crack A. This was seen earlier in the full model analysis of the first multiple defect problem. Figures 5.13 and 5.14 show the stress distributions near the crack tips for the second model. The shape of the distributions are quite similar to those obtained for the first multiple defect

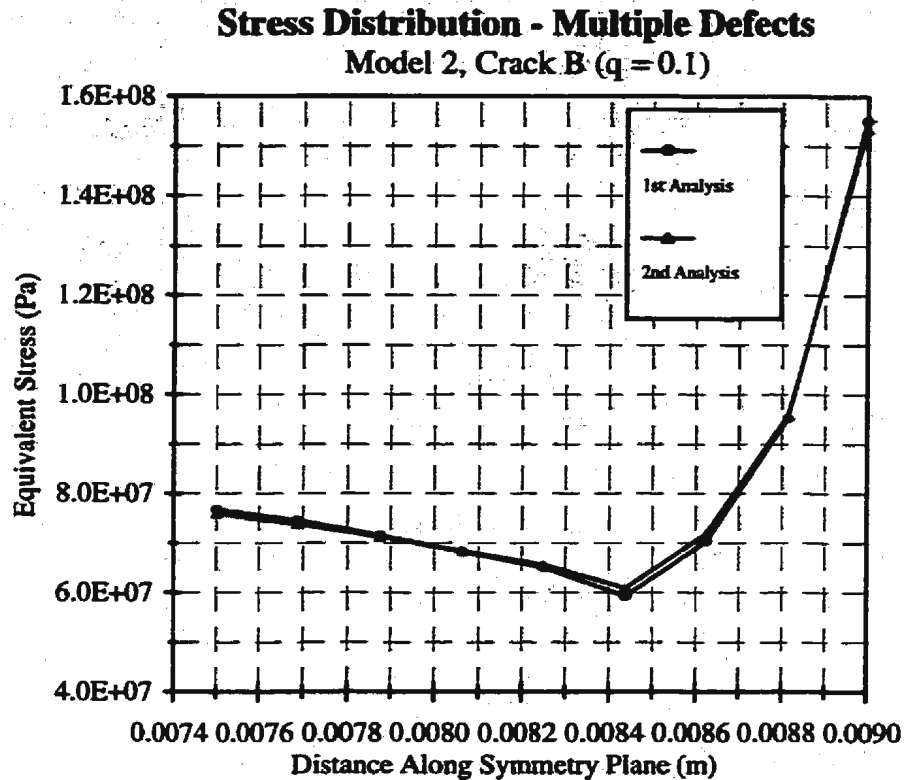


Figure 5.14 - Stress distributions near the crack tip (Model 2, Crack B).

model. The intersection of the two distributions for Crack A occurs at a location of approximately 6.62 mm from the inner surface of the pipe. The r-node stress for this intersection is approximately 130 MPa. The central crack in this model is much shallower. Therefore, a lower r-node stress is expected. This is indeed the case, as shown in Figure 5.14. The intersection of the first and second linear elastic distributions for Crack B occurs at a location of 8.83 mm from the inner surface of the pipe. The r-

node stress for this intersection is approximately 100 MPa. This value is less than that of Crack A. Therefore, the stress value to be used in the limit load calculation is that of the deeper crack. The limit load corresponding to this r-node stress value is 7.51 MPa. The nonlinear FEA result for the second model is 8.15 MPa. The Gloss r-node estimation compares very well for this particular geometry. The m_{α} -method gives 6.52 MPa for the limit load, which is also a reasonable lower bound estimate.

5.6 Discussion of Results

Several different pipe problems were presented in the preceding sections of this chapter, each of which involves one or more axial defects. Robust limit load analysis was conducted for each and compared to a nonlinear FEA result. The findings for each model are compiled in Table 5.1, along with error calculations based on the nonlinear finite element analysis results. In general, the robust estimation techniques provide good estimates of collapse loads when compared to nonlinear finite element analysis results.

Plots of the stress distributions for the first and second linear elastic analyses along the remaining ligament were obtained for each model. The intersection of the two distributions indicated the location and stress level of redistribution nodes from which limit loads were calculated. The plots shown are for the regions adjacent to the crack tip, where the major r-node is expected. In most cases, the stress distribution along the entire ligament reveals other intersections in areas remote from the crack tip region (stress

distributions along the entire ligament are found in Appendix C). The stress values for these intersections are usually much lower than those near the crack tip. In Chapter 4, it was explained that it is possible to have multiple valid r-nodes present. This typically occurs under pure bending conditions. If the r-nodes are valid and stress values are similar, averaging of all r-node stresses and using the resulting stress value in calculating the collapse load is recommended. If there is doubt as to the validity of any r-nodes, or

Table 5.1 - Limit Load Results for Pipe Models

Pipe Model	Gloss R-node		m _r -method		Nonlinear FEA
	P _L	% Error	P _L	% Error	
Single External Axial Defect					
2 mm defect	8.14 MPa	16.3%	8.07 MPa	17.0%	9.72 MPa
3 mm defect	6.74 MPa	16.4%	6.70 MPa	16.9%	8.06 MPa
4 mm defect	5.14 MPa	18.5%	5.00 MPa	20.8%	6.31 MPa
Single Internal Axial Defect					
2 mm defect	8.88 MPa	9.5%	8.11 MPa	17.3%	9.81 MPa
Thick Wall Pipe - External Axial Defect					
2 mm defect	132.00 MPa	3.0%	124.01 MPa	8.9%	136.09 MPa
Multiple External Axial Defects					
Model 1	6.98 MPa	15.5%	6.54 MPa	20.8%	8.26 MPa
Model 2	7.51 MPa	7.9%	6.52 MPa	20.0%	8.15 MPa

there are complexities in the geometry and loading it is prudent to use the highest r-node equivalent stress value in the limit load calculation. In the majority of cases with multiple valid r-nodes, the averaged result will lead to a collapse load estimate which compare

very well to that determined by nonlinear FEA. The limit load results presented in Table 5.1 are obtained by using the maximum r-node stress value obtained for each model. This conservative approach is chosen in order to avoid overpredictions in collapse loads due to the inherent uncertainties in material behaviour and complexities in the geometry leading to numerical modelling approximations for cracked components. The uncertainties in material behaviour may be examined separately using reliability analysis, however, the other uncertainties must be considered. Although conservative, the results presented are acceptable estimates of the collapse load as compared to the nonlinear FEA values and provide much better estimates than methods such as the lower bound theorem which can be conservative by 50% or more. The manner in which collapse loads were obtained from a nonlinear analysis using the ANSYS software can lead to some uncertainty. The load is applied in increasingly large load increments until excessive displacements occur or predefined plasticity limits are reached which do not allow the solution of the problem. At this point, the previously applied load step is bisected and the solution process continues. The bisection process continues until the load increment reaches a sufficiently small value such that no further application of load can occur without excessive displacement or plastic strain. Uncertainty arises in the size of the load gap between which the problem can be solved and the onset of excessive displacement. This can be overcome by manually selecting the applied load increment and carefully controlling the load application following the onset of plasticity. This uncertainty, while not very large, may allow a robust estimation to fall either above or below the nonlinear FEA estimate, in which case, the robust estimate may be questioned. There is also uncertainty

introduced in the assumption of elastic-perfectly plastic material behaviour. Therefore, comparisons with nonlinear FEA estimates must be fully considered before discounting any robust estimate results. Although comparison with nonlinear FEA results is acceptable for illustrating the power of the techniques described, further work is required to obtain experimental or other reliable results that may be used for comparison purposes.

The m_α -method also provides reasonable collapse load estimations. For the most part, m_α results are slightly more conservative than those obtained by the Gloss r-node approach (refer to Table 5.1). This is the opposite of the results obtained in Chapter 4, however, this is explained by the limited size of the volume available for stress redistribution in the pipe models and the requirement of reducing the modulus adjustment index. It is important to note that most results obtained using the m_α -method require more than one iteration. The most common problem is a negative discriminant in the final calculation of the m_α multiplier, as discussed in Chapter 4. This difficulty is easily overcome by performing multiple iterations. This process is automated in the macro used to obtain the given results. For cases which require multiple iterations, acceptable results are normally obtained within three or four iterations. Although processing time is somewhat longer, results are obtained more quickly than with a nonlinear FEA analysis. As well, there is no additional effort required once the macro is in place. The advantage of the m_α -method is in its ability to give a quick result without having to plot and interpret stress distributions.

CHAPTER 6

CONCLUSIONS

6.1 Contributions of the Thesis

One of the most important contributions of the thesis is in providing a relatively simple and systematic procedure for applying the Gloss r-node and m_r robust techniques. The theory behind each method is, for the most part, complex, thus, creating difficulty in the actual application. The procedures outlined allow the methods to be applied without a thorough knowledge of the theory. However, the user must have some knowledge of the structure being analyzed and some appreciation for the magnitude of the final result. As in most analysis techniques, there are pitfalls and traps that have to be avoided in order to achieve a satisfactory result.

This thesis extends the use of the Gloss r-node and m_r -methods of robust limit load

analysis to cracked components or structures. The methods are first applied to standard fracture geometries and compared to nonlinear finite element analysis and analytical limit load solutions for these geometries. In each case, the robust techniques provided adequate and acceptable results that could readily be used in analysis or assessment type activities. This is especially true of the R5 and R6 Failure Assessment Procedures outlined by Nuclear Electric in the United Kingdom. These assessment procedures are widely accepted around the world for the analysis of cracked components. The assessment procedure is entirely dependent on reference stress and a length parameter, each of which requires calculation of the structures limit load. The R5 and R6 procedures list several limit load calculation schemes for various geometries. However, there are numerous cases where a standard limit load solution is unavailable. The availability of a robust limit load estimation tool will greatly aid in the assessment of complex crack geometries which may not otherwise be viable. Both the Gloss r-node and m_g -methods of robust analysis would be of great benefit to users of the R5 and R6 failure assessment procedures.

This thesis also introduces an improved r-node visualization method which shows r-nodes as contours, enabling the user to quickly identify peaks and provide a quick picture of the load controlled locations within the structure. Examples of this are illustrated in Chapter 4 for the standard specimens, while r-node plots for the more complex pipe geometries are provided in Appendix C.

Perhaps the most important contribution of this thesis is the effort that has gone into advancing the robust techniques to complex multiple crack geometries as demonstrated in Chapter 5. The results obtained for these problems are very encouraging and illustrate the extensive capabilities of the techniques. Limit load solutions for complex crack geometries are generally not available, while nonlinear finite element solutions are extremely time consuming and require extensive computing resources. The robust methods are quick, accurate and easily implemented. Although further work is required to fully gauge the capabilities and limitations of these techniques, the results obtained through this research clearly indicate the usefulness of these tools in the assessment of cracked components.

6.2 Future Efforts

There are several routes to be explored in the application of the Gloss r-node and m_x techniques to cracked components. The analysis of finite length cracks of variable depth (i.e. the semi-elliptical shaped defect) is most definitely an area in which the techniques may be applied. This, of course, will require the use of three dimensional models and careful plotting of stress distributions for a successful analysis. The ability to analyze multiple defects has been shown in this thesis for simplified cases. However, future research should be directed toward the analysis of a measurable crack colony, encountered in the field, for evaluation purposes. In addition, the problem of circumferential defects in piping and pressure vessels has become of interest to industry.

The application of robust analysis to these problems was not explored in this thesis, but is an obvious extension of this work.

Another area for future work is the determination of elastic-plastic fracture mechanics parameters using robust analysis. Preliminary efforts have been made to this end and should be continued. The nature of modern materials is such that analysis of cracked components requires the use of elastic-plastic fracture mechanics in lieu of linear elastic fracture mechanics. If robust analysis can provide an effective means of determining elastic-plastic fracture mechanics parameters, it would provide a great step forward in the field.

The use of robust analysis has been shown to be quite effective in determining limit load estimates for the problems considered in this thesis. However, as the previous discussion illustrates, there are many other potential applications for robust analysis.

REFERENCES

Transportation Safety Board (1992). Pipeline Commodity Occurrence Report, Report Nos. P92T005, P91H0041 and P91H0117.

Jones, D.A. (1992). *Principles and Prevention of Corrosion*, Maxwell Macmillan Canada, Toronto, Ontario, 568 p.

Calladine, C.R. (1969). *Engineering Plasticity*, Pergamon Press, New York, 1969, 318 p.

Inoue, N., Nakagawa, H., Nakayama, T., Shimono, M. and Tanaka, T. (1977). "Lower Bounds to the Collapse Load of a Thick Circular Cylinder Subjected to Internal Pressure and Shear," *Journal of Applied Mechanics*, pp. 766-768.

Krasovskii, A.Ya., Orynyak, I.V. and Torop, V.M. (1990). "Ductile Failure of Cylindrical Bodies with Axial Cracks Loaded by Internal Pressure," *Strength of Materials*, Vol. 22, pp. 172-177.

Orynyak, I.V. and Borodii, M.V. (1994). "A Ductile Model for a Pipe with an Axial Surface Crack," *Engineering Fracture Mechanics*, Vol. 49, no. 2, pp. 287-294.

Orynyak, I.V. (1993). "Calculating the Pressure of Ductile Failure of a Pipe with an Axial Through Crack," *Strength of Materials*, Vol. 25, pp. 266-274.

Orynyak, I.V., Torop, V.M. and Borodii, M.V. (1996). "Ductile Fracture of a Pipe with a Part-Through Slot," *International Journal of Pressure Vessels and Piping*, Vol. 65, pp.171-179.

Kiefner, J.F., Maxey, W.A., Eiber, R.J. and Duffy, A.R. (1973). "Failure Stress Levels of Flaws in Pressurized Cylinders," *Progress in Flaw Growth and Fracture Toughness Testing, ASTM STP 536*, American Society of Testing and Materials, pp. 461-481.

Lancaster, E.R. and Palmer, S.C. (1996). "Burst Pressures of Pipes Containing Defects," *Proceedings of the Institution of Mechanical Engineers, Part E, Journal of Process Mechanical Engineering*, Vol. 210, issue E1, pp. 19-27.

Jaske, C.E., Beavers, J.A. and Harle, B.A. (1996). "Effect of Stress Corrosion Cracking on Integrity and Remaining Life of Natural Gas Pipelines," *Corrosion 96 - NACE International Annual Conference and Exposition*, Paper # 255, Dublin, Ohio

Zarrabi, K. (1994). "Plastic Collapse Pressures for Defected Cylindrical Vessels,"

International Journal of Pressure Vessels and Piping, Vol. 60, pp. 65-69.

Cheung, Y.K. and Wu, Chang-Chun (1993). "Incompatible Numerical Simulation of the Axisymmetric Cracked Body Made of Ideally Elastic-Plastic Material," *Engineering Fracture Mechanics*, Vol.45, no. 3, pp. 399-405.

Mackenzie, D. and Boyle, J.T. (1993). "A Method of Estimating Limit Loads by Iterative Elastic Analysis I - Simple Examples," *International Journal of Pressure Vessels and Piping*, Vol. 53, pp. 77-95.

Nadarajah, C., Mackenzie, D. and Boyle, J.T., "A Method of Estimating Limit Loads by Iterative Elastic Analysis II - Nozzle Sphere Interactions with Internal Pressure and Radial Load," *International Journal of Pressure Vessels and Piping*, Vol. 53, pp. 97-119.

Shi, Jinhua, Mackenzie, D. and Boyle, J.T., "A Method of Estimating Limit Loads by Iterative Elastic Analysis III - Torispherical Heads Under Internal Pressure," *International Journal of Pressure Vessels and Piping*, Vol. 53, pp. 121-142.

Seshadri, R. (1991). "The Generalized Local Stress Strain (GLOSS) Analysis - Theory and Applications," *ASME Journal of Pressure Vessel Technology*, Vol.113, pp. 219-227.

Sehadri, R. and Fernando, C.P.D. (1992). "Limit Loads of Mechanical Components and Structures Using the GLOSS R-node Method," *ASME Journal of Pressure Vessel Technology*, Vol. 114, pp. 201-208.

Seshadri, R. (1995). "Inelastic Evaluation of Mechanical and Structural Components Using the Generalized Local Stress Strain Method of Analysis," *Nuclear Engineering and Design*, Vol. 153, pp. 287-303.

Seshadri, R. and Kizhatil, R. (1995). "Robust Approximate Methods for Estimating Inelastic Fracture Parameters," *ASME Journal of Pressure Vessel Technology*, Vol. 117, pp. 115-123.

Calladine, C.R. and Drucker, D.C. (1962). "Nesting Surfaces for Constant Rate of Energy Dissipation in Creep," *Quarterly of Applied Mathematics*, Vol. 20, pp. 79-84.

Boyle, J.T. (1982). "The Theorem of Nesting Surfaces in Steady Creep and Its Application to Generalized Models and Limit Reference Stresses," *Res Mechanica*, Vol. 4, pp. 275-294.

Mura, T. and Lee, S.L. (1963). "Application of Variational Principles to Limit Analysis," *Quarterly of Applied Mathematics*, Vol. 21, no. 3, pp. 243-248.

Mura, T., Rimawi, W.H. and Lee, S.L. (1965). "Extended Theorems of Limit Analysis," *Quarterly of Applied Mathematics*, Vol. 23, no. 2, pp. 171-179.

Seshadri, R. and Mangalaramanan, S.P. (1996). "Lower Bound Limit Loads Using Variational Concepts: The m_α -Method," *Engineering & Applied Science Technical Report Series*, Report No. 96-01, Memorial University of Newfoundland, St. John's, Newfoundland, Canada.

Barsoum, R.S., (1976). "On the Use of Isoparametric Finite Elements in Linear Fracture Mechanics," *International Journal for Numerical Methods in Engineering*, Vol. 10, pp. 25-37.

Rice, J.R. and Rosengren, G.F., (1968). "Plane Strain Deformation Near a Crack Tip in a Power-Law Hardening Material," *Journal of the Mechanics and Physics of Solids*, Vol.16, pp. 1-12.

Anderson, T.L., (1991). *Fracture Mechanics Fundamentals and Applications*, CRC Press Inc., Boca Raton, Florida, 793 p.

Seshadri, R., (1996). "In Search of the Redistribution Nodes," Proceedings of the International Conference on Pipes and Pressure Vessels, Singapore.

Mangalaramanan, S.P., (1997). Personal Consultation, Memorial University of Newfoundland, St. John's, Newfoundland, Canada.

APPENDIX A

ANSYS Input Files and Macro Code

ANSYS Input Files - Standard Fracture Specimens

CT Specimen:

/batch

/title,CT Specimen - Linear Analysis

*set,a,.0466 ! Set model geometry values
*set,w,.1
*set,b,.003
*set,r,.0125
*set,ym,211e09
*set,ys,488.43e06

/prep7

et,1,plane2,,,3 ! 6 noded triangular element
mp,ex,1,211e9 ! Young's Modulus (Pa)
mp,nuxy,1,0.3 ! Poisson's ratio

tb,bkin,1,1 ! Set plastic material properties
tbdata,1,ys,0 ! for nonlinear analysis

real,1
r,1,b

k,1,0,.005 ! Definition of model keypoints
k,2,.005,0
k,3,a,0
k,4,w,0
k,5,w,0.625*w
k,6,-1.5*r,0.625*w
k,7,-1.5*r,.005
k,8,0,.0315
k,9,0,.0315+r
k,10,0,.0315,w

l,1,2 ! Definition of lines from
l,2,3 ! keypoints
l,3,4
l,4,5
l,5,6

```

1,6,7
1,7,1

lesize,3,.005          ! Set element edge length for
lesize,4,.005          ! selected lines during meshing
lesize,5,.005
lesize,6,.005

circle,8,r,10,9,,4     ! Generate a circle for CT model
                        ! load application

kscon,3,0.001,1,9      ! Generate crack-tip elements

al,1,2,3,4,5,6,7       ! Define areas from lines
al,8,9,10,11

asba,1,2                ! Subtract area 2 from area 1

amesh,3                 ! Mesh resulting area 3

fini

/solu

antype,0

nropt,1,,off           ! Set solver options for nonlinear
autots,on              ! analysis
pred,on,,on
ncnv,0
outres,all,all

nset,s,loc,x,w         ! Set boundary conditions
nset,r,loc,y,0
d,all,ux,0
nset,all

lset,s,line,,3
nsl,s,1
d,all,uy,0
nset,all
lset,all

```

lselect,s,line,,8,11,3
nselect,s,1
f,all,fy,1500
nselect,all
lselect,all

! Load application

time,3
nsubst,200

**! Set number of load steps and substeps
! for nonlinear analysis**

save
solve

fini

exit

SENB Specimen:

/batch

! SINGLE EDGE NOTCHED BEND SPECIMEN
! Half Model

/prep7

/title, SENB Specimen

et,1,plane2,,,3 **! 6 noded triangular element**
mp,ex,1,211e9 **! Young's Modulus (Pa)**
mp,nuxy,,0.3 **! Poisson's ratio**

tb,bkin,1,1 **! Setting plastic material properties**
tbdata,1,488.43e6,0 **! for nonlinear analysis**

k,1,0,0 **! Define model keypoints**
k,2,0.19375,0
k,3,0.19375,.00625
k,4,0.2,0.025
k,5,0.2,0.05
k,6,0.2,0.1
k,7,0,0.1

l,1,2 **! Define lines**
l,2,3
l,3,4
l,4,5
l,5,6
l,6,7
l,7,1

r,1,0.003 **! Model thickness (m)**

kscon,5,0.001,,5,9 **! Create crack-tip elements**

lesize,all,0.05 **! Define element edge length for meshing**

al,all **! Define area**

real,1

amesh,1 ! Mesh area

finish

/solution

antype,0 ! Setting solver options for
nropt,1,,off ! nonlinear analysis

autots,on
pred,on,,on
ncnv,0
outres,all,all

nsel,s,loc,x,0 ! Define boundary conditions
nsel,r,loc,y,0
d,all,uy,0
nsel,all

lsel,s,line,,5
nsl,s,1
d,all,ux,0
lsel,all
nsel,all

nsel,s,loc,x,0.2 ! Apply load
nsel,r,loc,y,0.1
f,all,fy,-6000
nsel,all

time,3 ! Set number of load steps and substeps
nsubst,200

save
solve

finish
exit

SENT Specimen:

/batch

! SINGLE EDGE NOTCHED TENSION PANEL

! Half Model

/prep7

/title,SENT Specimen

et,1,plane2,,,3

! 6 noded triangular element

r,1,0.003

! Component thickness (m)

mp,ex,1,211e9

! Young's Modulus (Pa)

mp,nuxy,1,0.3

! Poisson's ratio

k,1,0,0

! Define model keypoints

k,2,0.03,0

k,3,0.05,0

k,4,0.05,0.1

k,5,0,0.1

l,1,2

! Define lines

l,2,3

l,3,4

l,4,5

l,5,1

kscon,2,0.001,0.5,9

! Create crack-tip elements

lesize,all,0.005

! Set element edge length for meshing

al,all

! Define area

amesh,1

! Mesh area

finish

/solution

antype,0

! Set solver options for nonlinear

autots,on

! analysis

outres,all,all

pred,on,,on

nropt,1,,off
ncnv,0

lsel,s,line,,2
nsl,s,1
d,all,uy,0
lsel,all

! Set boundary conditions

nset,s,loc,x,0.05
nset,r,loc,y,0
d,all,ux,0
nset,all

tb,bkin,1,1
tbdata,1,488.43e6,0

**! Set plastic material properties for
! nonlinear analysis**

time,3
nsubst,200

! Set number of load steps and substeps

nset,s,loc,y,0.1
nset,r,loc,x,.02,.03
f,all,fy,200
nset,all

! Load application

save
solve

finish
exit

ANSYS Input Files - Pipe Models

Typical Single Axial Defect Model:

/batch

/title,Pipe Model - 2mm Defect

*set,ym,211e9

*set,ys,488.43e6

/prep7

et,1,plane2,,,2

mp,ex,1,ym

mp,nuxy,1,0.3

tb,bkin,1,1

tbdata,1,ys,0

k,1,0,0,0

k,2,.447,0

k,3,.455,0

k,4,.457,.0002

k,5,0,.457

k,6,-.457,0

k,7,-.447,0

k,8,0,.447

l,2,3

l,3,4

larc,4,5,1,.457

larc,5,6,1,.457

l,6,7

larc,2,8,1,.447

larc,8,7,1,.447

lesize,1,.001

lesize,2,.001

lesize,3,.005,,,4

lesize,4,.005

lesize,6,.005,,,4

lesize,5,.005

lesize,7,.005

kscon,3,.0005,1,9

a,2,3,4,5,8

a,5,6,7,8

amesh,all

fini

/solu

antype,0

nropt,1,,off

autots,on

pred,on,,on

ncnv,0

outres,all,all

nsel,s,node,,2

d,all,ux,0

nsel,all

lsel,s,line,,1

nsll,s,1

d,all,uy,0

nsel,all

lsel,all

lsel,s,line,,5

nsll,s,1

d,all,uy,0

nsel,all

lsel,all

! lsel,s,line,,6,7

! nsll,s,1

! sf,all,pres,2e6

! nsel,all

! lsel,all

lsel,s,line,,6,7

sfl,all,pres,15e6

lsel,all

time,3

nsubst,200

save

solve

fini

! *use,repeat

! /inp,rmac3d

exit

Typical Internal Axial Defect Model:

/batch

/title,Pipe Model - Internal 2mm Defect

*set,ym,211e9

*set,ys,488.43e6

/prep7

et,1,plane2,,,2

mp,ex,1,ym

mp,nuxy,1,0.3

tb,bkin,1,1

tbdata,1,ys,0

k,1,0,0,0

k,2,.447,0

k,3,.449,0

k,4,.457,0

k,5,0,.457

k,6,-.457,0

k,7,-.447,0

k,8,0,.447

l,2,3

l,3,4

larc,4,5,1,.457

larc,5,6,1,.457

l,6,7

larc,2,8,1,.447

larc,8,7,1,.447

lesize,1,.001

lesize,2,.001

lesize,3,.005,,,4

lesize,4,.005

lesize,6,.005,,,4

lesize,5,.005

lesize,7,.005

kscon,3,0005,1,9

a,2,3,4,5,8

a,5,6,7,8

amesh,all

fini

/solu

antype,0

nropt,1,,off

autots,on

pred,on,,on

ncnv,0

outres,all,all

nselect,s,loc,x,-457

nselect,r,loc,y,0

d,all,ux,0

nselect,all

lselect,s,line,,2

nselectll,s,1

d,all,uy,0

nselect,all

lselect,all

lselect,s,line,,5

nselectll,s,1

d,all,uy,0

nselect,all

lselect,all

! lselect,s,line,,6,7

! nselectll,s,1

! sf,all,pres,2e6

! nselect,all

! lselect,all

lselect,s,line,,6,7

sfl,all,pres,15e6

lsel,all

time,3

nsubst,200

save

solve

fini

! *use,repeat

! /inp,rmac3d

exit

Thick Wall Pipe External Defect:

/batch

/title,Pipe Model - 2mm Defect

*set,ym,211e9

*set,ys,488.43e6

/prep7

et,1,plane2,,,2

mp,ex,1,ym

mp,nuxy,1,0.3

tb,bkin,1,1

tldata,1,ys,0

k,1,0,0,0

k,2,-.357,0

k,3,.455,0

k,4,.457,.0002

k,5,0,.457

k,6,-.457,0

k,7,-.357,0

k,8,0,.357

l,2,3

l,3,4

larc,4,5,1,.457

larc,5,6,1,.457

l,6,7

larc,2,8,1,.357

larc,8,7,1,.357

lesize,1,.005

lesize,2,.005

lesize,3,.01,,,4

lesize,4,.01

lesize,6,.01,,,4

lesize,5,.01

lesize,7,.01

kscon,3,.0005,1,9

a,2,3,4,5,8

a,5,6,7,8

amesh,all

fini

/solu

antype,0

nropt,1,,off

autots,on

pred,on,,on

ncnv,0

outres,all,all

nselect,s,loc,x,-.457

nselect,r,loc,y,0

d,all,ux,0

nselect,all

lselect,s,line,,1

nselectll,s,1

d,all,uy,0

nselect,all

lselect,all

lselect,s,line,,5

nselectll,s,1

d,all,uy,0

nselect,all

lselect,all

! lselect,s,line,,6,7

! nselectll,s,1

! sf,all,pres,2e6

! nselect,all

! lselect,all

lselect,s,line,,6,7

sfl,all,pres,150e6

lsel,all

time,3
nsubst,200

save
solve

fini

! *use,repeat
! /inp,rmac3d

exit

Multiple Defects Full Model:

/batch

/title, Pipe Model - Multiple Defects

*set,ym,211e9
*set,ys,488.43e6

/prep7

et,1,plane2,,,2
mp,ex,1,ym
mp,nuxy,1,0.3

tb,bkin,1,1
tbdata,1,ys,0

k,1,0,0,0
csys,1
k,2,.454,0
k,3,.457,.02
k,4,.457,.5
k,5,.447,.5
k,6,.447,-.5
k,7,.457,-.5
k,8,.457,-.02

k,9,.455,1
k,10,.457,1.02
k,11,.457,1.5
k,12,.447,1.5
k,24,.457,.98

k,13,.455,-1
k,14,.457,-.98
k,15,.447,-1.5
k,16,.457,-1.5
k,17,.457,-1.02

csys,0
k,18,0,.457
k,19,0,.447

k,20,-.457,0
k,21,-.447,0
k,22,0,-.457
k,23,0,-.447

l,2,3
l,2,8
l,4,5
l,6,7
l,9,10
l,9,24
l,11,12
l,13,14
l,15,16
l,13,17
l,18,19
l,22,23

larc,3,4,1,.457
larc,8,7,1,.457
larc,5,6,1,.447
larc,4,24,1,.457
larc,10,11,1,.457
larc,5,12,1,.447
larc,7,14,1,.457
larc,17,16,1,.457
larc,6,15,1,.447

larc,11,18,1,.457
larc,12,19,1,.447
larc,16,22,1,.457
larc,15,23,1,.447
larc,18,20,1,.457
larc,20,22,1,.457
larc,19,21,1,.447
larc,21,23,1,.447

lesize,3,.001
lesize,4,.001
lesize,7,.001
lesize,9,.001
lesize,15,.001
lesize,18,.001

lesize,21,.001
lesize,22,.005,,,4
lesize,23,.005,,,4
lesize,24,.005,,,4
lesize,25,.005,,,4
lesize,26,.005
lesize,27,.005
lesize,28,.005
lesize,29,.005

kscon,2,.0005,1,18
kscon,9,.0005,1,18
kscon,13,.0005,1,18

a,2,3,4,5,6,7,8
a,9,10,11,12,5,4,24
a,13,14,7,6,15,16,17
a,11,12,19,18
a,15,16,22,23
a,18,20,21,19
a,20,22,23,21

amesh,all

fini

/solu

antype,0

nropt,1,,off

autots,on

pred,on,,on

ncnv,0

outres,all,all

nselect,s,loc,x,4539,4541

nselect,r,loc,y,0

d,all,uy,0

d,all,ux,0

nselect,all

nselect,s,loc,x,0

```
nset,r,loc,y,.447  
d,all,ux,0  
nset,all
```

```
nset,s,loc,x,-.447  
nset,r,loc,y,0  
d,all,uy,0  
nset,all
```

```
csys,1  
! nset,s,loc,x,.447  
! sf,all,pres,2e6  
! nset,all
```

```
nset,s,loc,x,.447  
sf,all,pres,15e6  
nset,all
```

```
csys,0
```

```
time,3  
nsubst,200
```

```
save  
solve
```

```
fini
```

```
! *use,repeat  
! /inp,rmac3d
```

```
exit
```

Multiple Defects Half Model:

/batch

/title,Pipe Model - Multiple Defects

*set,ym,211e9

*set,ys,488.43e6

/prep7

et,1,plane2,,,2

mp,ex,1,ym

mp,nuxy,1,0.3

tb,bkin,1,1

tbdata,1,ys,0

k,1,0,0,0

csys,1

k,2,.456,0

k,3,.457,.02

k,4,.457,.5

k,5,.447,.5

! k,6,.447,-.5

! k,7,.457,-.5

! k,8,.457,-.02

k,9,.454,1

k,10,.457,1.02

k,11,.457,1.5

k,12,.447,1.5

k,24,.457,.98

! k,13,.454,-1

! k,14,.457,-.98

! k,15,.447,-1.5

! k,16,.457,-1.5

! k,17,.457,-1.02

k,25,.447,0

k,26,.447,1

! k,27,.447,-1

csys,0
k,18,0,.457
k,19,0,.447
k,20,-.457,0
k,21,-.447,0
! k,22,0,-.457
! k,23,0,-.447

l,2,3
! l,2,8
l,4,5
! l,6,7
l,9,10
l,9,24
l,11,12
! l,13,14
! l,15,16
! l,13,17
l,18,19
! l,22,23
l,21,20
l,25,2

larc,3,4,1,.457
! larc,8,7,1,.457
larc,5,25,1,.447
! larc,25,6,1,.447
larc,4,24,1,.457
larc,10,11,1,.457
larc,12,26,1,.447
larc,26,5,1,.447
! larc,7,14,1,.457
! larc,17,16,1,.457
! larc,6,27,1,.447
! larc,27,15,1,.447

larc,11,18,1,.457
larc,12,19,1,.447
! larc,16,22,1,.457
! larc,15,23,1,.447
larc,18,20,1,.457
! larc,20,22,1,.457
larc,19,21,1,.447

! larc,21,23,1,447

lesize,2,.001
lesize,5,.001
lesize,6,.005
lesize,7,.005
lesize,8,.001
lesize,9,.001
lesize,10,.001
lesize,11,.001
lesize,12,.001
lesize,13,.001
lesize,14,.001
lesize,15,.005,,,4
lesize,16,.005,,,4
lesize,17,.005
lesize,18,.005
! lesize,23,.001
! lesize,24,.001
! lesize,25,.005,,,4
! lesize,26,.005,,,4
! lesize,27,.005,,,4
! lesize,28,.005,,,4
! lesize,29,.005
! lesize,30,.005
! lesize,31,.005
! lesize,32,.005

kscon,2,.0005,1,18
kscon,9,.0005,1,18
kscon,13,.0005,1,18

a,2,3,4,5,25 ! 6,7,8
a,9,10,11,12,26,5,4,24
! a,13,14,7,6,27,15,16,17
a,11,12,19,18
! a,15,16,22,23
a,18,20,21,19
! a,20,22,23,21

amesh,all

fini

/solu

antype,0

nropt,1,,off

autots,on

pred,on,,on

ncnv,0

outres,all,all

nselect,loc,x,.4539,.4541

nselect,r,loc,y,0

d,all,uy,0

d,all,ux,0

nselect,all

! nselect,s,loc,x,0

! nselect,r,loc,y,.447

! d,all,ux,0

! nselect,all

nselect,s,loc,x,-.447

nselect,r,loc,y,0

d,all,uy,0

nselect,all

lselect,s,line,,7

nselect,l,s,1

d,all,uy,0

nselect,all

lselect,all

lselect,s,line,,8

nselect,l,s,1

d,all,uy,0

nselect,all

lselect,all

csys,1

! nselect,s,loc,x,.447

! sf,all,pres,2e6

! nselect,all

```
nset,s,loc,x,.447  
sf,all,pres,15e6  
nset,all
```

```
csys,0
```

```
time,3  
nsubst,200
```

```
save  
solve
```

```
fini
```

```
! *use,repeat  
! /inp,rmac3d
```

```
exit
```

ANSYS Macro Code

Improved Gloss R-node Macro:

```
! #####
! # ELASTIC MODULUS SOFTENING MACRO FOR R-NODE ANALYSIS #
! #####
!
! *****
! * note: *
! * the parameters "ym" and "ys" should be defined in the main *
! * program *
! *****
!
!
! -----
! I - L I N E A R   A N A L Y S I S
! -----
! Suited for:
! (1) 2-dimensional plane elements
! - 3-noded triangular elements
! - 6-noded triangular elements
! - 4-noded quadrilateral elements
! - 8-noded quadrilateral elements
! (2) 3-dimensional solid elements
! - 4-noded tetrahedral elements
! - 10-noded tetrahedral elements
! - 8-noded solid elements
! - 20-noded solid elements

/post1

*dim,dum1,array,1
*dim,dum2,array,1
*dim,dum3,array,1
*dim,xcord,array,1
*dim,ycord,array,1
*dim,zcord,array,1
*dim,tri,array,4
*dim,quad,array,4
*dim,tetra,array,4
*dim,brick,array,6
*dim,zz,array,1
```

*dim,zdum1,array,1
*dim,zdum2,array,1
*dim,zdum3,array,1
*dim,zdum4,array,1
*dim,zdum5,array,10000
*dim,varbl1,array,1
*dim,varbl2,array,1
*dim,varbl3,array,1
*dim,varbl4,array,1
*dim,varbl5,array,1
*dim,varbl6,array,1
*dim,varbl7,array,1
*dim,varbl8,array,1

Set,1
Etable,sigc,s,eqv
Etable,vol,volu

=====
=====
! Sorted element stresses and volumes are stored in the file "esort1"
! Unsorted element stresses and volumes are stored in the file "estrs1"
=====
=====

*get,max1,elem,0,num,max

Esort,etab,sigc,0
/out,esort1
Pretab,sigc,vol
/out
Eusort

*cfopen,estrs1
*do,kk,1,max1
*get,sigc1,elem,kk,etab,sigc
*get,vol1,elem,kk,volu
*get,xcoord,elem,kk,cent,x
*get,ycoord,elem,kk,cent,y
*get,zcoord,elem,kk,cent,z
Xcord(1)=xcoord
Ycord(1)=ycoord

```

Zcord(1)=zcoord
Dum1(1)=kk
Dum2(1)=sigc1
Dum3(1)=vol1
*vwrite,dum1(1),dum2(1),dum3(1),xcord(1),ycord(1),zcord(1)
(x,f6.1,5(2x,e21.10))
*enddo
*cfclos
!_____

```

```

!=====begin grouping adjacent element pairs=====

```

```

*get,cent1,elem,5,cent,z      ! two arbitrary
*get,cent2,elem,27,cent,z     ! elements
*if,cent1,eq,0,then
  *if,cent2,eq,0,then
    Prob=2                    ! 2-dimensional problem
  *endif
  *else
    Prob=3                    ! 3-dimensional problem
  *endif

*get,telem,elem,0,count

*c fopen,egroup

*do,ij,1,telem
  Esel,s,elem,,ij
  Nsle,s
  *get,nnode,node,0,count
  Esel,all
  Nsel,all
  Zz(1)=ij

  *if,prob,eq,2,then
    *if,nnode,eq,3,then
      *get,tri(1),elem,ij,adj,1
      *get,tri(2),elem,ij,adj,2
      *get,tri(3),elem,ij,adj,3
      *get,tri(4),elem,ij,adj,4 ! for the sake of stif42
      *vwrite,zz(1),tri(1)
      (2(2x,f7.1))
      *vwrite,zz(1),tri(2)
    *endif
  *endif

```

```

(2(2x,f7.1))
*vwrite,zz(1),tri(3)
(2(2x,f7.1))
*vwrite,zz(1),tri(4) ! for the sake of stif42 forced
(2(2x,f7.1)) ! into triangle
*endif
*if,nnode,eq,6,then
*get,tri(1),elem,ij,adj,1
*get,tri(2),elem,ij,adj,2
*get,tri(3),elem,ij,adj,3
*vwrite,zz(1),tri(1)
(2(2x,f7.1))
*vwrite,zz(1),tri(2)
(2(2x,f7.1))
*vwrite,zz(1),tri(3)
(2(2x,f7.1))
*endif
*if,nnode,eq,4,then
*get,quad(1),elem,ij,adj,1
*get,quad(2),elem,ij,adj,2
*get,quad(3),elem,ij,adj,3
*get,quad(4),elem,ij,adj,4
*vwrite,zz(1),quad(1)
(2(2x,f7.1))
*vwrite,zz(1),quad(2)
(2(2x,f7.1))
*vwrite,zz(1),quad(3)
(2(2x,f7.1))
*vwrite,zz(1),quad(4)
(2(2x,f7.1))
*endif
*if,nnode,eq,8,then
*get,quad(1),elem,ij,adj,1
*get,quad(2),elem,ij,adj,2
*get,quad(3),elem,ij,adj,3
*get,quad(4),elem,ij,adj,4
*vwrite,zz(1),quad(1)
(2(2x,f7.1))
*vwrite,zz(1),quad(2)
(2(2x,f7.1))
*vwrite,zz(1),quad(3)
(2(2x,f7.1))
*vwrite,zz(1),quad(4)

```

```

      (2(2x,f7.1))
    *endif
  *endif

  *if,prob,eq,3,then
    *if,nnode,eq,4,then
      *get,tetra(1),elem,ij,adj,1
      *get,tetra(2),elem,ij,adj,2
      *get,tetra(3),elem,ij,adj,3
      *get,tetra(4),elem,ij,adj,4
      *vwrite,zz(1),tetra(1)
      (2(2x,f7.1))
      *vwrite,zz(1),tetra(2)
      (2(2x,f7.1))
      *vwrite,zz(1),tetra(3)
      (2(2x,f7.1))
      *vwrite,zz(1),tetra(4)
      (2(2x,f7.1))
    *endif
    *if,nnode,eq,10,then
      *get,tetra(1),elem,ij,adj,1
      *get,tetra(2),elem,ij,adj,2
      *get,tetra(3),elem,ij,adj,3
      *get,tetra(4),elem,ij,adj,4
      *vwrite,zz(1),tetra(1)
      (2(2x,f7.1))
      *vwrite,zz(1),tetra(2)
      (2(2x,f7.1))
      *vwrite,zz(1),tetra(3)
      (2(2x,f7.1))
      *vwrite,zz(1),tetra(4)
      (2(2x,f7.1))
    *endif
    *if,nnode,eq,8,then
      *get,brick(1),elem,ij,adj,1
      *get,brick(2),elem,ij,adj,2
      *get,brick(3),elem,ij,adj,3
      *get,brick(4),elem,ij,adj,4
      *get,brick(5),elem,ij,adj,5
      *get,brick(6),elem,ij,adj,6
      *vwrite,zz(1),brick(1)
      (2(2x,f7.1))
      *vwrite,zz(1),brick(2)

```

```

(2(2x,f7.1))
  *vwrite,zz(1),brick(3)
(2(2x,f7.1))
  *vwrite,zz(1),brick(4)
(2(2x,f7.1))
  *vwrite,zz(1),brick(5)
(2(2x,f7.1))
  *vwrite,zz(1),brick(6)
(2(2x,f7.1))
*endif
*if,nnode,eq,20,then
  *get,brick(1),elem,ij,adj,1
  *get,brick(2),elem,ij,adj,2
  *get,brick(3),elem,ij,adj,3
  *get,brick(4),elem,ij,adj,4
  *get,brick(5),elem,ij,adj,5
  *get,brick(6),elem,ij,adj,6
  *vwrite,zz(1),brick(1)
(2(2x,f7.1))
  *vwrite,zz(1),brick(2)
(2(2x,f7.1))
  *vwrite,zz(1),brick(3)
(2(2x,f7.1))
  *vwrite,zz(1),brick(4)
(2(2x,f7.1))
  *vwrite,zz(1),brick(5)
(2(2x,f7.1))
  *vwrite,zz(1),brick(6)
(2(2x,f7.1))
*endif
*endif
/gop
Elem_num=ij
/nop
*enddo
*cfclos

=====end grouping adjacent element
pairs=====

```

! -----open a file to store all external nodes of the component-----

*c fopen,extnodes

Nsel,s,ext

*get,ztotnod,node,0,count

Zz(1)=ztotnod

*vwrite,zz(1)

(X,f7.0)

*get,znodnum,node,0,num,min

*do,zk,1,ztotnod

*get,zxcord,node,znodnum,loc,x

*get,zycord,node,znodnum,loc,y

*get,zzcord,node,znodnum,loc,z

Zdum1(1)=znodnum

Zdum2(1)=zxcord

Zdum3(1)=zycord

Zdum4(1)=zzcord

*vwrite,zdum1(1),zdum2(1),zdum3(1),zdum4(1)

(X,f6.0,3(2x,e21.10))

*get,znodnum,node,znodnum,nxth

*enddo

*cfclos

Nsel,all

Esel,all

=====end node selection=====

=====

! For selective softening remove the comment below

c*** esel,s,etab,sigc,ys,(ys*10e10)

=====

*set,mn,2

*c fopen,exval

*get,kk,elem,0,count

Alfa=1

*do,l,1,kk

*get,min1,elem,0,num,min

```

*get,steq,elem,min1,etab,sigc
*set,esec,((ys/steq)**alfa)*ym
*cfwrite,mp,ex,mn,esec
c*** *cfwrite,mp,nuxy,mn,0.49
*set,mn,mn+1
*set,min1,min1+1
*if,min1,le,max1,then
Esel,r,elem,,min1,max1
*endif
*enddo
*cfclos
!

```

```

=====
Esel,all
c*** esel,s,etab,sigc,ys,(ys*10e10)
=====

```

```

*set,mn,2

*cfopen,exmod
*do,1,1,kk
*get,min1,elem,0,num,min
*cfwrite,mat,mn
*cfwrite,emodif,min1
*set,mn,mn+1
*set,min1,min1+1
*if,min1,le,max1,then
Esel,r,elem,,min1,max1
*endif
*enddo
*cfclos
Esel,all
Finish

```

```

!
!   II - LINEAR ANALYSIS
!
-----

```

```

/prep7
Resume

```

Ex,1,ym
*use,exval
*use,exmod
Finish

/solu
Save
Solve
Finish

/post1

*dim,dum1,array,1
*dim,dum2,array,1
*dim,dum3,array,1

Set,1
Etable,sigc,s,eqv
Etable,vol,volu

=====
=====
! Sorted element stresses and volumes are stored in the file "esort2"
! Unsorted element stresses and volumes are stored in the file "estrs2"
=====
=====

*get,max1,elem,0,num,max

Esort,etab,sigc,0
/out,esort2
Pretab,sigc,vol
/out
Eusort

*cfoopen,estrs2
*do,kk,1,max1
*get,sigc3,elem,kk,etab,sigc
*get,vol2,elem,kk,volu
Dum1(1)=kk
Dum2(1)=sigc3
Dum3(1)=vol2
*vwrite,kk,sigc3,vol2

(x,f6.1,3x,e21.10,3x,e21.10)

*enddo

*cfclos

!-----

Finish

m_e-method Macros:

```
*set, YM, 211e9  
! *set, YS, 488.43e6  
/inp, iter1, ..., /itermac/  
/sys, mv RUN1 RUN2  
/inp, iter2, ..., /itermac/  
/sys, mv RUN2 RUN3  
/inp, iter3, ..., /itermac/  
/sys, mv RUN3 RUN4  
/inp, iter4, ..., /itermac/  
/sys, mv RUN4 RUN5  
/inp, iter5, ..., /itermac/  
/sys, mv RUN5 RUN6  
/inp, iter6, ..., /itermac/  
/sys, mv RUN6 RUN7  
/inp, iter7, ..., /itermac/  
/sys, mv RUN7 RUN8  
/inp, iter8, ..., /itermac/  
/sys, mv RUN8 RUN9  
/inp, iter9, ..., /itermac/  
/sys, mv RUN9 RUN10
```

```
/sys, rm vread  
/sys, rm MAX1  
/sys, rm EXVAL  
/sys, rm EXVAL.AUX
```

Iteration files:

```
! #####  
! #      ITERATION - I      #  
! #####  
  
! *****  
! * NOTE:                    *  
! * The parameter "YM" should be defined in the main program *  
! *****
```

! I - L I N E A R A N A L Y S I S

/post1

/nopr

*dim,dum1,array,1
*dim,dum2,array,1
*dim,dum3,array,1
*dim,dum4,array,1
*dim,dum5,array,1

Set,1
Etable,sigc,s,eqv
Etable,vol,volu

/out,esort1,,.../iterres/
Esort,etab,sigc,0
Pretab,sigc,vol
/out
Eusort

! Element stresses and volumes are stored in the file "estrs1"

*get,max1,elem,0,num,max

Dum4(1)=max1

```
*c fopen,max1
*v write,dum4(1)
(1x,f15.2)
*cfclos
```

```
/sys,cp max1 run1
```

```
*dim,esec1,array,max1 !
%% %% %% %% %% %% %% %% %% %% %% %% %% %% %% %% %% %% %% %% %%
```

```
*c fopen,estrsl,.../iterres/ ! %% %% %% %% %% %% %% %% %% %% %% %% %% %% %% %% %% %% %% %% %%
```

```
*do,k,1,max1
*get,sigc1,elem,k,etab,sigc
*get,voll,elem,k,volu
Dum1(1)=k
Dum2(1)=sigc1
Dum3(1)=voll
*v write,dum1(1),dum2(1),dum3(1)
(1x,f6.1,3x,e21.10,3x,e21.10)
*enddo
*cfclos
```

```
!-----
```

```
/nopr
```

```
c*** *cfclos
c*** !-----
```

```
=====
! For selective softening remove the comment below
c*** esel,s,etab,sigc,ys,(ys*10e10)
=====
```

```
*set,mn,2
*set,ys,100 ! arbitrary stress value
```

```
*c fopen,exval2,.../iterres/ ! %% %% %% %% %% %% %% %% %% %% %% %% %% %% %% %% %% %% %% %% %%
```

```
*get,k,elem,0,count
```

```
*do,l,1,k
```

```

*get,min1,elem,0,num,min
*get,steq,elem,min1,etab,sigc
*set,esec1(l),(ys/steq)*ym !%%%%%%%%%
*cfwrite,mp,ex,mn,esec1(l) !
%%%%%%%%%
*set,mn,mn+1
*set,min1,min1+1
*if,min1,le,max1,then
Esel,r,elem,,min1,max1
*endif
*enddo
*cfclos
!-----
/nopr

```

```

=====
Esel,all
c*** esel,s,etab,sigc,ys,(ys*10e10)
=====

```

```

*cfopen,exval,aux !%%%%%%%%%
*do,kk,1,max1,1
Dum5(1)=esec1(kk)
*vwrite,dum5(1) !%%%%%%%%%
(1x,e36.19)
*enddo
*cfclos

```

```

/nopr

```

```

*set,mn,2

```

```

*cfopen,exmod,.. /iterres/
*do,ll,1,k
*get,min1,elem,0,num,min
*cfwrite,mat,mn
*cfwrite,emodif,min1
*set,mn,mn+1
*set,min1,min1+1
*if,min1,le,max1,then
Esel,r,elem,,min1,max1
*endif
*enddo

```

*cfclos
Esel,all
Finish

/nopr

!
! l i - l I n e a r a n a l y s I s
!-----

/prep7
Resume

Mp,ex,1,ym
/inp,exval2,../iterres/ !%%%%%%%%%%
/inp,exmod,../iterres/
Finish

/solu
Save
Solve
Finish

/post1
Resume

*dim,dum1,array,1
*dim,dum2,array,1
*dim,dum3,array,1

Set,1
Etable,sigc,s,eqv
Etable,vol,volu

/out,esort2,../iterres/
Esort,etab,sigc,0
Pretab,sigc,vol
/out
Eusort

*get,max1,elem,0,num,max
*cfopen,estrs2,../iterres/ !
*do,k,1,max1

```
*get,sigc3,elem,k,etab,sigc
*get,vol2,elem,k,volu
Dum1(1)=k
Dum2(1)=sigc3
Dum3(1)=vol2
*vwrite,k,sigc3,vol2
(1x,f6.1,3x,e21.10,3x,e21.10)
*enddo
*cfclos
!-----
```

/nopr

Finish

```
/sys,cp ../itermac/iter1 iter1.aux
/sys,tail -20 iter1.aux > iter1a.aux
/sys,rm iter1.aux
/sys,cut -c2-72 iter1a.aux > vread.for
/sys,rm iter1a.aux
/sys,f77 -o vread vread.for
/sys,rm vread.for
/sys,vread
```

Iteration 2:

```
! #####
! #      ITERATION - II      #
! # ELASTIC MODULUS SOFTENING MACRO #
! #####
```

/post1

/nopr

Resume

Set,1
Etable,sigc,s,eqv

*get,max1,elem,0,num,max

*dim,ymodu,array,max1

*dim,esec2,array,max1

*dim,dum1,array,1

/inp,exval

/sys,rm exval

=====
! For selective softening remove the comment below
c*** esel,s,etab,sigc,ys,(ys*10e10)
=====

*set,mn,2

*set,yst,100e13 ! arbitrary stress value

*cfopen,exval3,.../iterres/ ! %%%%%%%%%%

*get,kk,elem,0,count

*do,ll,1,kk

*get,min1,elem,0,num,min

*get,steq,elem,min1,etab,sigc

*set,esec2(ll),(yst/steq)*ymodu(ll)

*cfwrite,mp,ex,mn,esec2(ll)

*set,mn,mn+1

*set,min1,min1+1

*if,min1,le,max1,then

Esel,r,elem,,min1,max1

*endif

*enddo

*cfclos

=====

/nopr

```
!-----  
Esel,all  
c*** esel,s,etab,sigc,ys,(ys*10e10)  
!-----
```

```
*cfopen,exval,aux  
*do,kj,1,max1  
Dum1(1)=esec2(kj)  
*vwrite,dum1(1)  
(1x,e39.12)  
*enddo  
*cfclos
```

```
/nopr
```

```
!-----  
!   L i n e a r   a n a l y s i s  
!-----
```

```
/prep7  
Resume
```

```
Ex,1,ym  
/inp,exval3,.../iterres/ !%%%%%%%%%%  
/inp,exmod,.../iterres/  
Finish
```

```
/solu  
Save  
Solve  
Finish
```

```
/post1  
Resume
```

```
Set,1  
Etable,sigc,s,eqv  
Etable,vol,volu
```

```
/out,esort3,.../iterres/  
Esort,etab,sigc,0
```

```
Pretab,sigc,vol
/out
Eusort

*get,max1,elem,0,num,max
*cfopen,estr3,../iterres/ !
*do,kl,1,max1
*get,sigc3,elem,kl,etab,sigc
*get,vol3,elem,kl,volu
*vwrite,kl,sigc3,vol3
(1x,f6.1,3x,e21.10,3x,e21.10)
*enddo
*cfclos
!
```

```
/nopr

Finish
```

```
/sys,vread
```

Iteration 3:

```
! #####
! #      ITERATION - III      #
! # ELASTIC MODULUS SOFTENING MACRO #
! #####
```

```
/post1
```

```
/nopr
```

```
Resume
```

```
Set,1
Etable,sigc,s,eqv
```

```
*get,max1,elem,0,num,max
```

```
*dim,ymodu,array,max1
*dim,esec2,array,max1
*dim,dum1,array,1
```

```
/inp,exval
```

```
/sys,rm exval
```

```
=====
! For selective softening remove the comment below
c*** esel,s,etab,sigc,ys,(ys*10e10)
=====
```

```
*set,mn,2
*set,yst,100 ! arbitrary stress value
```

```
*cfopen,exval4,../iterres/ ! %%%%%%%%%%
```

```
*get,kk,elem,0,count
```

```
*do,ll,1,kk
*get,min1,elem,0,num,min
*get,steq,elem,min1,etab,sigc
*set,esec2(ll),(yst/steq)*ymodu(ll)
*cfwrite,mp,ex,mn,esec2(ll)
*set,mn,mn+1
*set,min1,min1+1
*if,min1,le,max1,then
Esel,r,elem,,min1,max1
*endif
*enddo
*cfclos
!-----
```

```
/nopr
```

```
=====
Esel,all
c*** esel,s,etab,sigc,ys,(ys*10e10)
=====
```

```
*c fopen,exval,aux
*do,kj,1,max1
Dum1(1)=esec2(kj)
*vwrite,dum1(1)
(1x,e39.12)
*enddo
*cfclos
```

```
/nopr
```

```
!
! -----
!   l i n e a r   a n a l y s i s
! -----
!
```

```
/prep7
Resume
```

```
Ex,1,ym
/inp,exval4,.../iterres/ !%%%%%%%%%%
/inp,exmod,.../iterres/
Finish
```

```
/solu
Save
Solve
Finish
```

```
/post1
Resume
```

```
Set,1
Etable,sigc,s,eqv
Etable,vol,volu
```

```
/out,esort4,.../iterres/
Esort,etab,sigc,0
Pretab,sigc,vol
/out
Eusort
```

```
*get,max1,elem,0,num,max
*c fopen,estrs4,.../iterres/ !%%%%%%%%%%
```

```
*do,kl,1,max1
*get,sigc3,elem,kl,etab,sigc
*get,vol3,elem,kl,volu
*vwrite,kl,sigc3,vol3
(1x,f6.1,3x,e21.10,3x,e21.10)
*enddo
*cfclos
!
```

/nopr

Finish

/sys,vread

The remaining iteration files (4-9) continue from the three listed here. The only changes are the arbitrary stress value used in the modulus modification equation.

m_ Calculation - MATLAB Script File:

```
fname1=input('Enter first iteration file ','s');  
eval(['load ' fname1 ';' ])  
eval(['file1=' fname1 ';' ])
```

```
fname2=input('Enter second file ','s');  
eval(['load ' fname2 ';' ])  
eval(['file2=' fname2 ';' ])
```

```
tic  
check=10;  
A1=[file1 file2];  
[m n]=size(A1);  
[Y I]=sort(A1);  
for j=1:n  
    Y(:,j)=A1(I(:,2),j);  
end
```

```
for i=1:m  
    sq(i,:)= [Y(i,2)^2*Y(i,3) Y(i,5)^2*Y(i,6)];  
end
```

```
[s1 l1]=max(Y(:,2));  
[s2 l2]=max(Y(:,5));
```

```
if s1 < s2
```

```
disp('#####')  
disp('#### Equiv stress for first iteration is less than second ####')  
disp('#####')  
    s1,s2  
    check=0;  
end
```

```
if l1 ~= l2
```

```
disp('#####')  
disp('#### Maximum equiv stress does not occur at same element ####')  
disp('#####')  
    l1,l2  
    check=10;  
end
```

```

M1=sigy*(sum(Y(:,3)))^5/(sum(sq(:,1)))^5;
M2=sigy*(sum(Y(:,6)))^5/(sum(sq(:,2)))^5;

if M1 < M2

disp('#####')
disp('#### M for first analysis less than M for second analysis ####')
disp('#####')
    M1,M2
    check=0;
end

% if check ~= 0
    count=0;
    for i=m:-1:1
        count=count+1;
        refvol(count,1)=sigy*(sum(Y(i:m,3)))^5/(sum(sq(i:m,1)))^5;
        refvol(count,2)=sigy*(sum(Y(i:m,6)))^5/(sum(sq(i:m,2)))^5;
    end
    refvol(:,3)=refvol(:,1)-refvol(:,2);

    [k first]=max(sign(refvol(:,3)));
    % vref=sum(Y(m-(first-2):m,3));
    % mupper=sigy*vref^5/(sum(sq(m-(first-2):m,2)))^5;
    mupper=refvol((first),2)
    sigbar=max(Y(:,5))/sigy;
    if mupper*sigbar > (1+2^5)

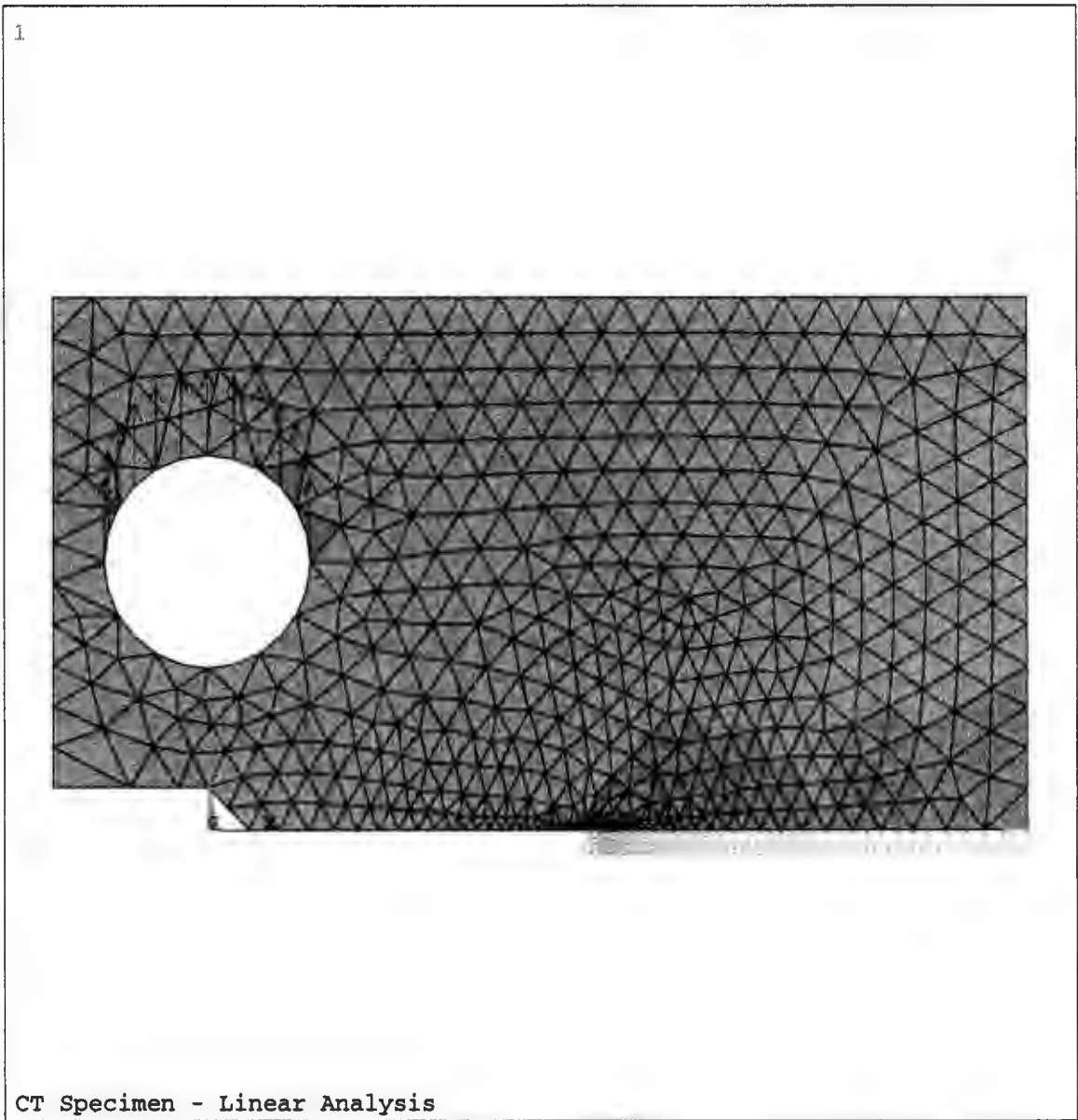
disp('#####')
disp('#####Negative check - use next iteration#####')
disp('#####')
        end
        coeffA=mupper^4*sigbar^4+4*mupper^2*sigbar^2-1;
        coeffB=-8*mupper^3*sigbar^2;
        coeffC=4*mupper^3*sigbar;
        m_alpha=max(roots([coeffA coeffB coeffC]))
        out=[Y sq refvol];
        save mdata.txt out -ascii
    % end

toc

```

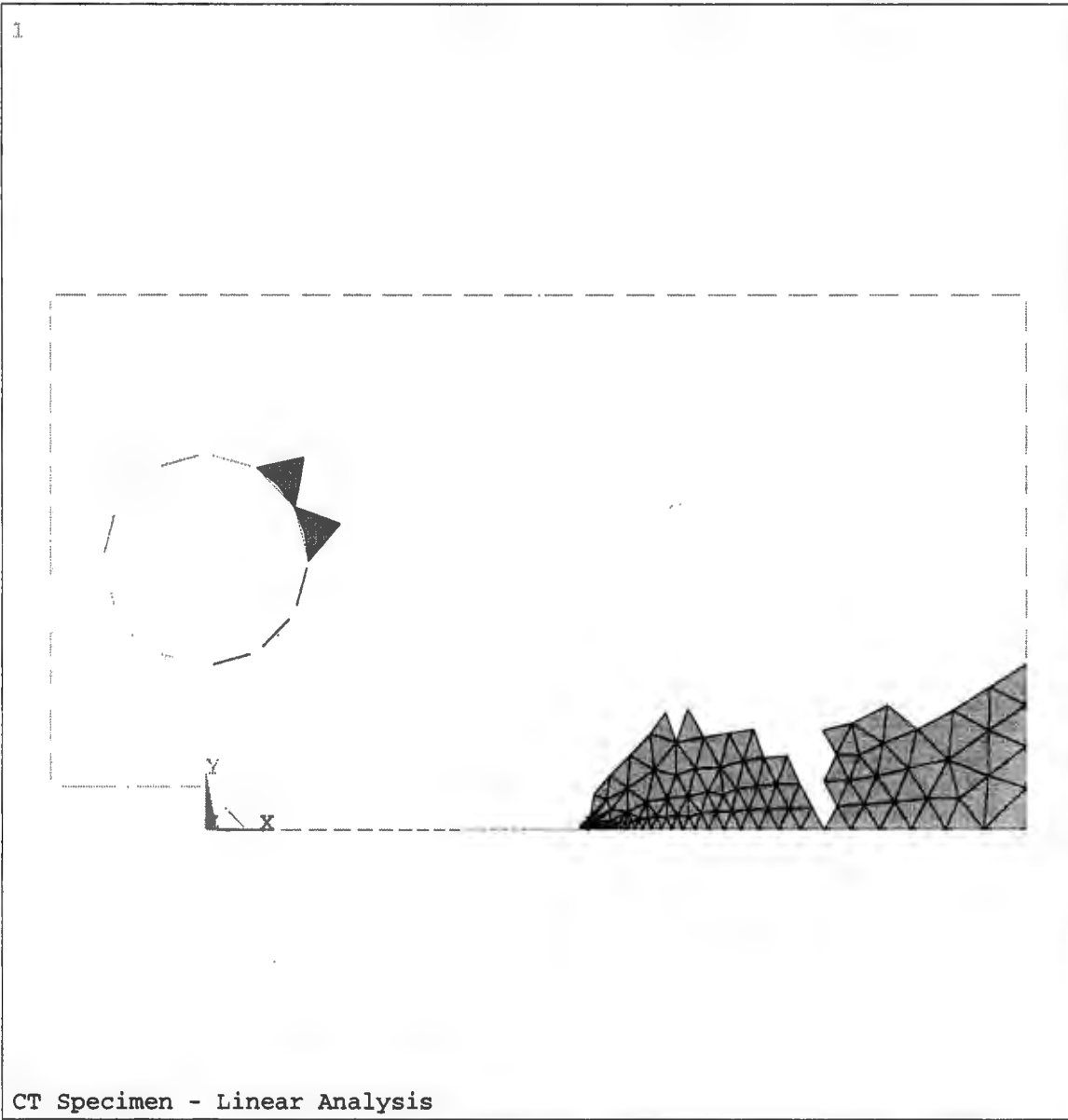
APPENDIX B

ANSYS Plots



```
ANSYS 5.2  
AUG 29 1997  
10:37:21  
PLOT NO. 1  
ELEMENTS  
TYPE NUM  
U  
F  
  
ZV =1  
DIST=.065313  
XF =.040625  
YF =.03125  
ZF =.05  
Z-BUFFER
```

Figure B.1 - Finite element mesh for compact tension specimen



ANSYS 5.2
 NOV 19 1997
 10:46:00
 PLOT NO. 1
 ELEMENTS
 TYPE NUM

ZV =1
 DIST=.065313
 XF =.040625
 YF =.03125
 ZF =.05
 Z-BUFFER

LINES
 TYPE NUM

ZV =1
 DIST=.065313
 XF =.040625
 YF =.03125
 Z-BUFFER

Figure B.2 - Plasticity spread at collapse for the compact tension specimen

ANSYS 5.2
AUG 30 1997
10:20:15
PLOT NO. 1

ELEMENTS
TYPE NUM
U F

ZV =1
DIST=.11
XF =.1
YF =.05
Z-BUFFER

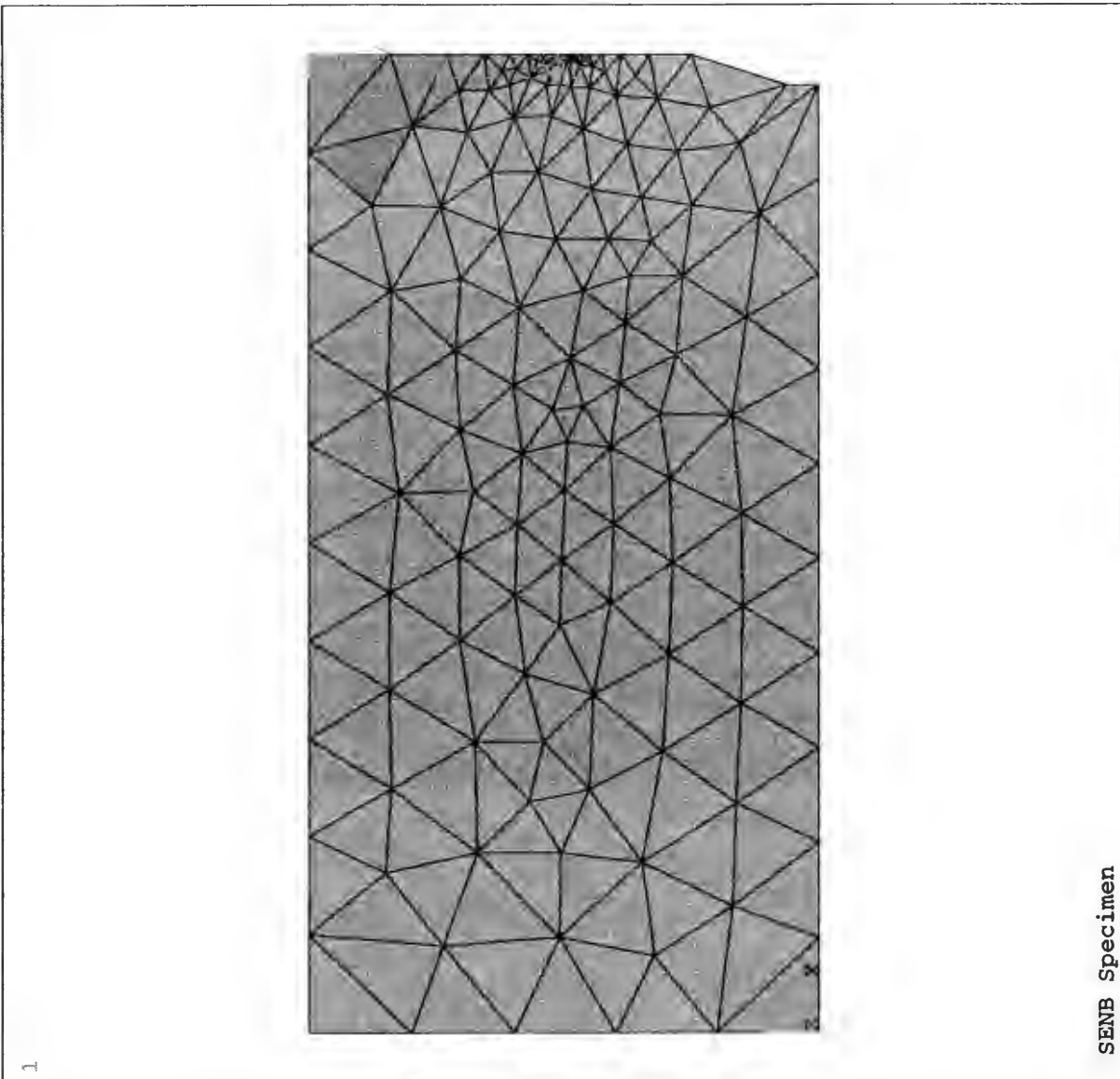


Figure B.3 - Finite element mesh for single edge notched bend specimen



ANSYS 5.2
 NOV 18 1997
 14:46:29
 PLOT NO. 1
 ELEMENTS
 TYPE NUM

ZV =1
 DIST=.11
 XF =.1
 YF =.05
 Z-BUFFER

LINES
 TYPE NUM

ZV =1
 DIST=.11
 XF =.1
 YF =.05
 Z-BUFFER

Figure B.4 - Plasticity spread at collapse for the single edge notched bend specimen

ANSYS 5.2
AUG 30 1997
10:57:18
PLOT NO. 1
ELEMENTS
TYPE NUM
U F
ZV =1
DIST=.055
XF =.025
YF =.05
Z-BUFFER

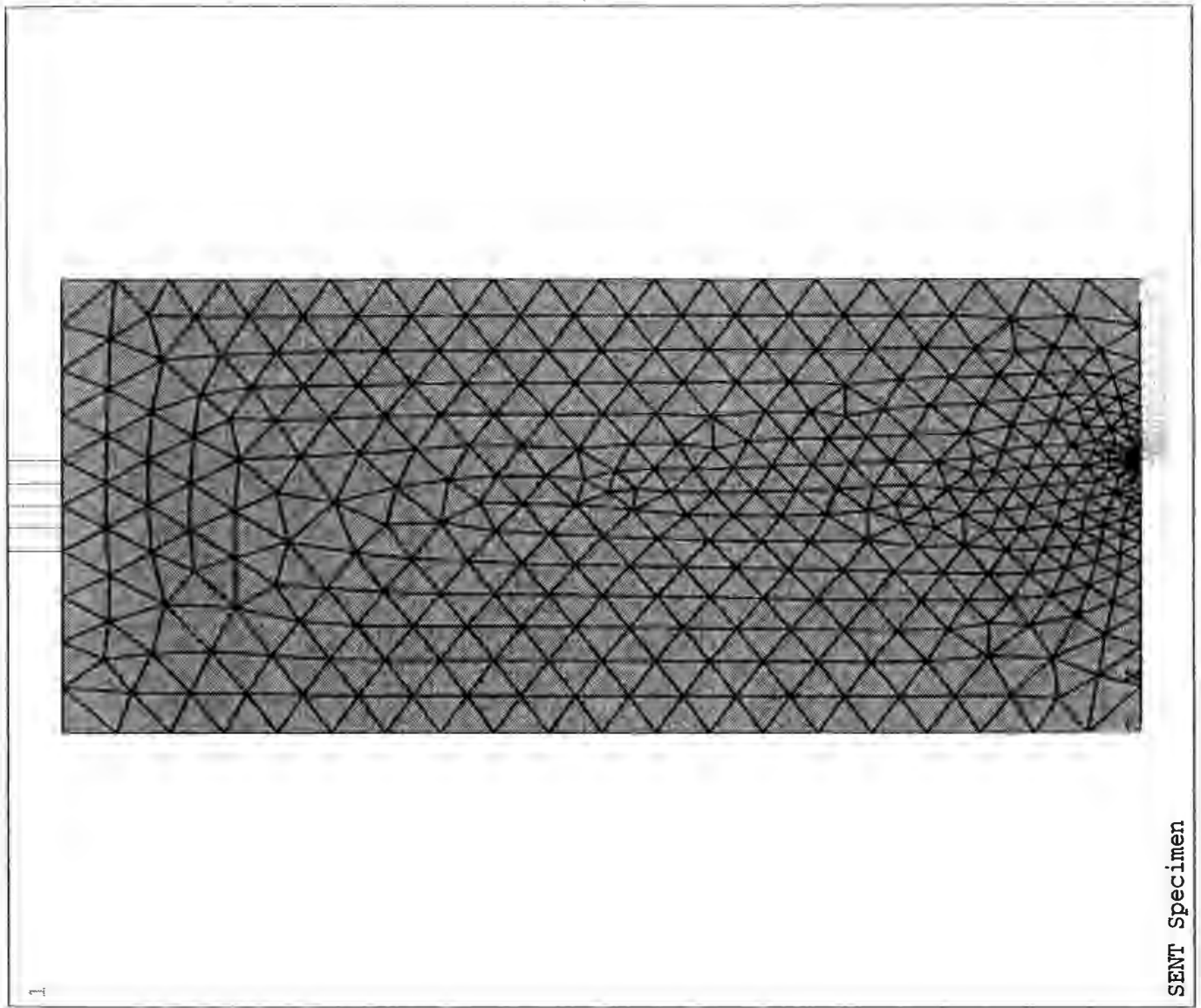


Figure B.5 - Finite element mesh for the single edge notched tension specimen

ANSYS 5.2
NOV 18 1997
14:57:38
PLOT NO. 1
ELEMENTS
TYPE NUM

U
F

ZV =1
DIST=.055
XF =.025
YF =.05
Z-BUFFER

LINES
TYPE NUM

ZV =1
DIST=.055
XF =.025
YF =.05
Z-BUFFER

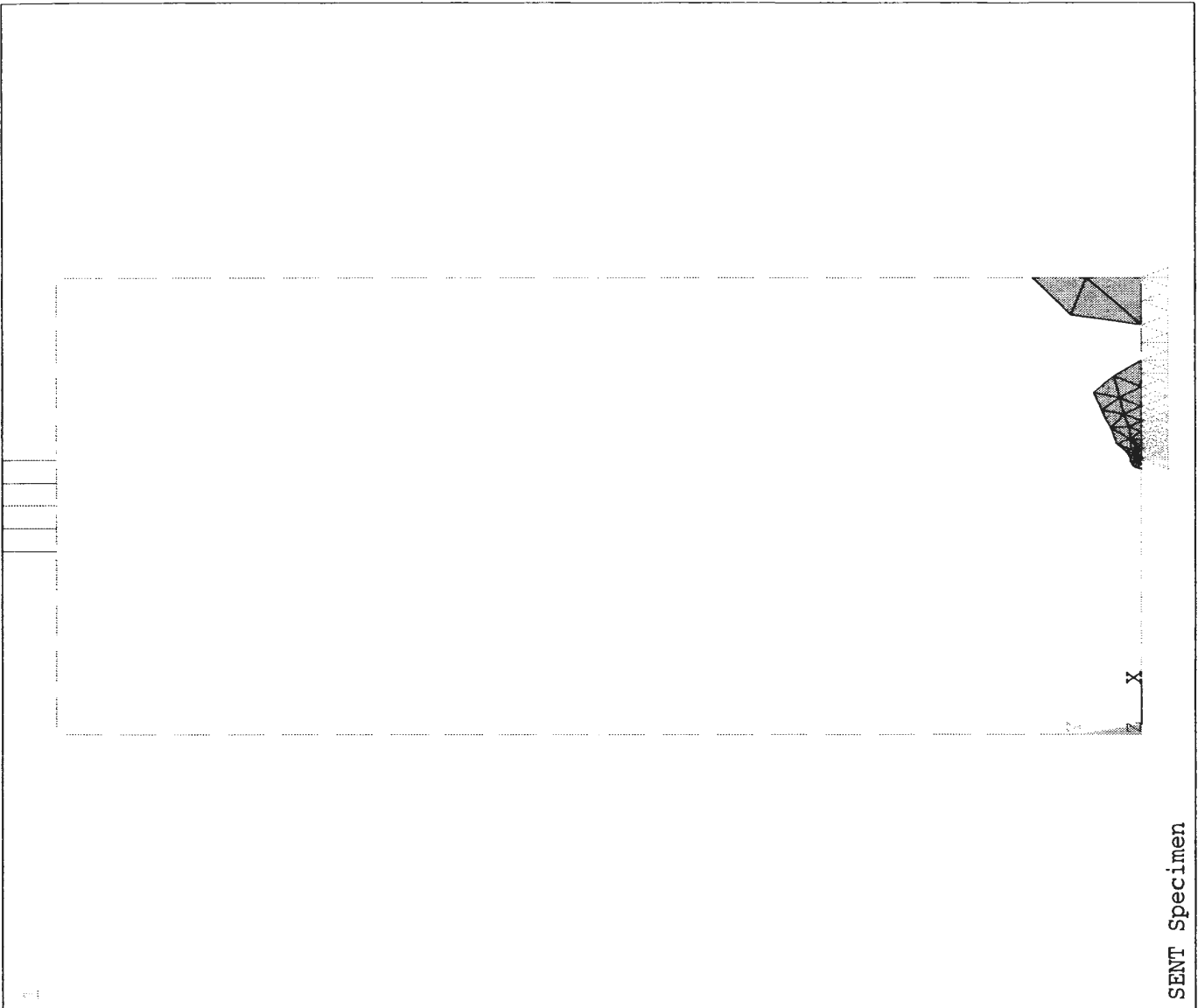
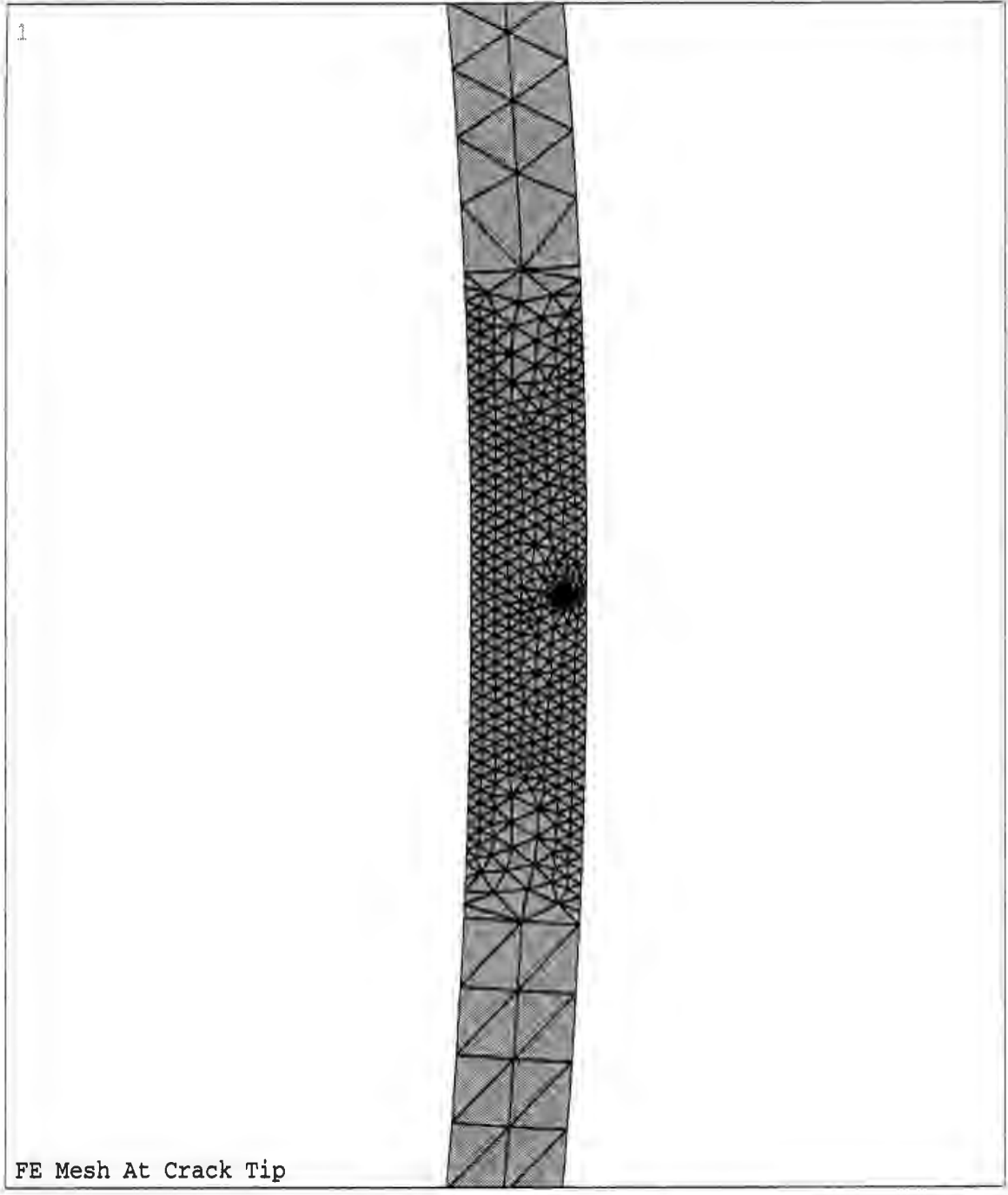


Figure B.6 - Plasticity spread at collapse for the single edge notched tension specimen



ANSYS 5.2
SEP 15 1997
14:34:41
PLOT NO. 1
ELEMENTS
TYPE NUM
U

ZV =1
*DIST=.043113
*XF =.450011
Z-BUFFER

FE Mesh At Crack Tip

Figure B.7 - Finite element mesh (Pipe model, 2 mm deep external defect)

ANSYS 5.2
SEP 15 1997
14:35:33
PLOT NO. 1
ELEMENTS
TYPE NUM

ZV =1
*DIST=.007097
*XF =.452022
*YF =.300E-03
Z-BUFFER

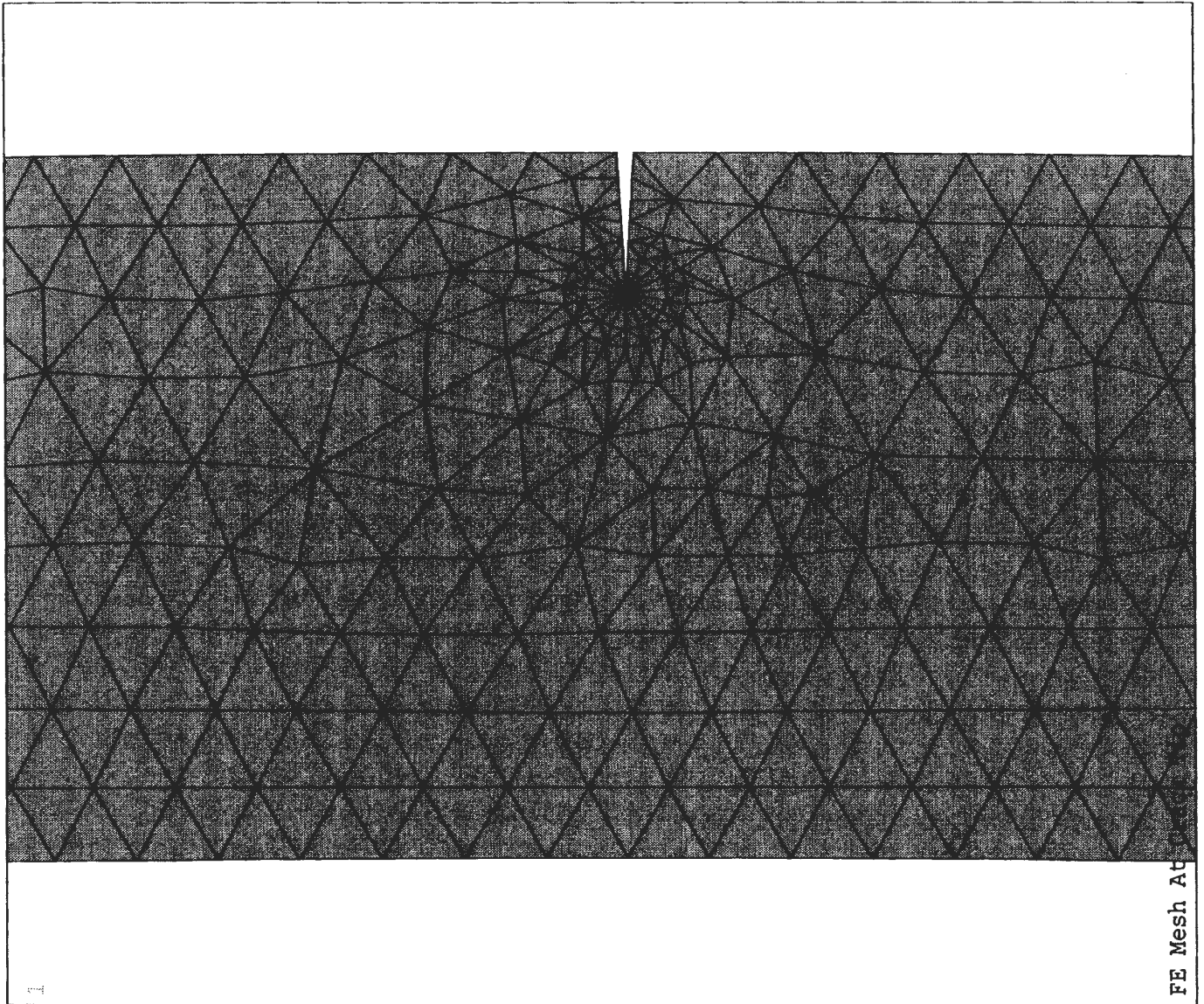


Figure B.8 - Finite element mesh at the crack tip (Pipe model, 2 mm external defect)

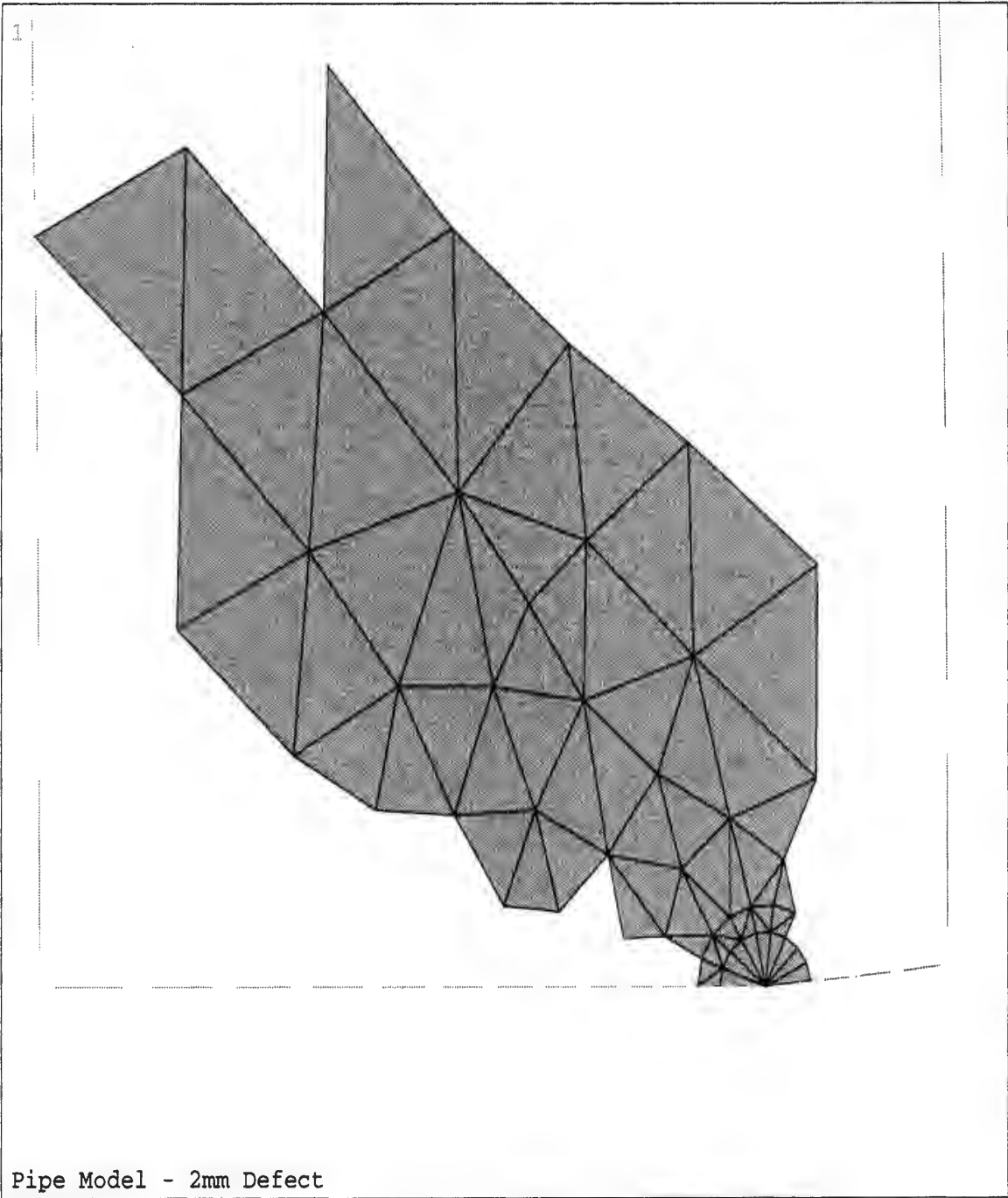


Figure B.9 - Plasticity spread at collapse (Pipe model - 2 mm external defect)

ANSYS 5.2
SEP 15 1997
14:51:30
PLOT NO. 1
ELEMENTS
TYPE NUM
0
ZV =1
*DIST=.036121
*XF =.452342
*YF =-.00233
Z-BUFFER

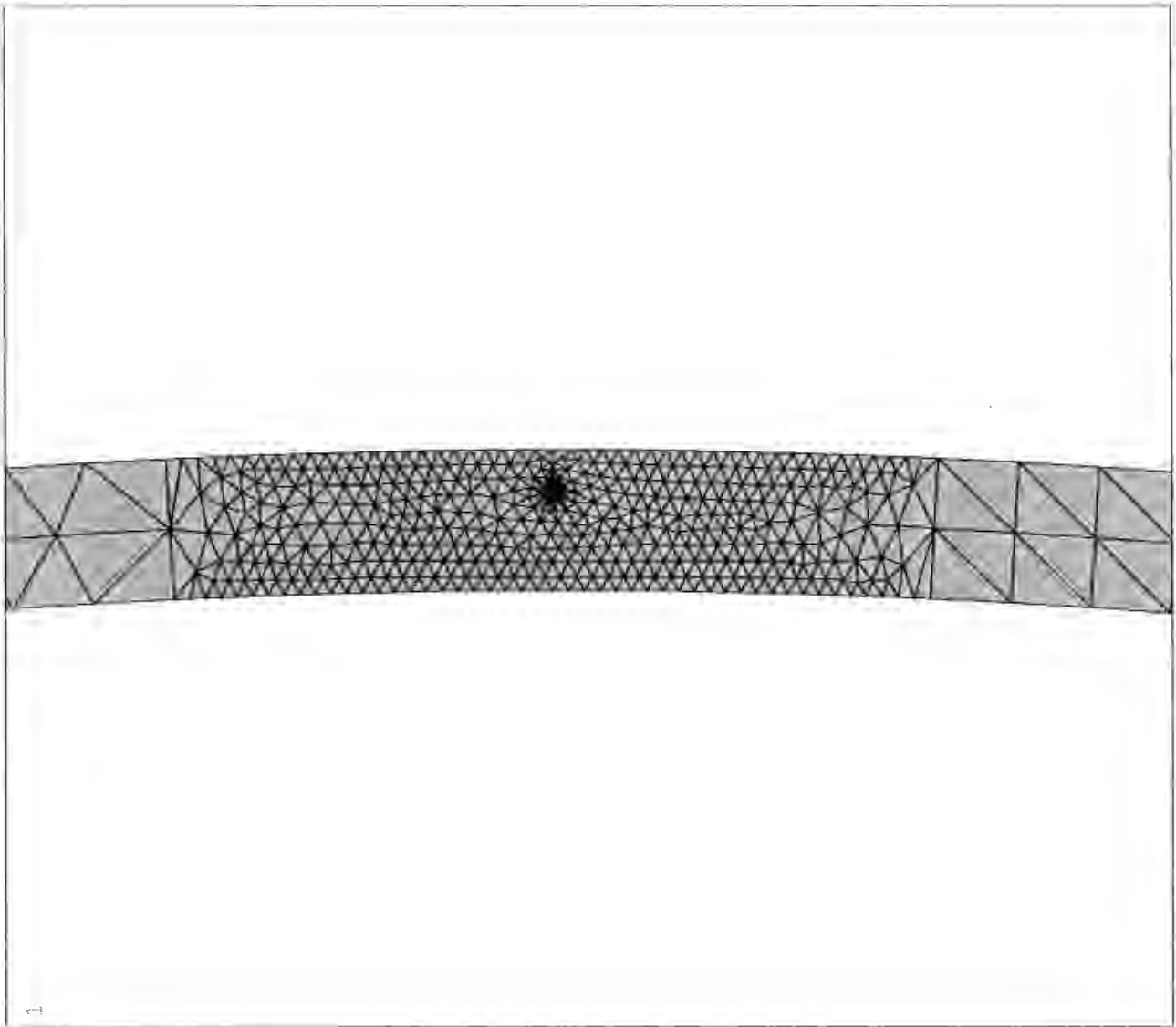


Figure B.10 - Finite element mesh (Pipe model, 3 mm deep external defect)

```
ANSYS 5.2
SEP 15 1997
14:52:10
PLOT NO. 1
ELEMENTS
TYPE NUM
U
ZV =1
*DIST=.007118
*XF =.451849
*YF =.181E-03
Z-BUFFER
```

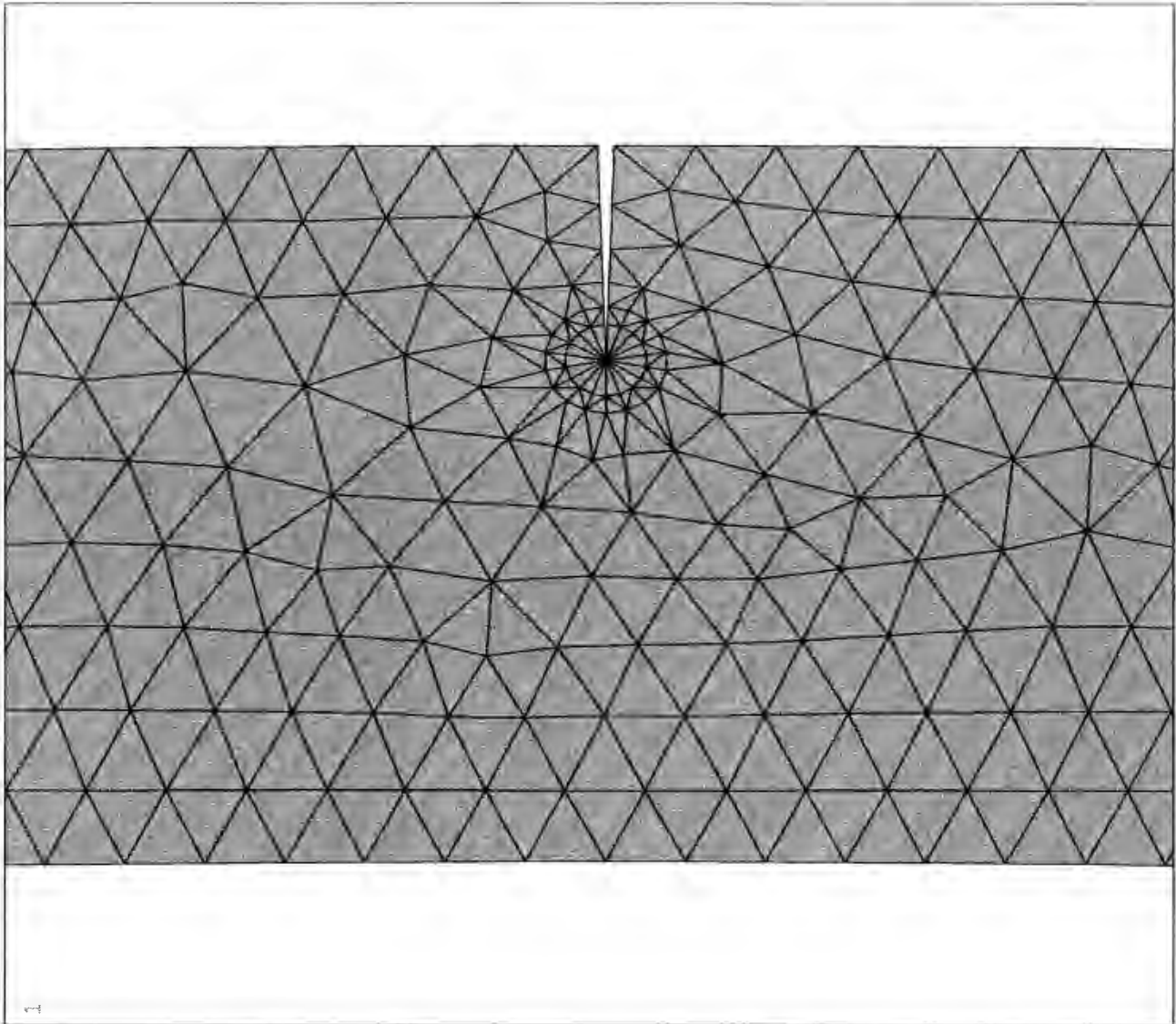
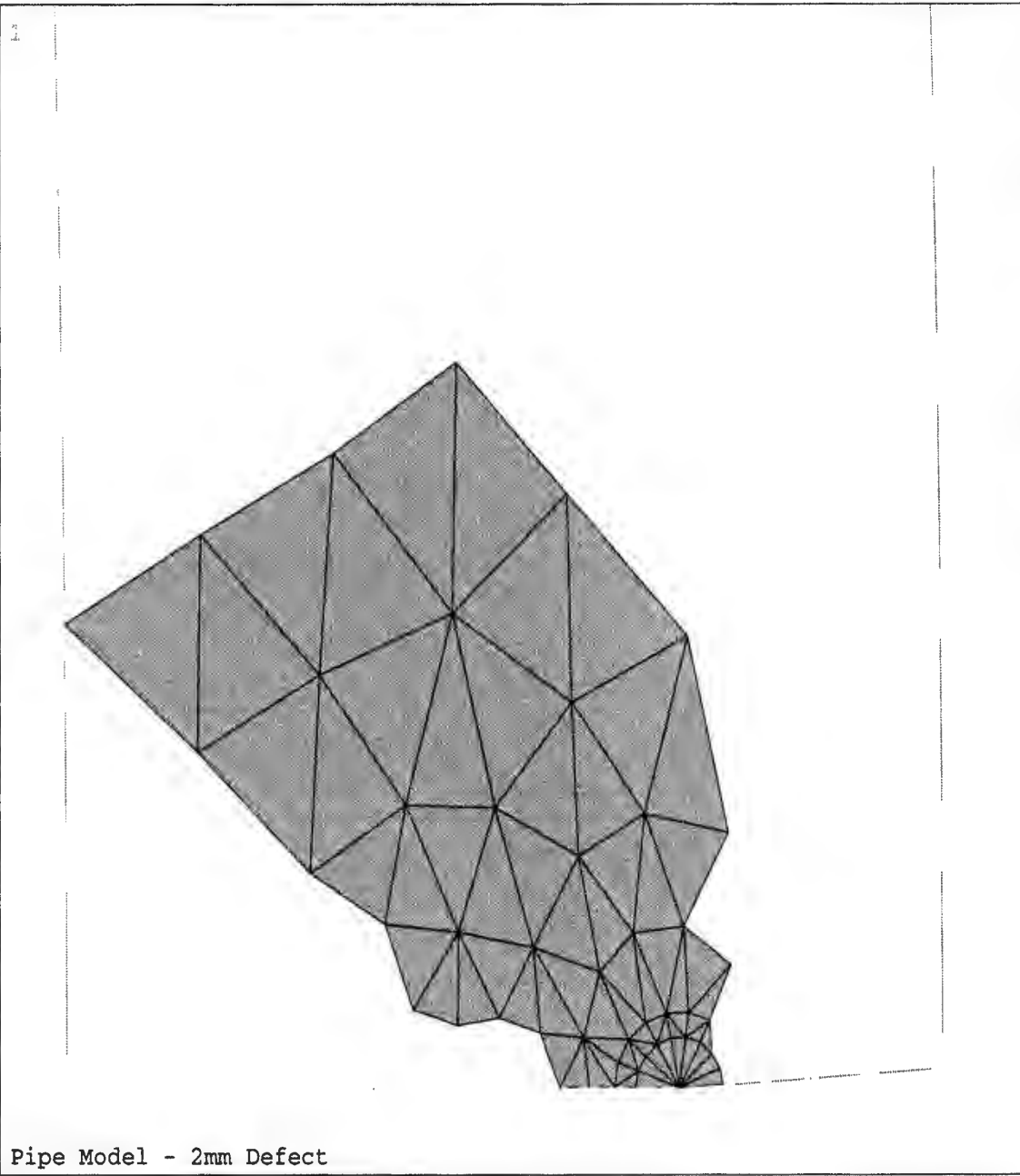


Figure B.11 - Finite element mesh at the crack tip (Pipe model, 3 mm external defect)



ANSYS 5.2
 NOV 20 1997
 09:59:54
 PLOT NO. 1
 ELEMENTS
 TYPE NUM

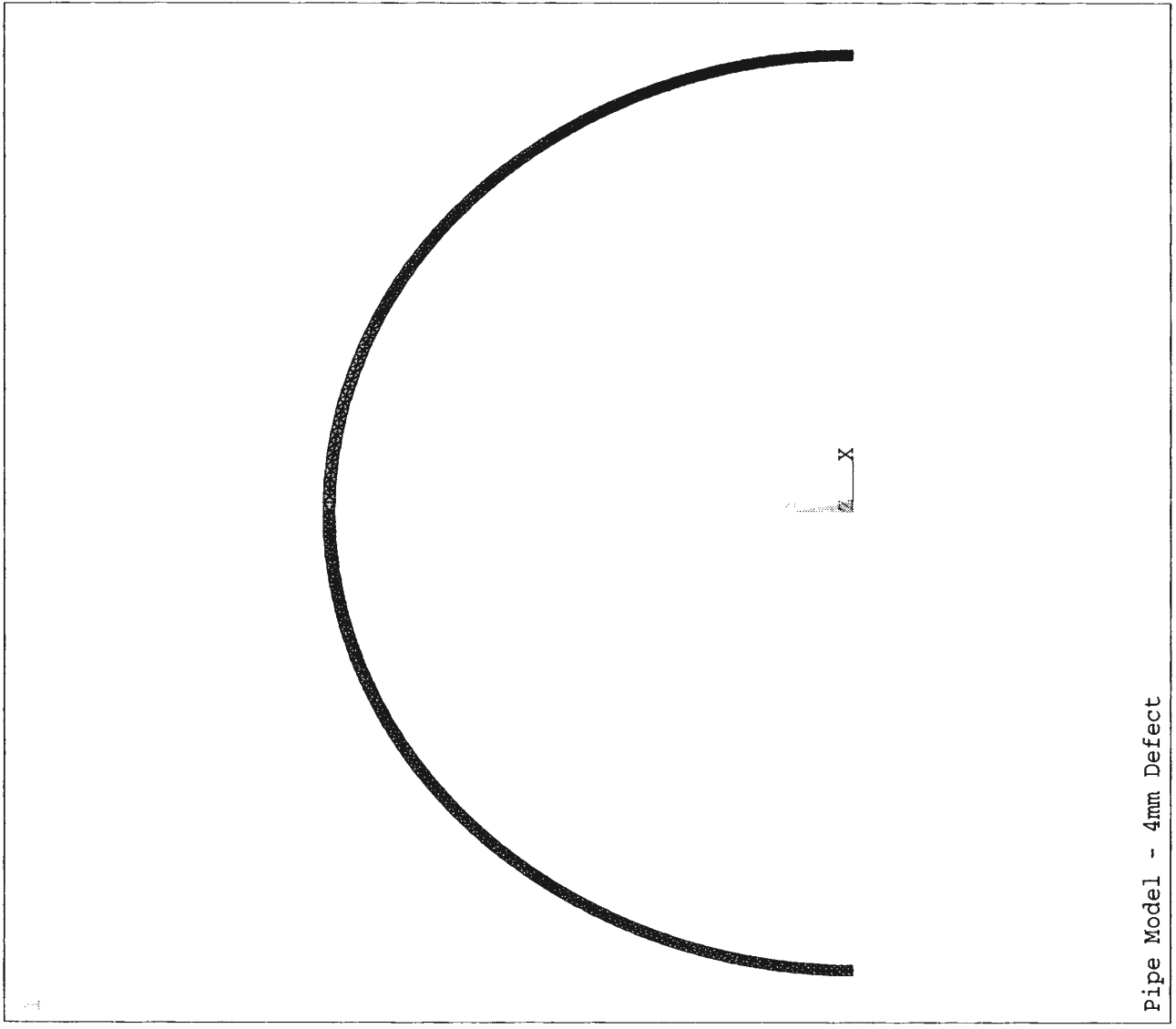
ZV =1
 *DIST=.005837
 *XF =.452074
 *YF =.004965
 Z-BUFFER

LINES
 TYPE NUM

ZV =1
 *DIST=.005837
 *XF =.452074
 *YF =.004965
 Z-BUFFER

Figure B.12 - Plasticity spread at collapse (Pipe model, 3 mm deep external defect

ANSYS 5.2
NOV 20 1997
13:24:07
PLOT NO. 1
ELEMENTS
TYPE NUM
ZV =1
DIST=.5027
YF =.2285
Z-BUFFER



Pipe Model - 4mm Defect

Figure B.13 - Finite element mesh (Pipe model, 4 mm deep external defect)

ANSYS 5.2
NOV 20 1997
13:25:39
PLOT NO. 1
ELEMENTS
TYPE NUM
ZV =1
*DIST=.00541
*XF =.451889
*YF =.003664
Z-BUFFER

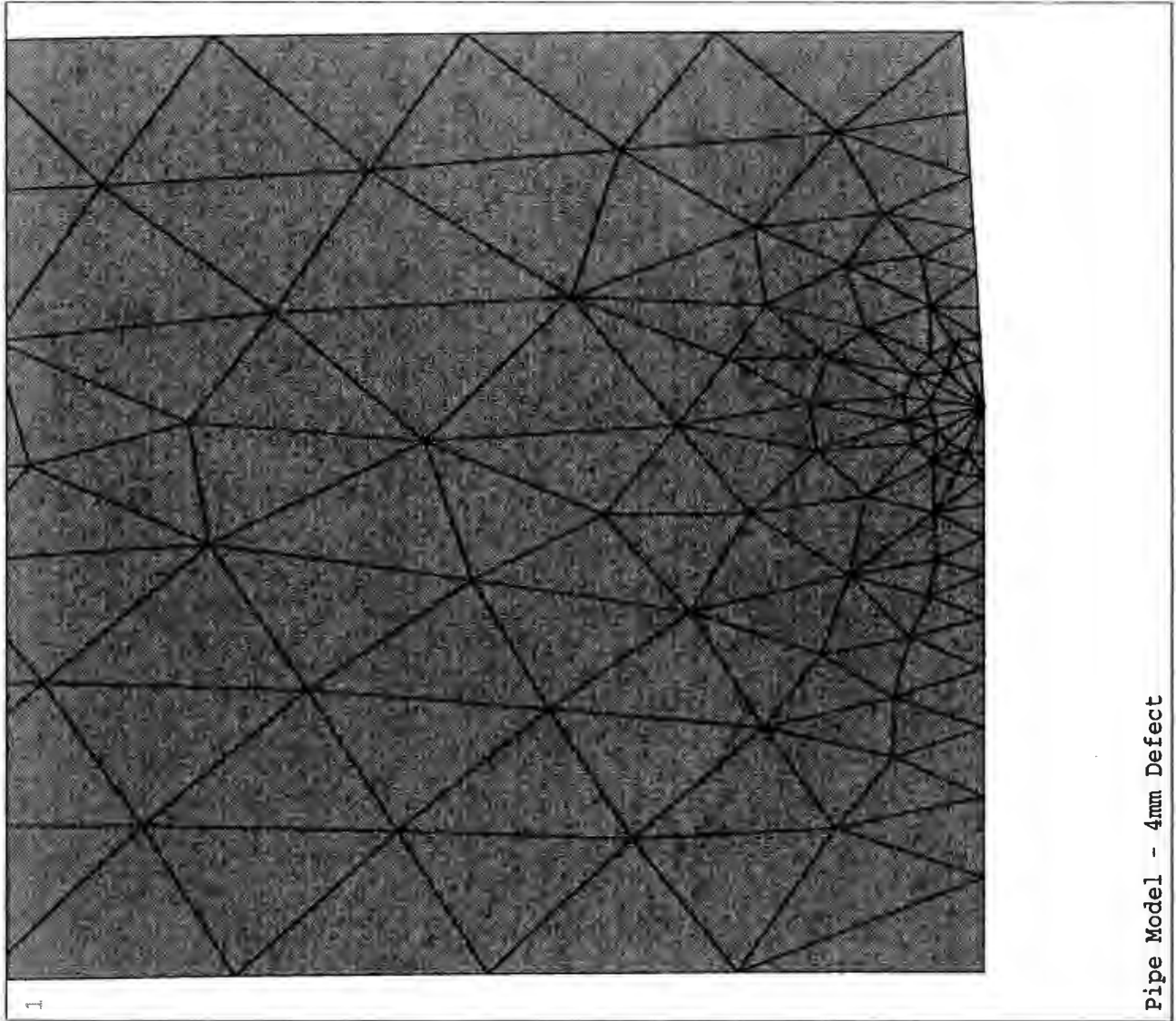
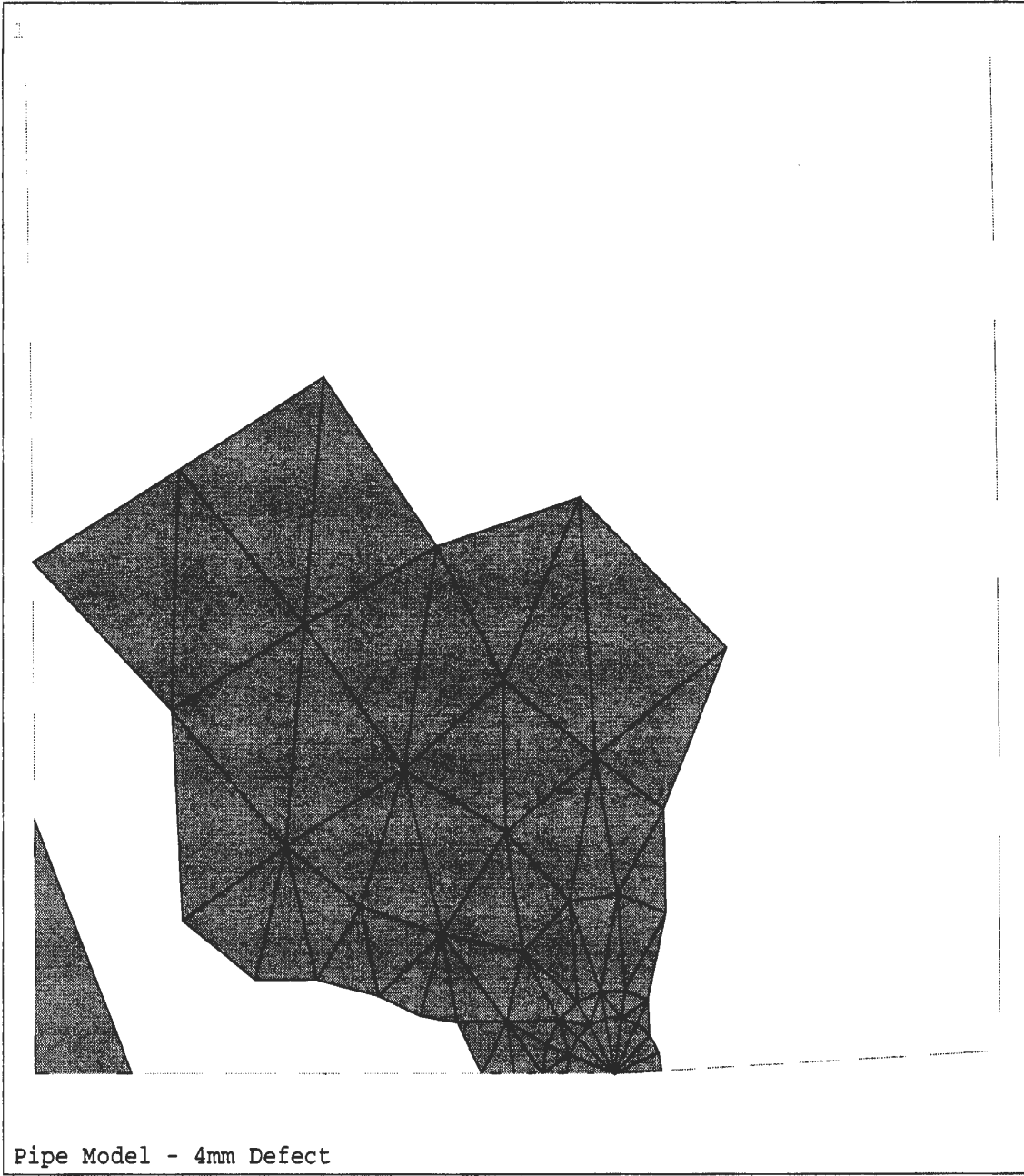


Figure B.14 - Finite element mesh at the crack tip (Pipe model, 4 mm external defect)



ANSYS 5.2
NOV 20 1997
10:19:13
PLOT NO. 1
ELEMENTS
TYPE NUM

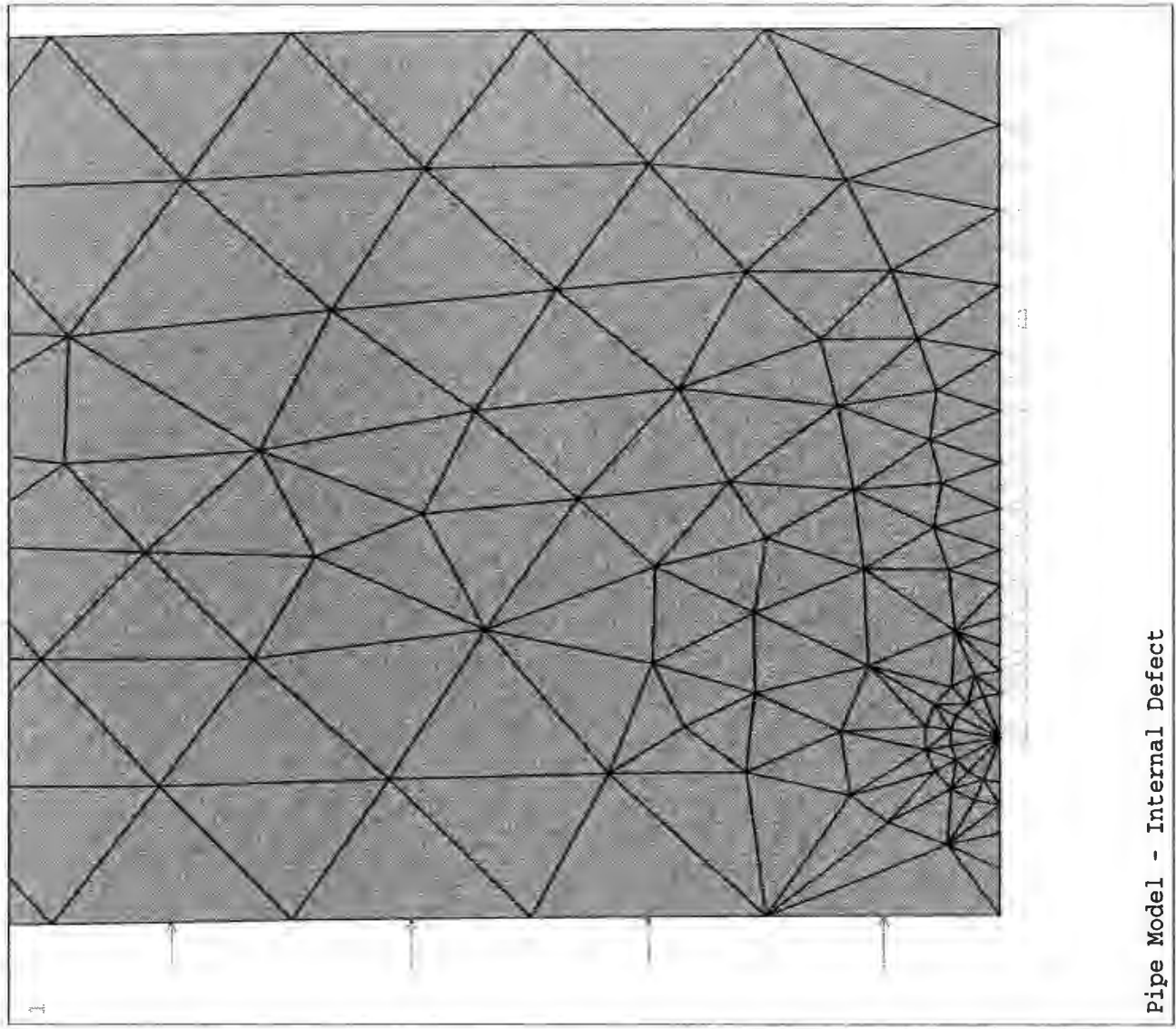
ZV =1
*DIST=.005296
*XF =.451963
*YF =.004384
Z-BUFFER

LINES
TYPE NUM

ZV =1
*DIST=.005296
*XF =.451963
*YF =.004384
Z-BUFFER

Figure B.15 - Plasticity spread at collapse (Pipe model, 4 mm deep external defect)

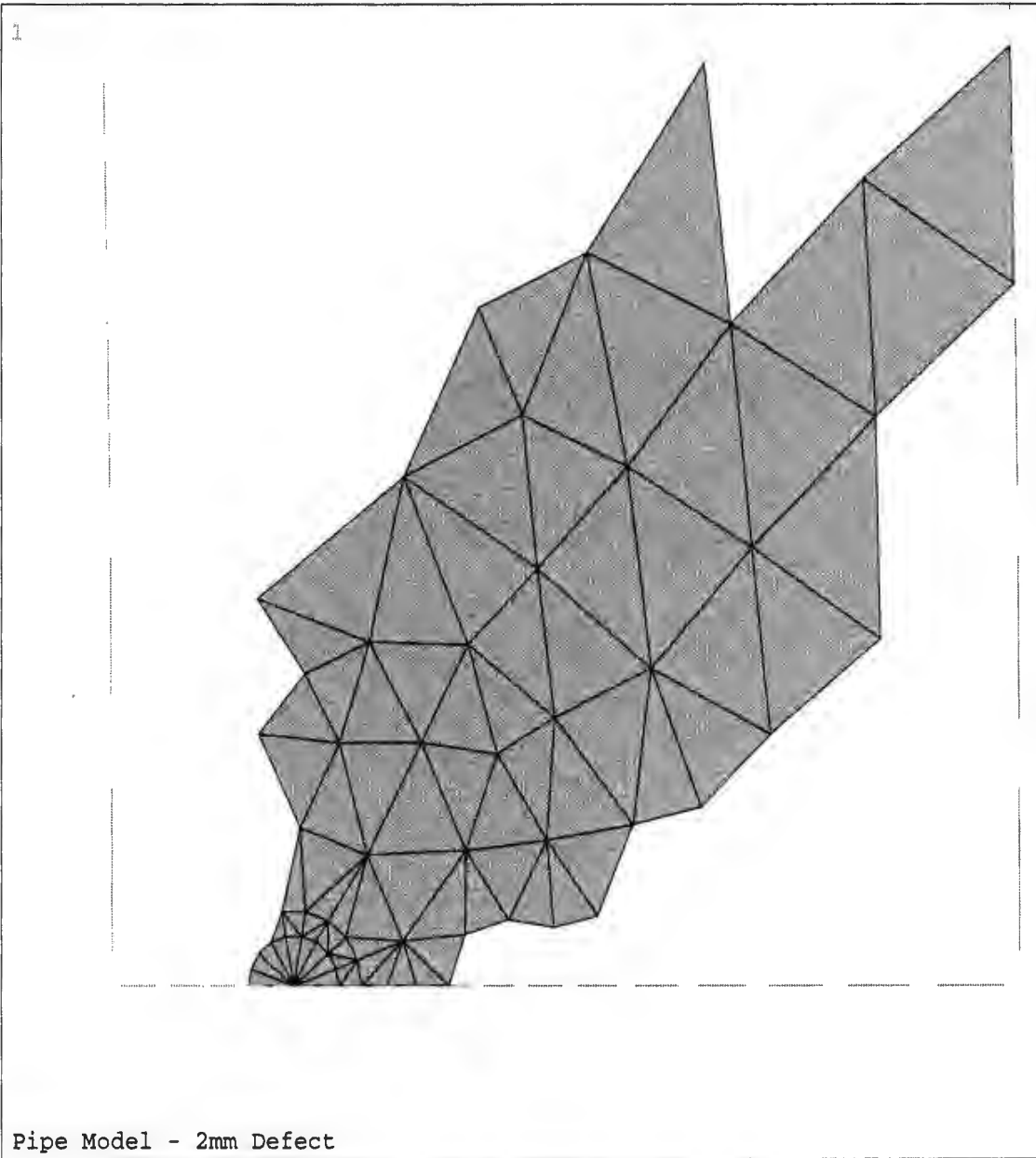
ANSYS 5.2
NOV 20 1997
13:41:39
PLOT NO. 1
ELEMENTS
TYPE NUM
U
PRES
ZV =1
*DIST=.005736
*XF =.451518
*YF =.004012
Z-BUFFER



Pipe Model - Internal Defect

Figure B.16 - Finite element mesh at crack tip (Pipe model, 2 mm internal defect)

Figure B.17 - Plasticity spread at collapse (Pipe model, 2 mm deep internal defect)



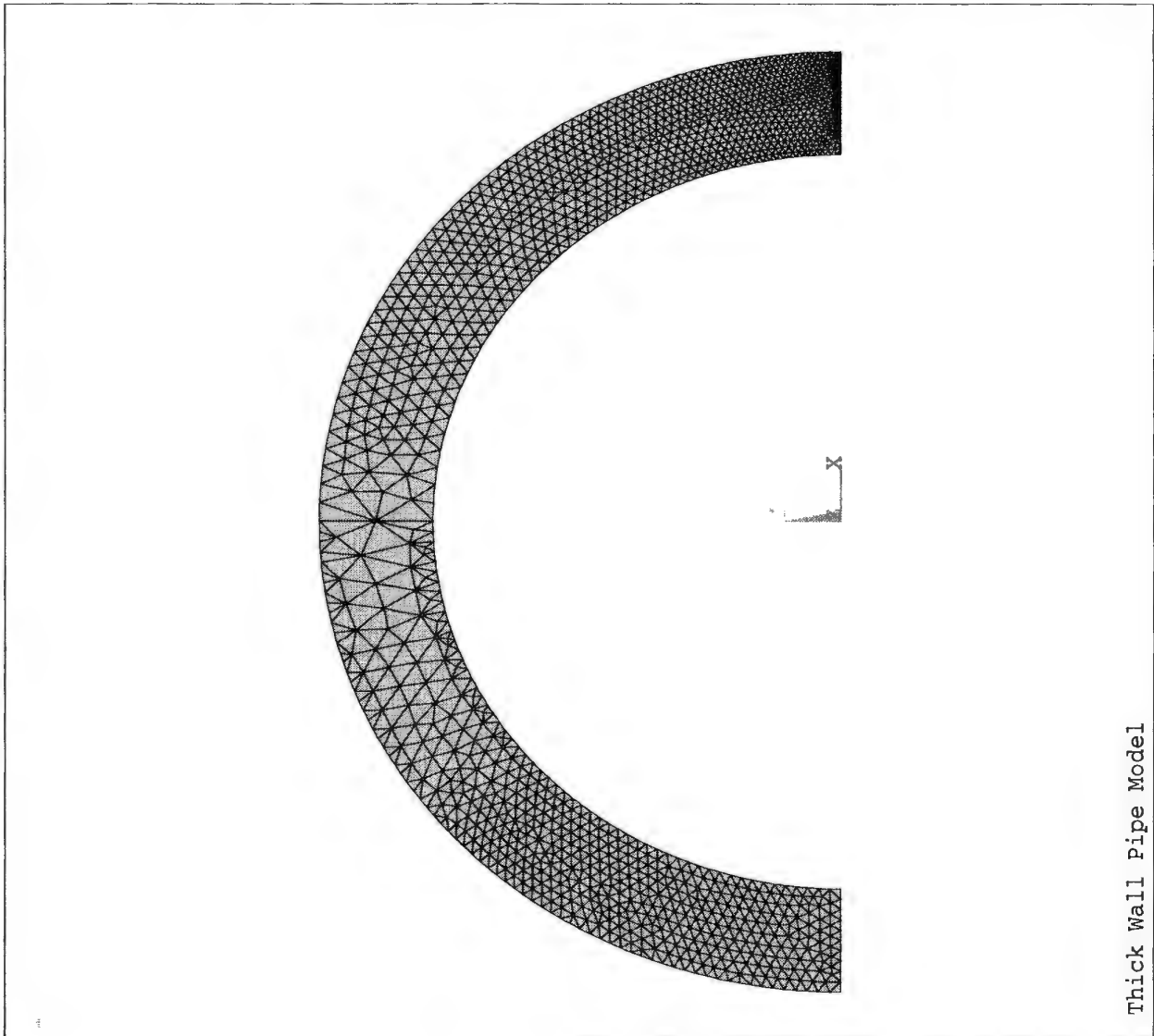
ANSYS 5.2
NOV 20 1997
13:47:16
PLOT NO. 1
ELEMENTS
TYPE NUM

ZV =1
*DIST=.005736
*XF =.451518
*YF =.004012
Z-BUFFER

LINES
TYPE NUM

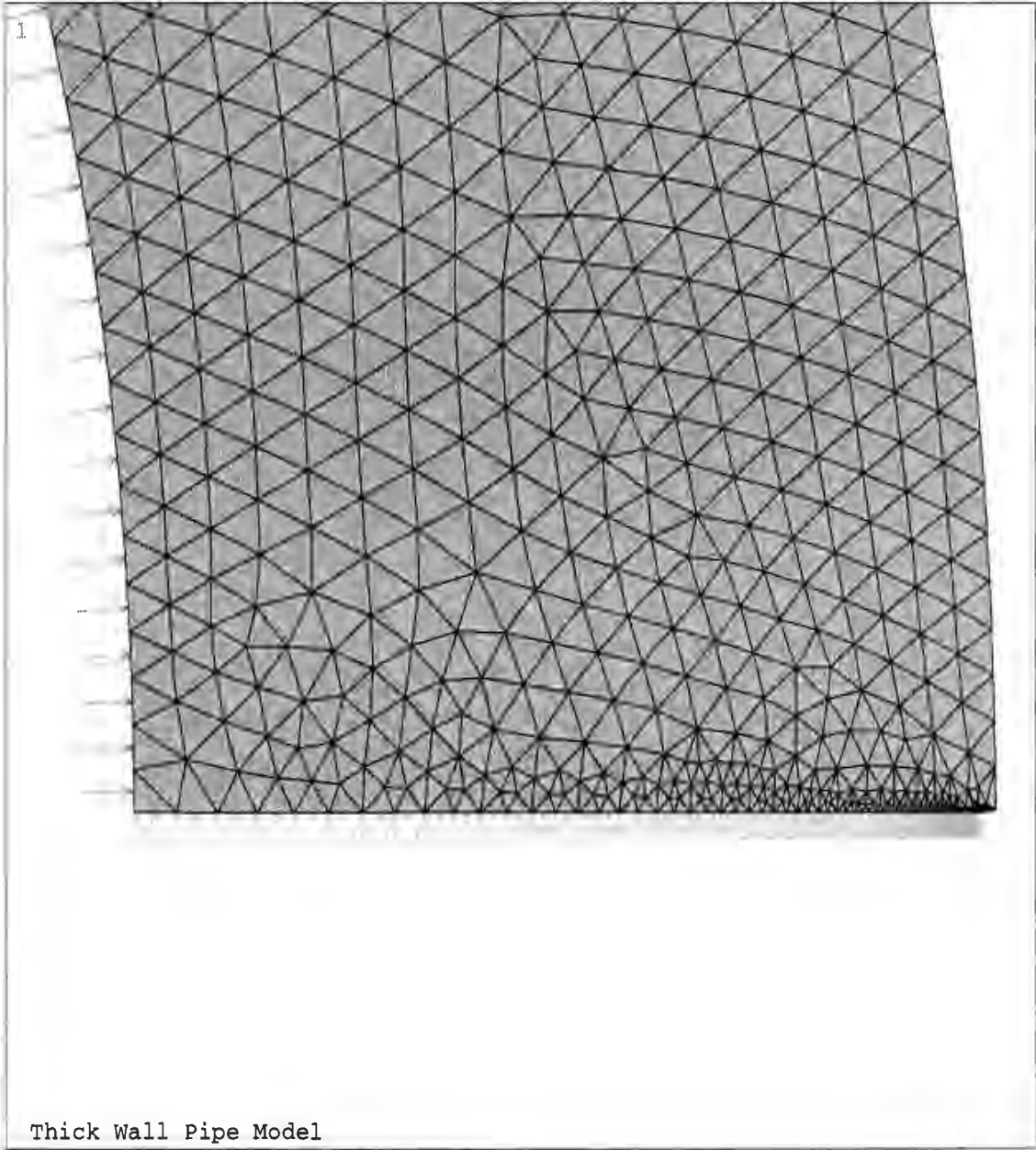
ZV =1
*DIST=.005736
*XF =.451518
*YF =.004012
Z-BUFFER

ANSYS 5.2
NOV 20 1997
15:09:54
PLOT NO. 1
ELEMENTS
TYPE NUM
ZV =1
DIST=.5027
YF =.2285
Z-BUFFER



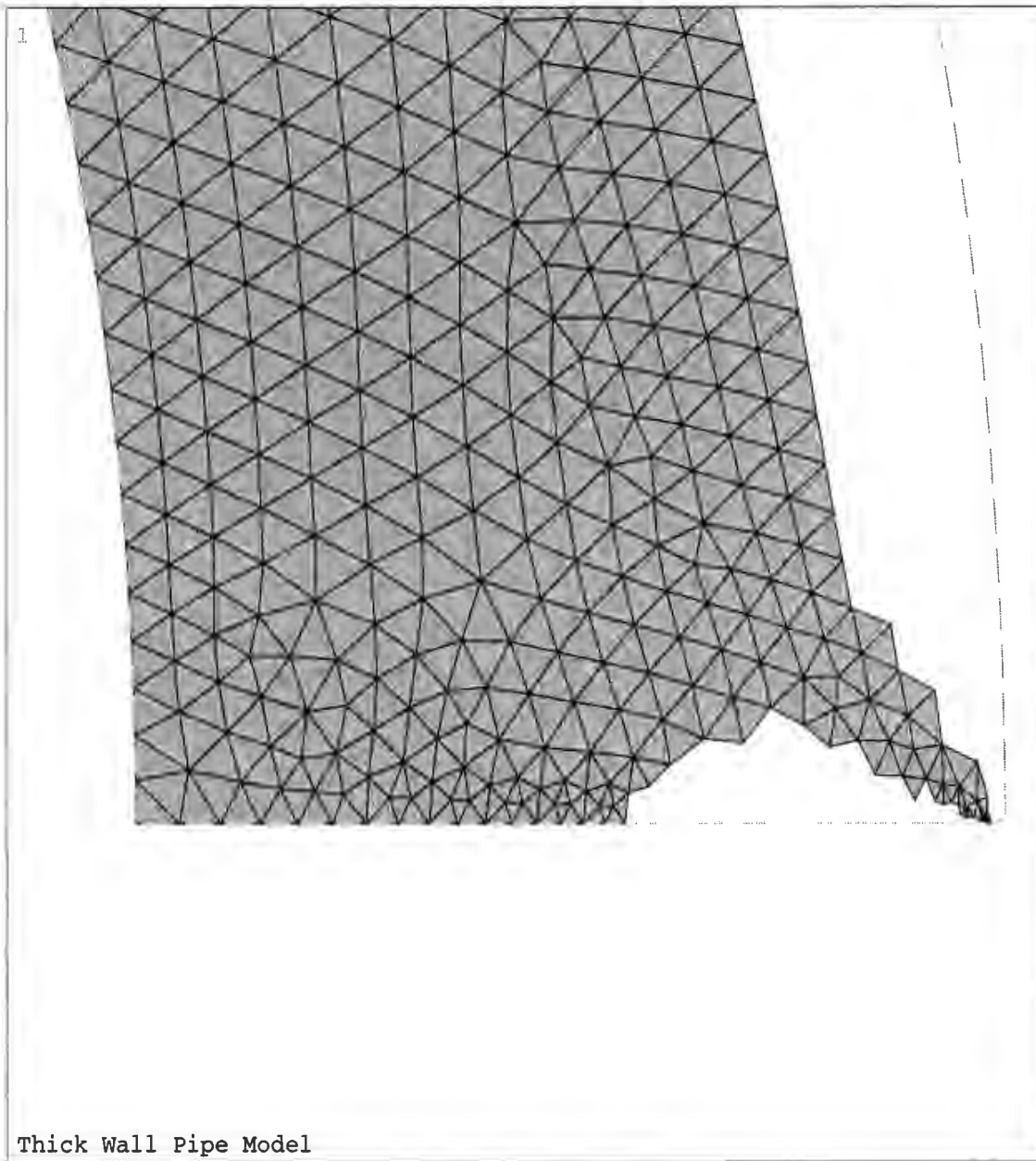
Thick Wall Pipe Model

Figure B.18 - Finite element mesh (Thick walled pipe model)



```
ANSYS 5.2  
NOV 20 1997  
15:12:25  
PLOT NO. 1  
ELEMENTS  
TYPE NUM  
U  
PRES  
  
ZV =1  
*DIST=.059721  
*XF =.401921  
*YF =.024617  
Z-BUFFER
```

Figure B.19 - Finite element mesh at crack tip (Thick walled pipe model)



```
ANSYS 5.2  
NOV 20 1997  
15:33:47  
PLOT NO. 1  
ELEMENTS  
TYPE NUM
```

```
ZV =1  
*DIST=.059721  
*XF =.401921  
*YF =.024617  
Z-BUFFER
```

```
LINES  
TYPE NUM
```

```
ZV =1  
*DIST=.059721  
*XF =.401921  
*YF =.024617  
Z-BUFFER
```

Figure B.20 - Plasticity spread at collapse (Thick walled pipe model)

ANSYS 5.2
NOV 20 1997
15:46:52
PLOT NO. 1
ELEMENTS
TYPE NUM
ZV =1
DIST=.5027
Z-BUFFER

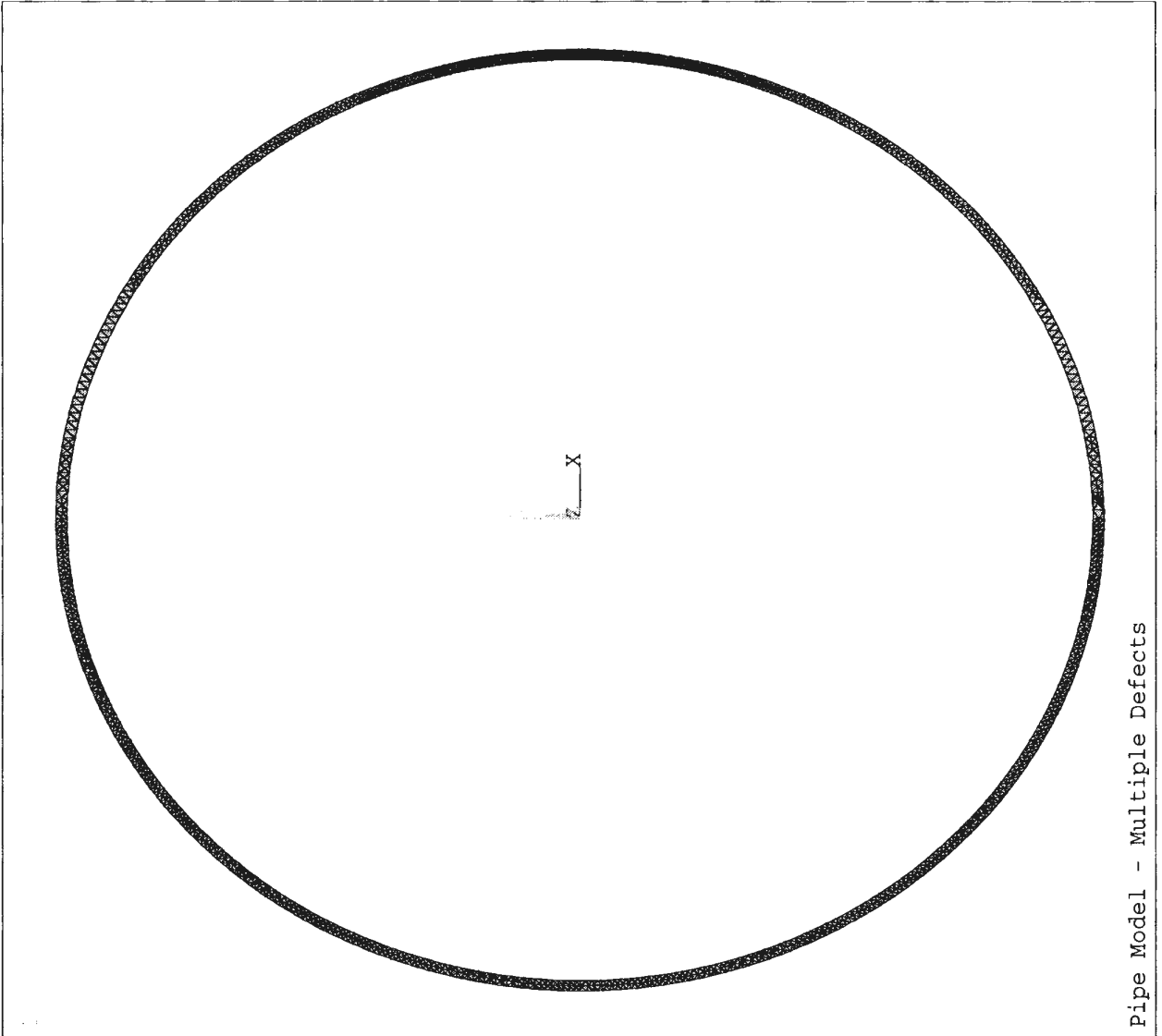


Figure B.21 - Finite element mesh (Multiple defects, Model 1)

```
ANSYS 5.2
NOV 20 1997
15:49:23
PLOT NO. 1
ELEMENTS
TYPE NUM 0
PRES
ZV =1
*DIST=.012348
*XF =.451668
*YF =.533E-04
Z-BUFFER
```

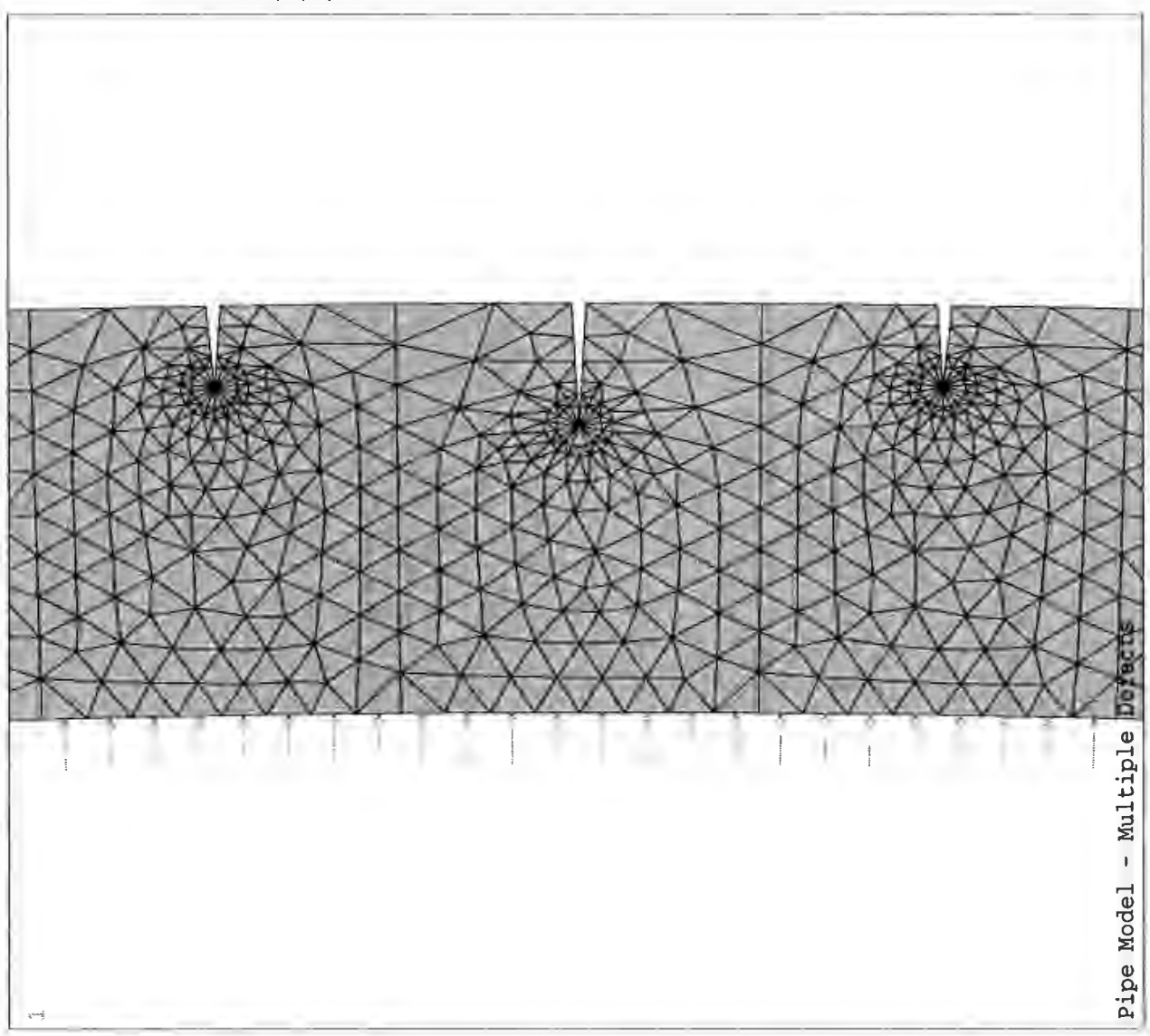
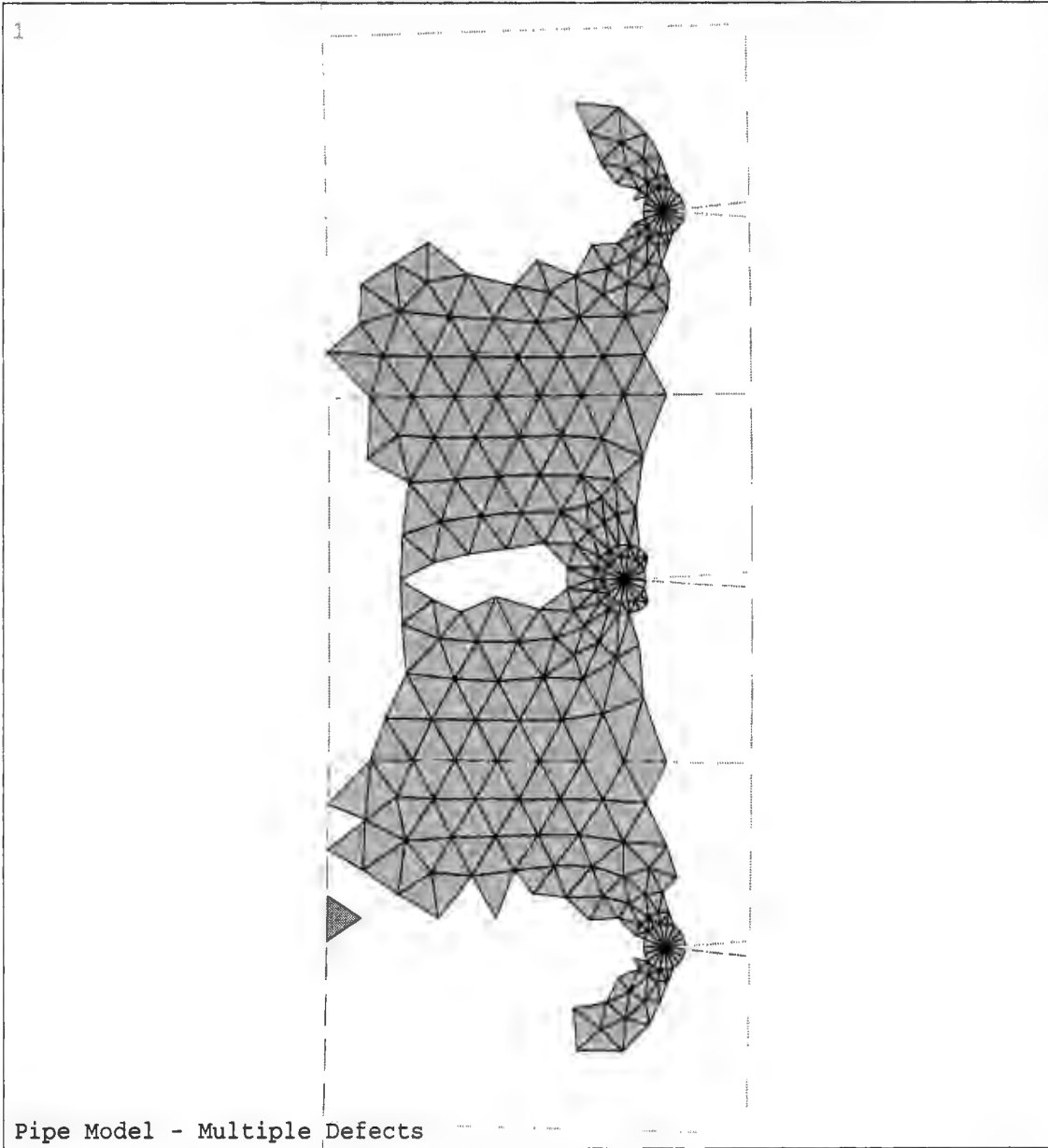


Figure B.22 - Finite element mesh at the crack tip (Multiple defects, Model 1)



ANSYS 5.2
 NOV 20 1997
 16:34:22
 PLOT NO. 1
 ELEMENTS
 TYPE NUM

ZV =1
 *DIST=.012348
 *XF =.451668
 *YF =.533E-04
 Z-BUFFER

LINES
 TYPE NUM

ZV =1
 *DIST=.012348
 *XF =.451668
 *YF =.533E-04
 Z-BUFFER

Figure B.23 - Plasticity spread at collapse (Multiple defects, Model 1)

ANSYS 5.2
NOV 20 1997
16:46:24
PLOT NO. 1
ELEMENTS
TYPE NUM

ZV =1
DIST=.5027
YF =.2285
Z-BUFFER

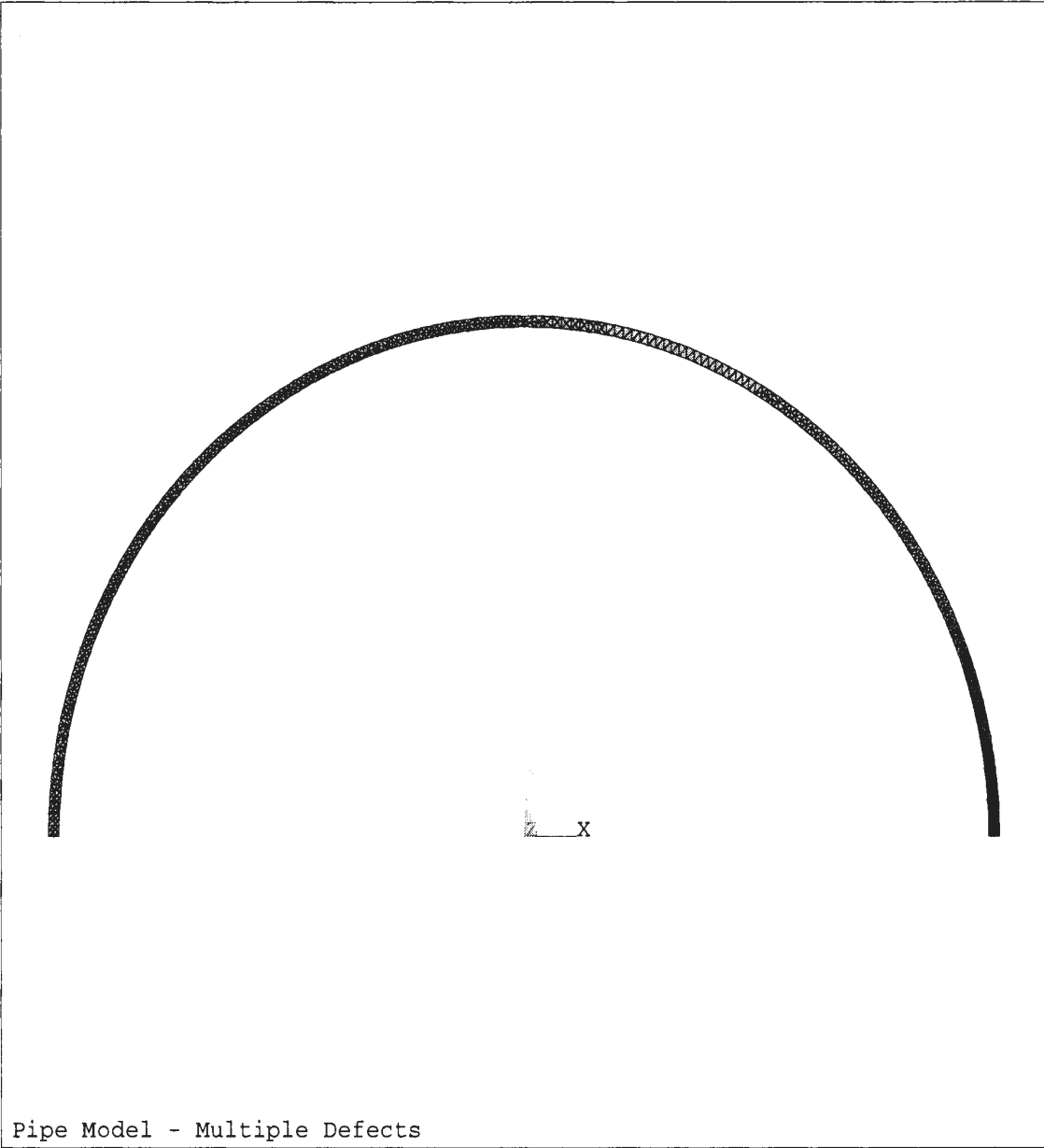
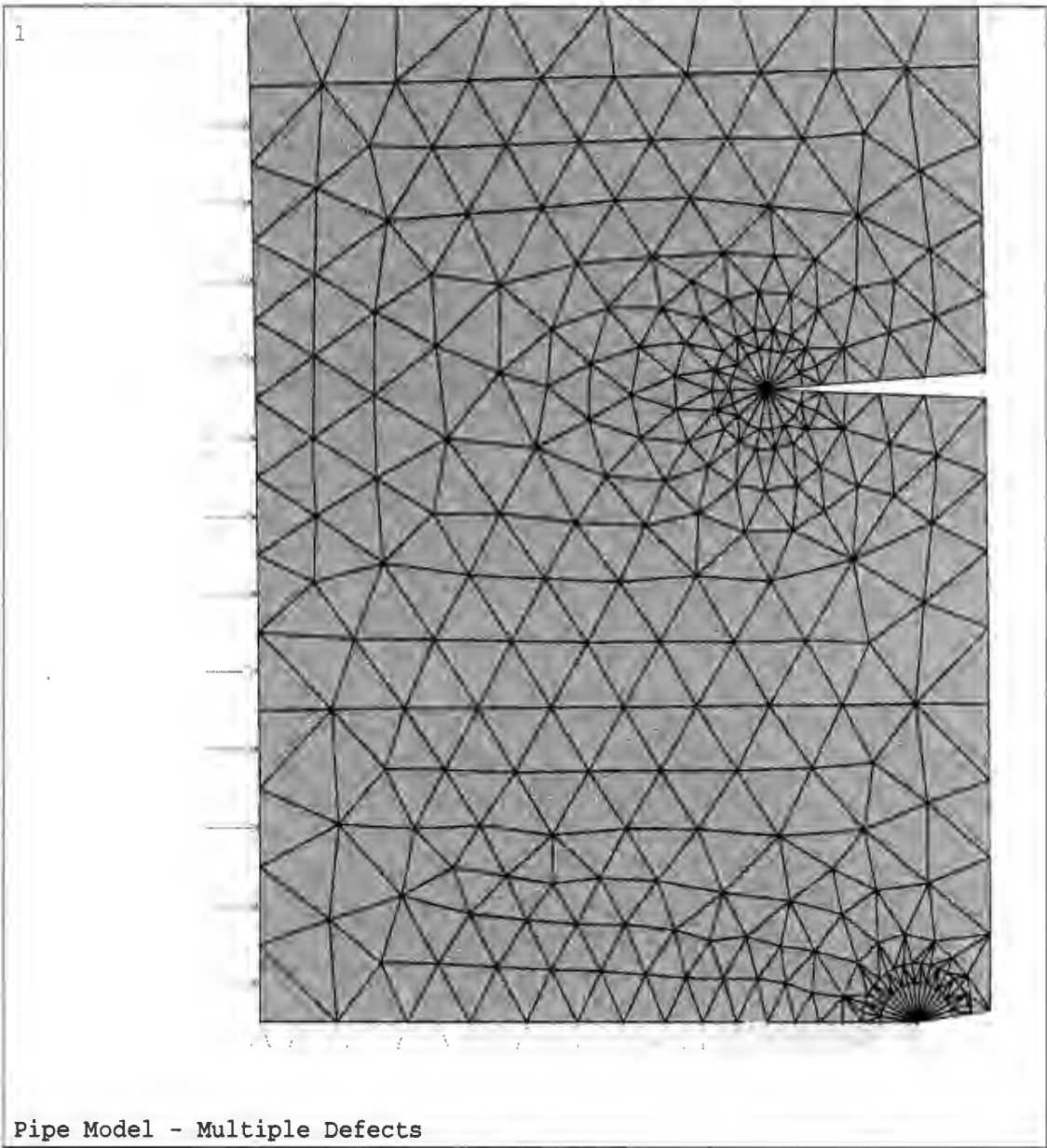


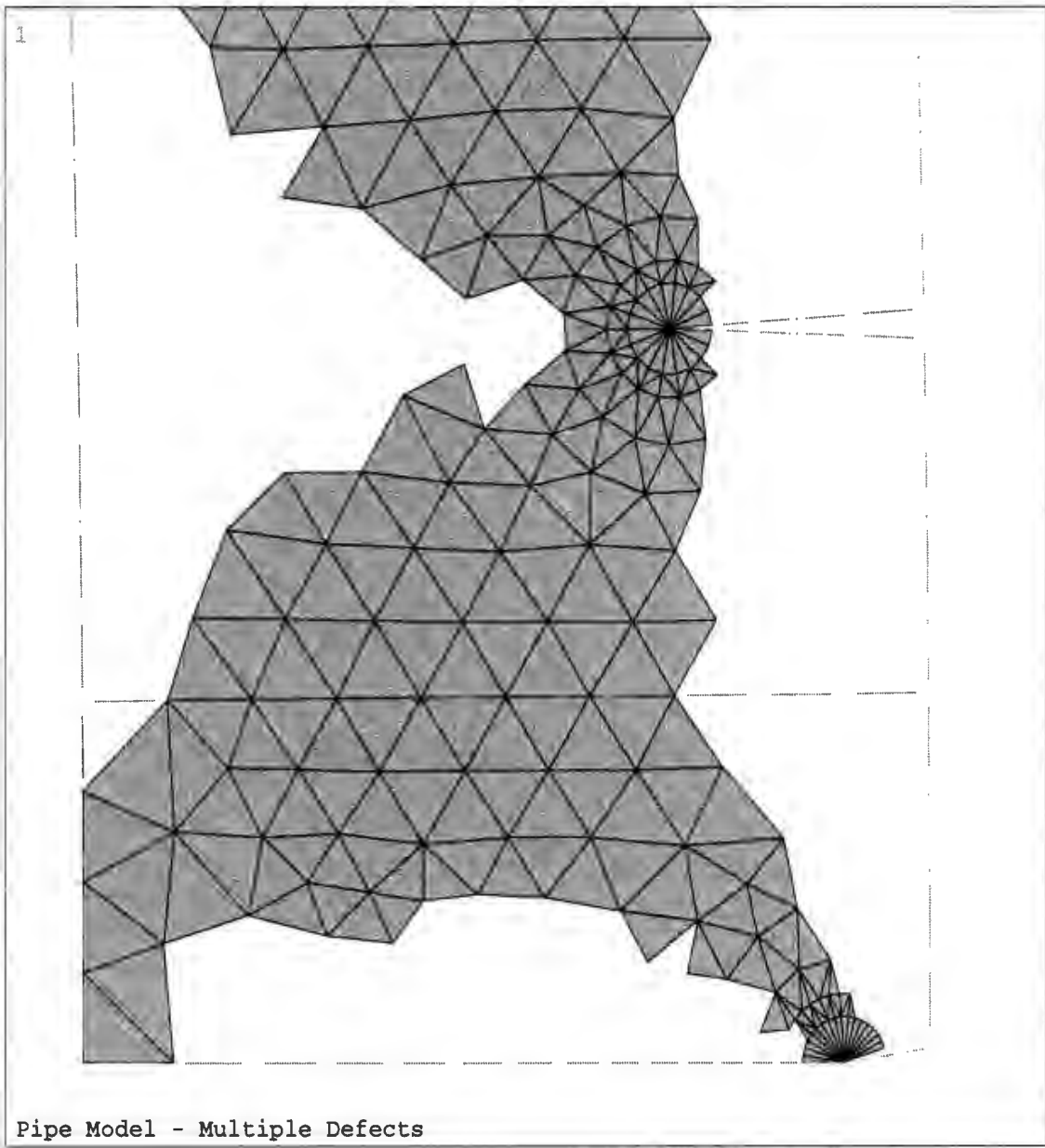
Figure B.24 - Finite element mesh (Multiple defects, Model 2)



```
ANSYS 5.2  
NOV 20 1997  
16:52:57  
PLOT NO. 1  
ELEMENTS  
TYPE NUM  
U  
PRES  
  
ZV =1  
*DIST=.007134  
*XF =.450629  
*YF =.005558  
Z-BUFFER
```

Figure B.25 - Finite element mesh at the crack tip (Multiple defects, Model 2)

Figure B.26 - Plasticity spread at collapse (Multiple defects, Model 2)



ANSYS 5.2
NOV 20 1997
17:48:12
PLOT NO. 1
ELEMENTS
TYPE NUM

ZV =1
*DIST=.006151
*XF =.452226
*YF =.005237
Z-BUFFER

LINES
TYPE NUM

ZV =1
*DIST=.006151
*XF =.452226
*YF =.005237
Z-BUFFER

APPENDIX C

Full Stress Distributions and R-node Plots for Pipe Models

Stress Distribution - 2 mm Defect
Softening Exponent $q = 0.1$

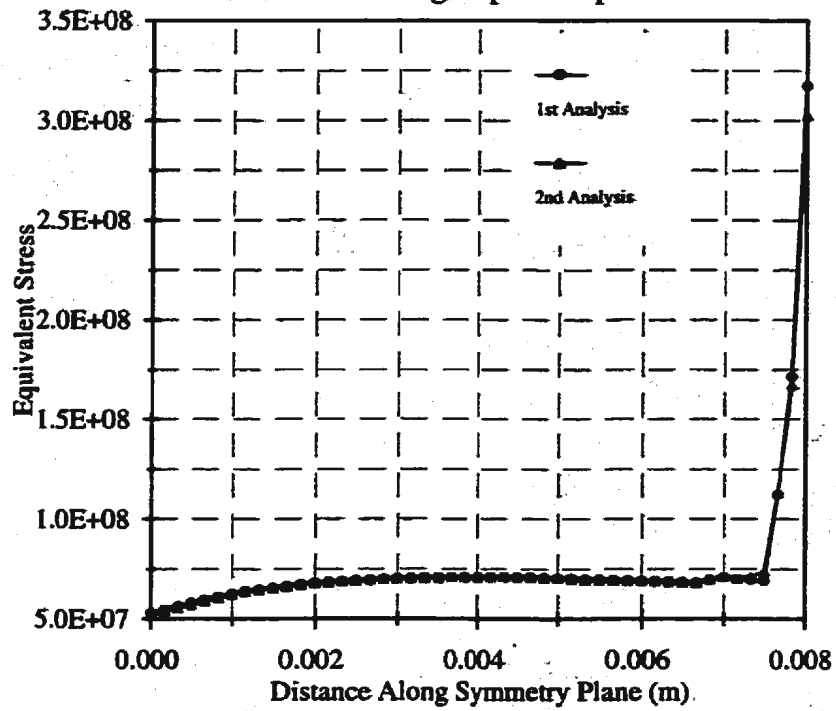


Figure C.1 - Stress distributions along uncracked ligament (Pipe model, 2 mm deep external defect).

Stress Distribution - 3 mm Defect
Softening Exponent $q = 0.1$

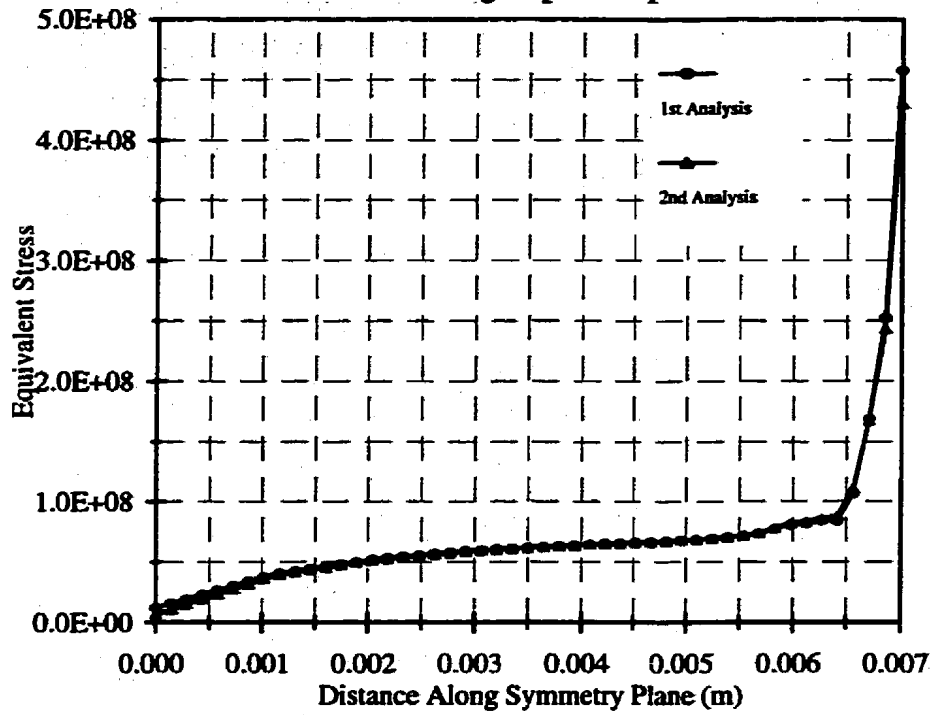


Figure C.2 - Stress distributions along uncracked ligament (Pipe model, 3 mm deep external defect)

Stress Distribution - 4 mm Defect
Softening Exponent $q = 0.1$

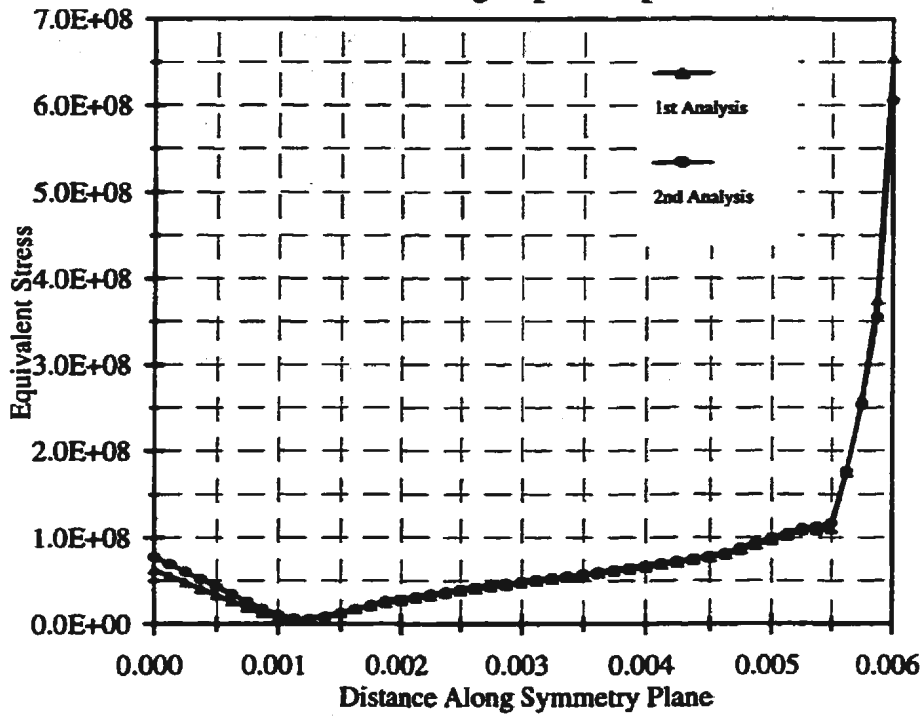


Figure C.3 - Stress distributions along uncracked ligament (Pipe model, 4 mm deep external defect)

Stress Distribution - Internal Defect
Softening Exponent $q = 0.1$

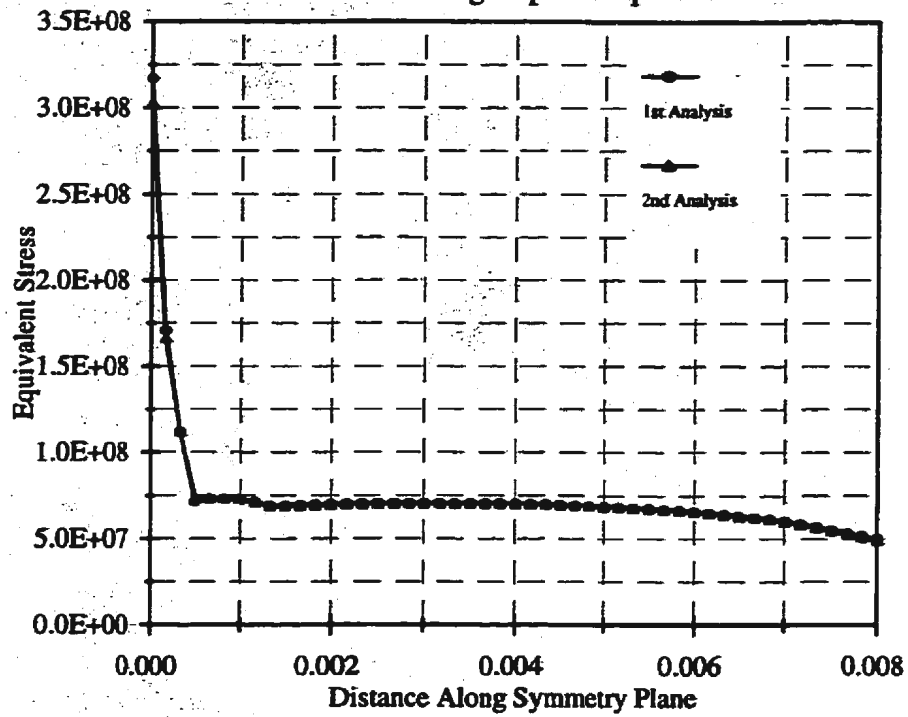


Figure C.4 - Stress distributions along uncracked ligament (Pipe model, 2 mm deep internal defect)

Stress Distribution - Thick Wall Pipe External Defect - 2 mm

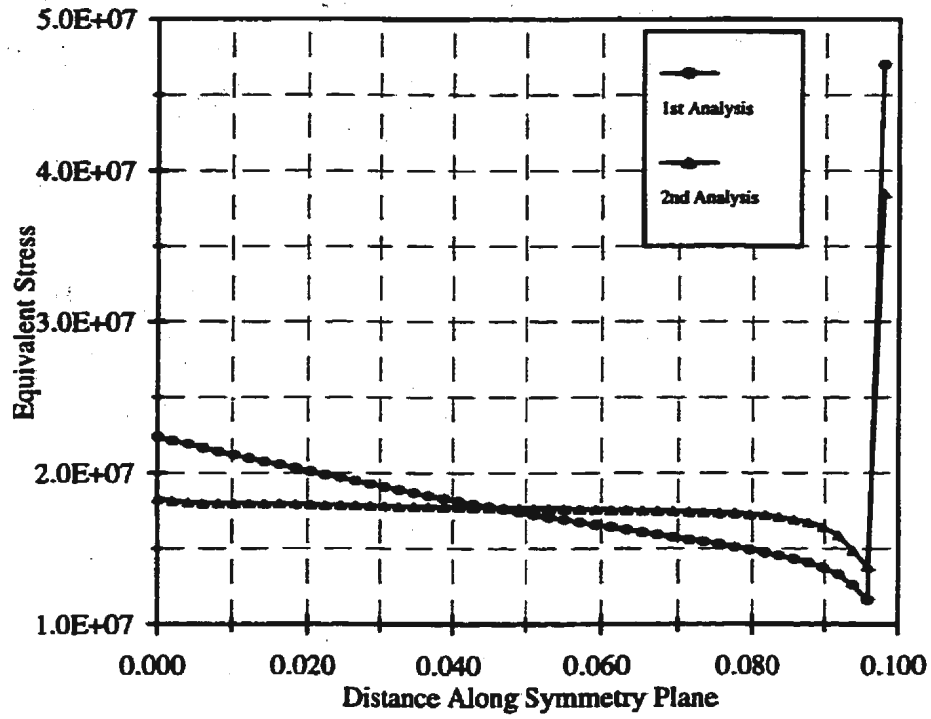


Figure C.5 - Stress distributions along uncracked ligament (Thick wall pipe, 2 mm deep external defect)

Stress Distribution - Multiple Defects
Model 1, Crack A (q = 0.1)

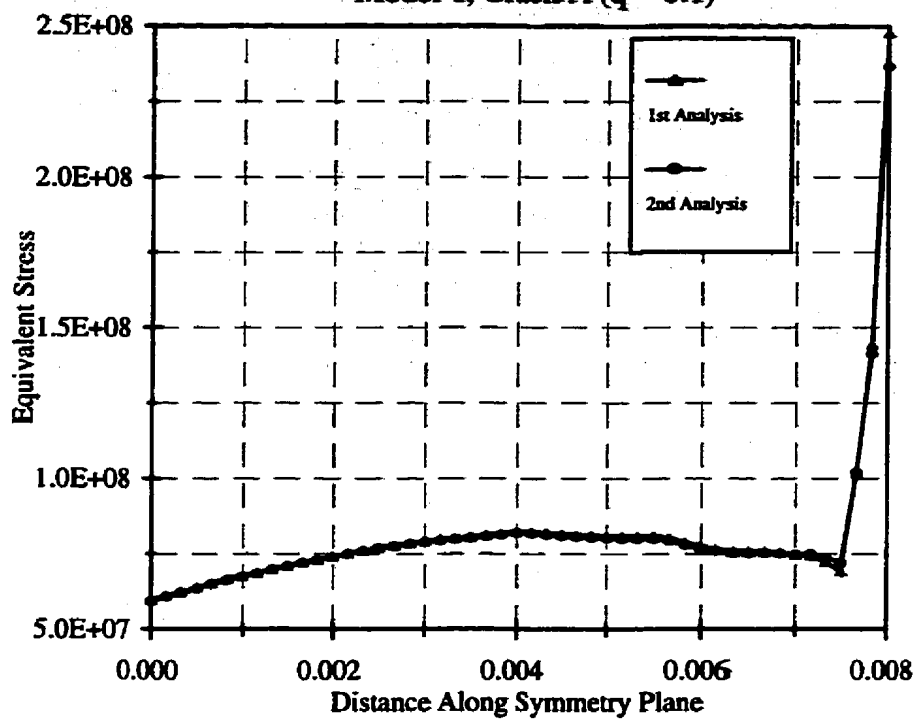


Figure C.6 - Stress distributions along uncracked ligament (Multiple defects, Model 1, Crack A)

Stress Distribution - Multiple Defects
Model 1, Crack B (q = 0.1)

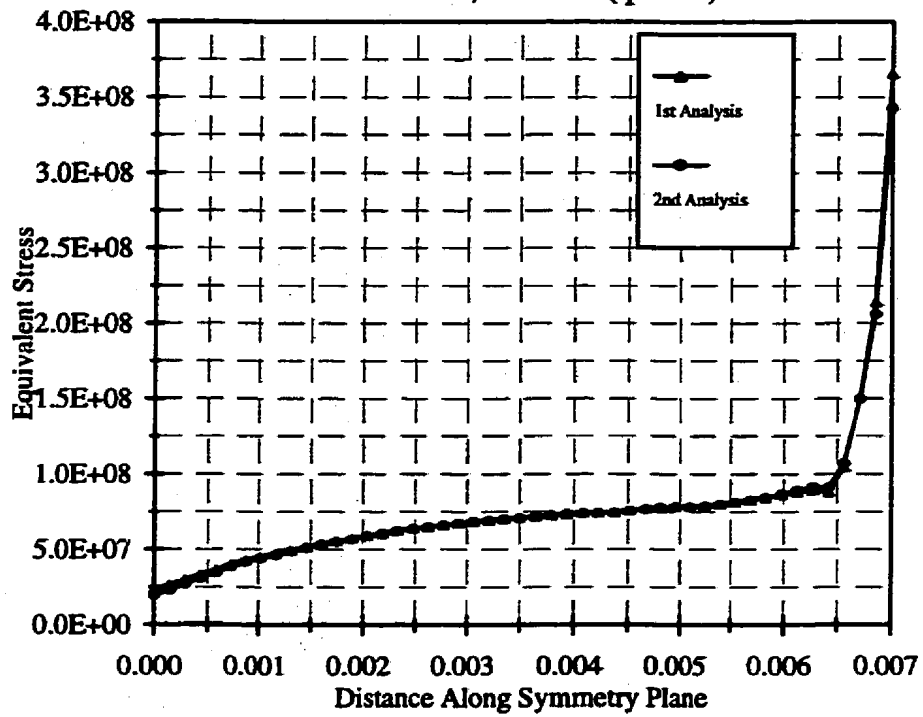


Figure C.7 - Stress distributions along uncracked ligament (Multiple defects, Model 1, Crack B)

Stress Distribution - Multiple Defects
Model 1, Crack C ($q = 0.1$)

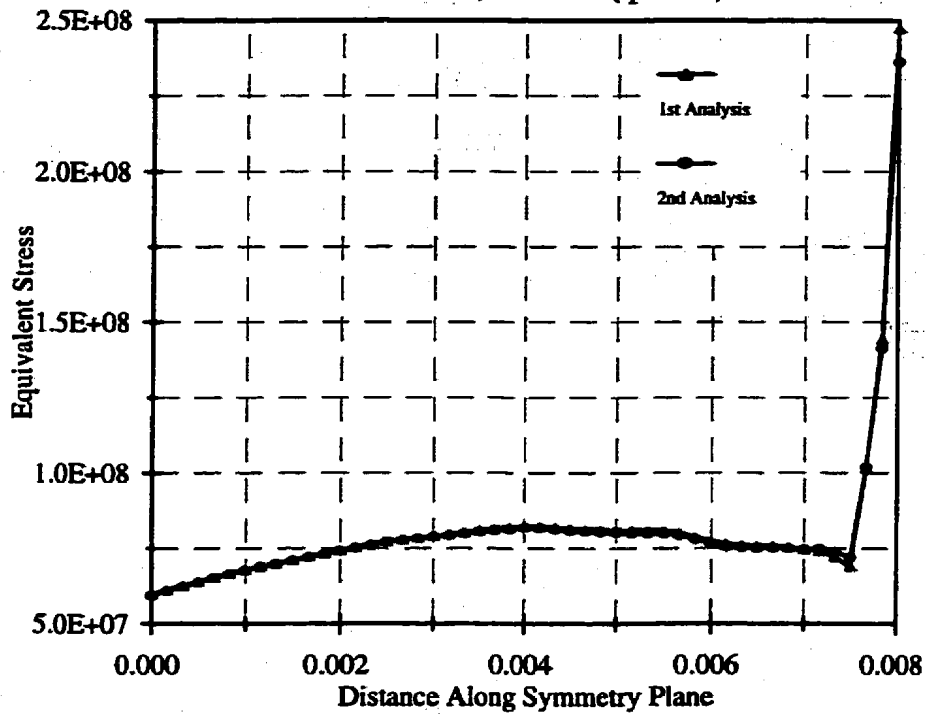


Figure C.8 - Stress distributions along uncracked ligament (Multiple defects, Model 1, Crack C)

Stress Distribution - Multiple Defects
Model 2, Crack A ($q = 0.1$)

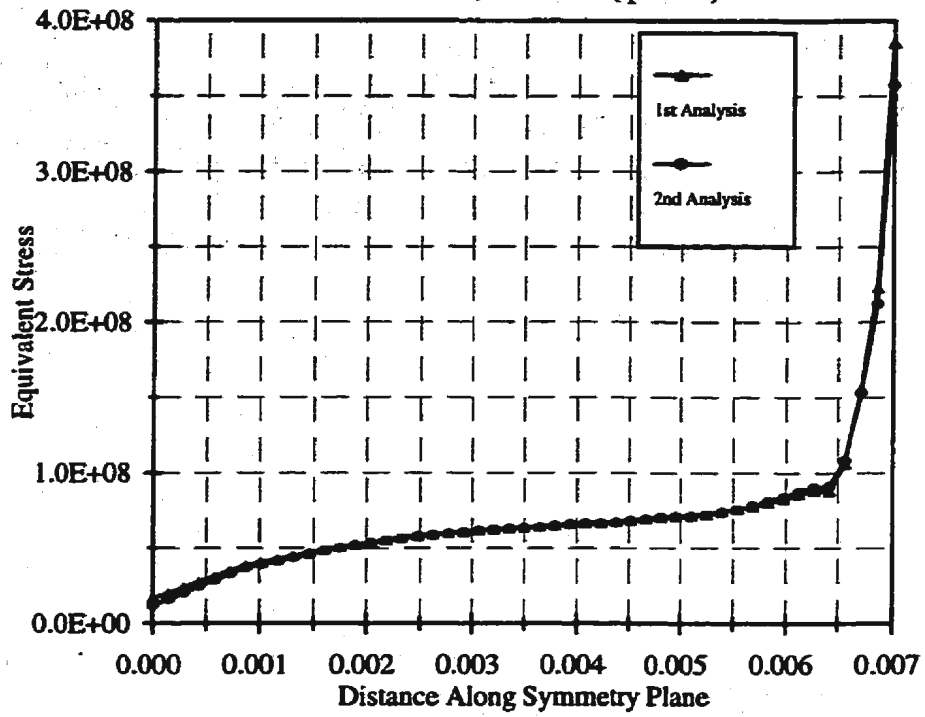


Figure C.9 - Stress distributions along uncracked ligament (Multiple defects, Model 2, Crack A)

Stress Distribution - Multiple Defects
Model 2, Crack B ($q = 0.1$)

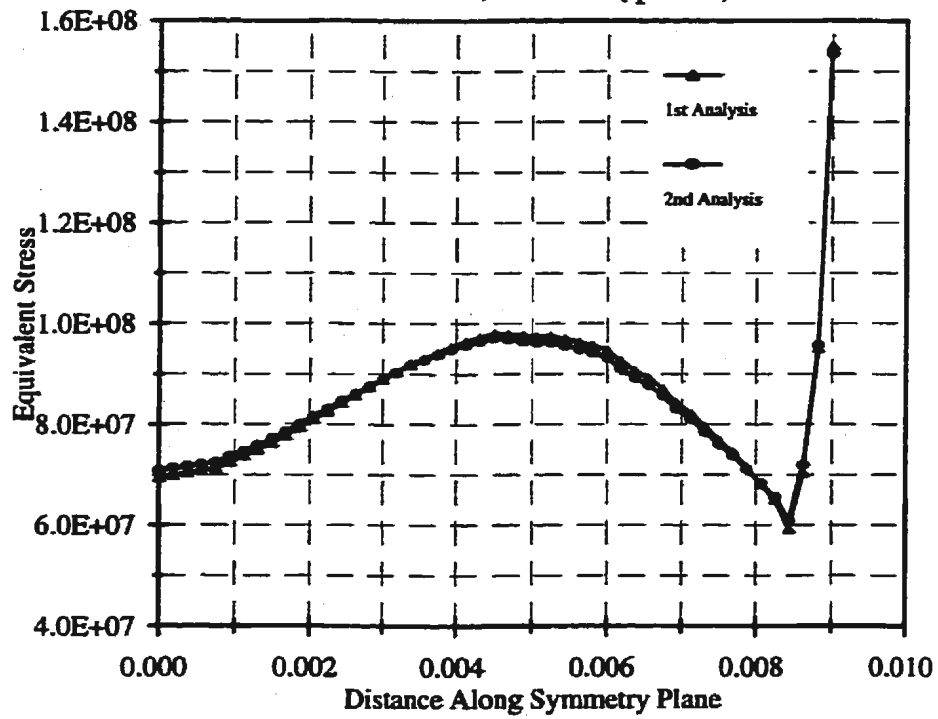


Figure C.10 - Stress distributions along uncracked ligament (Multiple defects, Model 2, Crack B)

ANSYS 5.2
NOV 21 1997
10:24:17
PLOT NO. 1
ELEMENTS
MAT NUM
F M

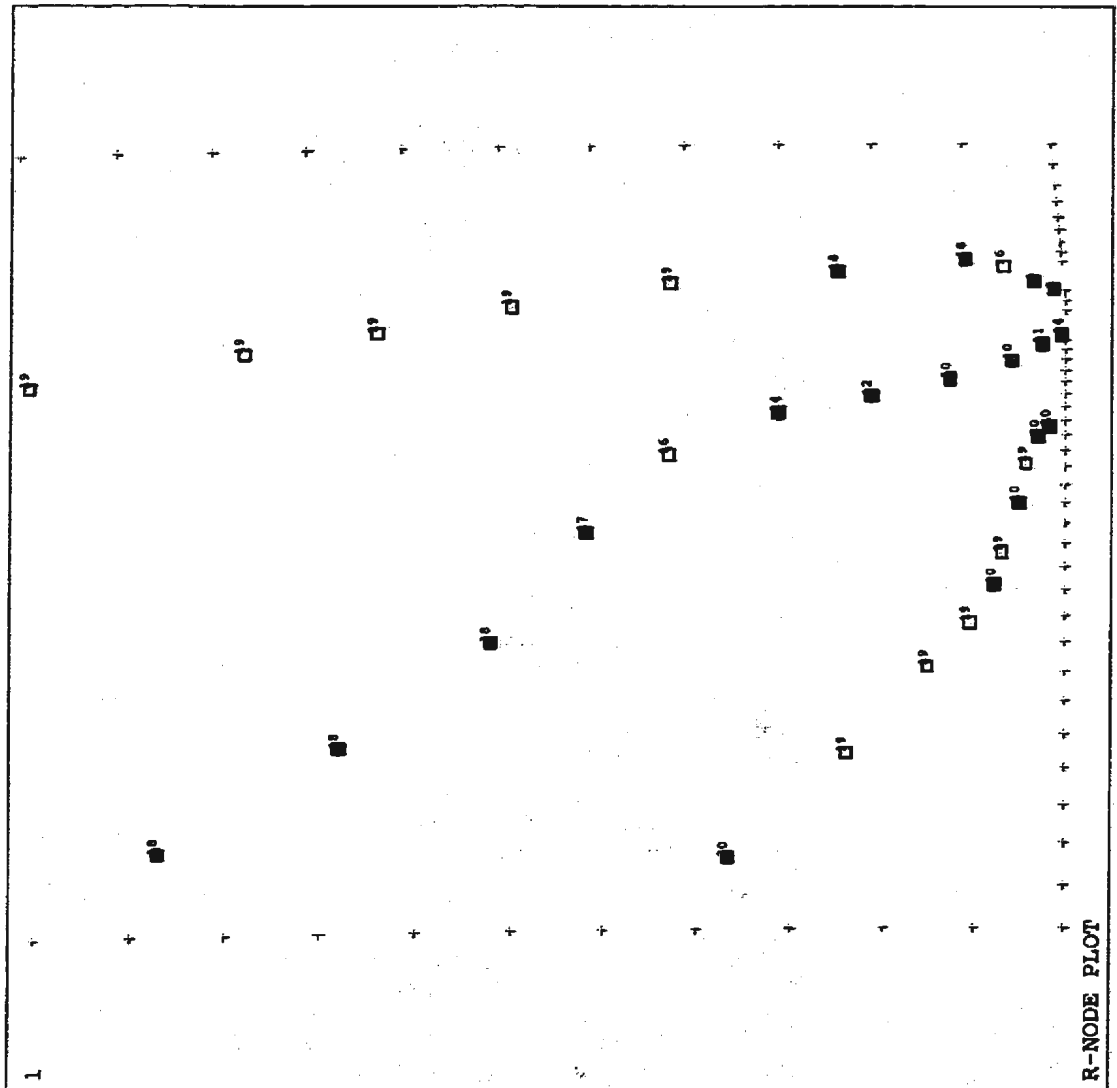


Figure C.11 - R-node plot (Pipe model, 2 mm deep external defect)

Table C.1 - R-node stress ranges (Pipe model, 2 mm deep external defect)

COLOR NUMBER	R-NODE STRESS RANGE	TOTAL ELEMENTS
1	0.1706159E+09 to 0.1656797E+09	1
2	0.1656797E+09 to 0.1607435E+09	0
3	0.1607435E+09 to 0.1558073E+09	0
4	0.1558073E+09 to 0.1508712E+09	0
5	0.1508712E+09 to 0.1459350E+09	0
6	0.1459350E+09 to 0.1409988E+09	1
7	0.1409988E+09 to 0.1360627E+09	0
8	0.1360627E+09 to 0.1311265E+09	0
9	0.1311265E+09 to 0.1261903E+09	0
10	0.1261903E+09 to 0.1212541E+09	2
11	0.1212541E+09 to 0.1163180E+09	1
12	0.1163180E+09 to 0.1113818E+09	1
13	0.1113818E+09 to 0.1064456E+09	0
14	0.1064456E+09 to 0.1015095E+09	2
15	0.1015095E+09 to 0.9657327E+08	0
16	0.9657327E+08 to 0.9163710E+08	2
17	0.9163710E+08 to 0.8670093E+08	1
18	0.8670093E+08 to 0.8176476E+08	5
19	0.8176476E+08 to 0.7682858E+08	298
20	0.7682858E+08 to 0.7189242E+08	5

ANSYS 5.2
NOV 21 1997
10:37:09
PLOT NO. 1
ELEMENTS
MAT NUM
F M

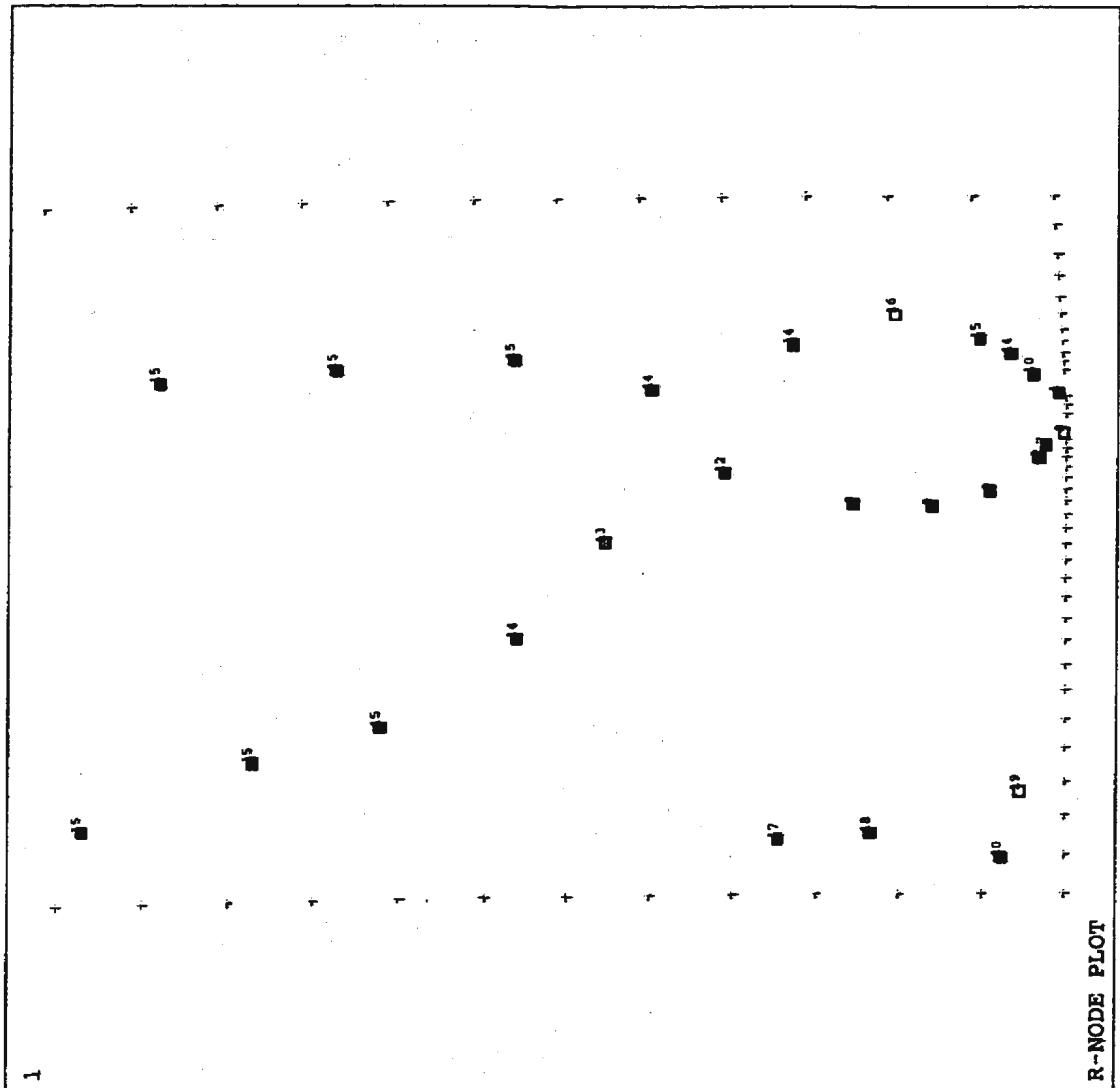


Figure C.12 - R-node plot (Pipe model, 3 mm deep external defect)

Table C.2 - R-node stress ranges (Pipe model, 3 mm deep external defect)

COLOR NUMBER	R-NODE STRESS RANGE	TOTAL ELEMENTS
1	0.2153581E+09 to 0.2060887E+09	1
2	0.2060887E+09 to 0.1968192E+09	0
3	0.1968192E+09 to 0.1875498E+09	0
4	0.1875498E+09 to 0.1782803E+09	0
5	0.1782803E+09 to 0.1690109E+09	0
6	0.1690109E+09 to 0.1597414E+09	0
7	0.1597414E+09 to 0.1504720E+09	1
8	0.1504720E+09 to 0.1412025E+09	1
9	0.1412025E+09 to 0.1319331E+09	4
10	0.1319331E+09 to 0.1226637E+09	1
11	0.1226637E+09 to 0.1133942E+09	0
12	0.1133942E+09 to 0.1041248E+09	1
13	0.1041248E+09 to 0.9485533E+08	1
14	0.9485533E+08 to 0.8558587E+08	4
15	0.8558587E+08 to 0.7631643E+08	313
16	0.7631643E+08 to 0.6704700E+08	1
17	0.6704700E+08 to 0.5777754E+08	1
18	0.5777754E+08 to 0.4850810E+08	1
19	0.4850810E+08 to 0.3923866E+08	1
20	0.3923866E+08 to 0.2996921E+08	1

ANSYS 5.2
NOV 21 1997
10:49:50
PLOT NO. 1
ELEMENTS
MAT NUM
F
M

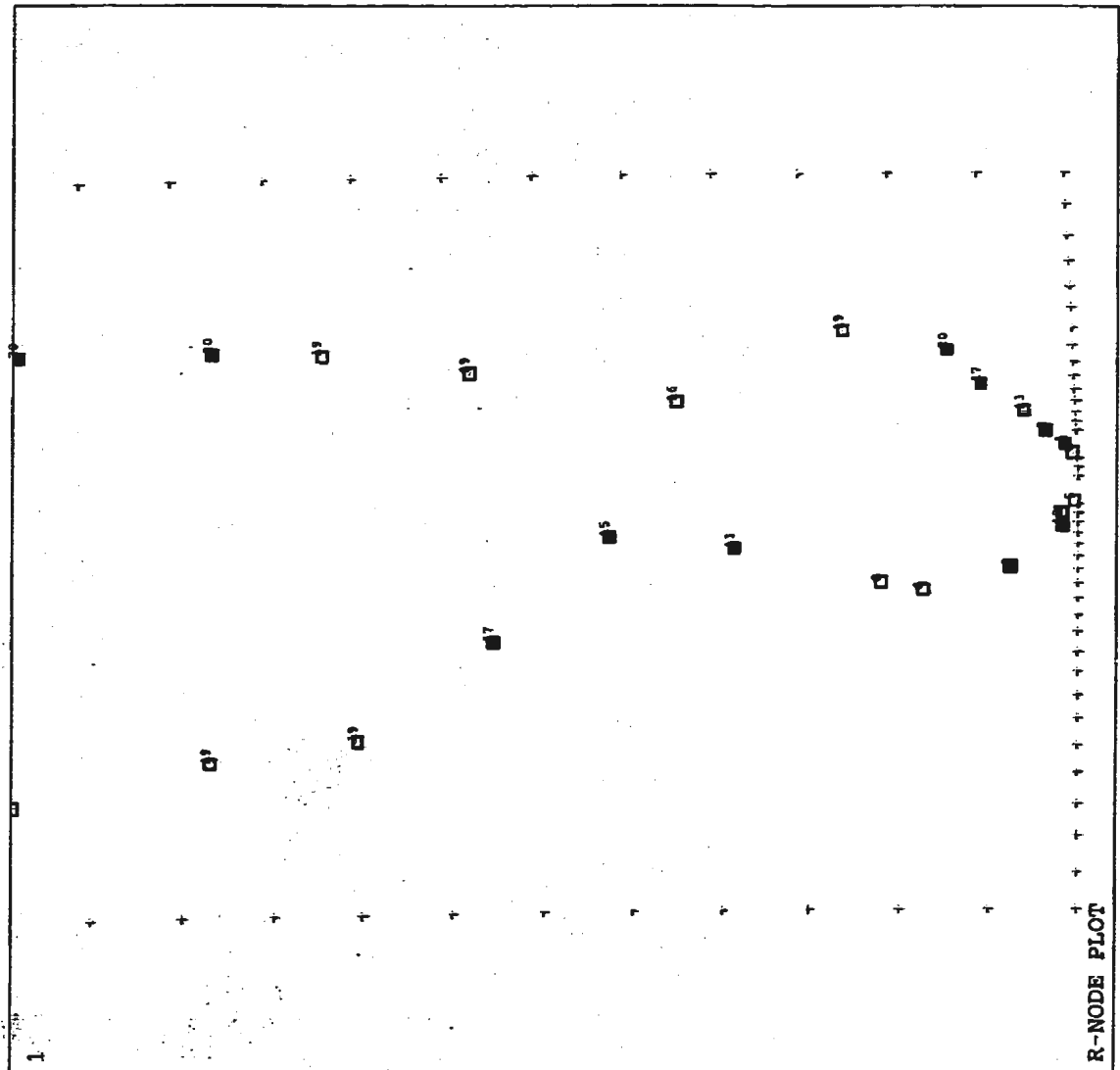


Figure C.13 - R-node plot (Pipe model, 4 mm deep external defect)

Table C.3 - R-node stress ranges (Pipe model, 4 mm external defect)

COLOR NUMBER	R-NODE STRESS RANGE	TOTAL ELEMENTS
1	0.2171057E+09 to 0.2098592E+09	1
2	0.2098592E+09 to 0.2026126E+09	0
3	0.2026126E+09 to 0.1953661E+09	0
4	0.1953661E+09 to 0.1881196E+09	0
5	0.1881196E+09 to 0.1808731E+09	1
6	0.1808731E+09 to 0.1736266E+09	0
7	0.1736266E+09 to 0.1663801E+09	0
8	0.1663801E+09 to 0.1591336E+09	4
9	0.1591336E+09 to 0.1518871E+09	2
10	0.1518871E+09 to 0.1446406E+09	0
11	0.1446406E+09 to 0.1373940E+09	1
12	0.1373940E+09 to 0.1301475E+09	1
13	0.1301475E+09 to 0.1229010E+09	1
14	0.1229010E+09 to 0.1156545E+09	0
15	0.1156545E+09 to 0.1084080E+09	1
16	0.1084080E+09 to 0.1011615E+09	1
17	0.1011615E+09 to 0.9391500E+08	2
18	0.9391500E+08 to 0.8666850E+08	0
19	0.8666850E+08 to 0.7942198E+08	342
20	0.7942198E+08 to 0.7217547E+08	7

ANSYS 5.2
NOV 21 1997
11:05:26
PLOT NO. 1
ELEMENTS
MAT NUM
F
M

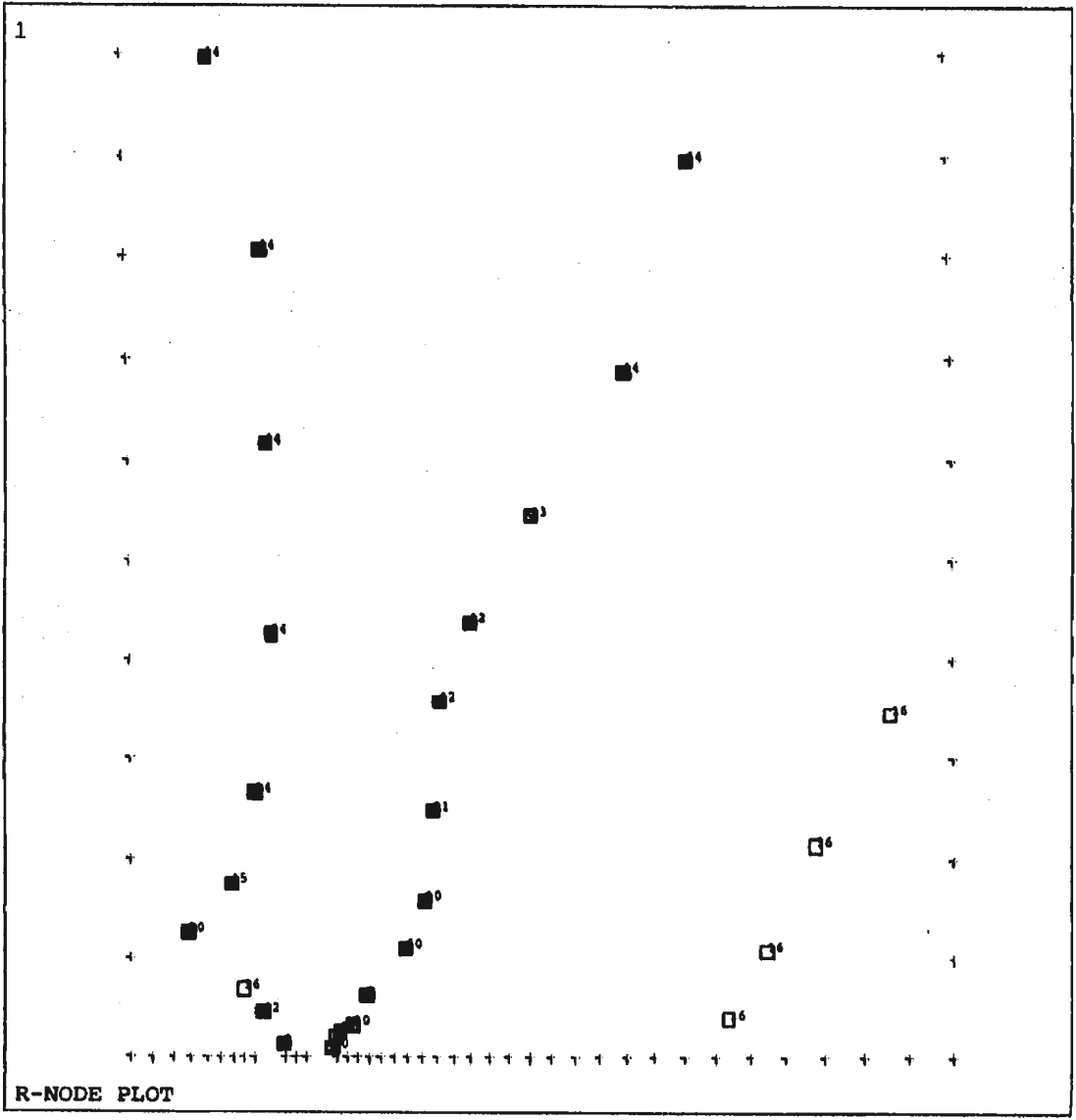


Figure C.14 - R-node plot (Pipe model, 2 mm deep internal defect)

Table C.4 - R-node stress ranges (Pipe model, 2 mm deep internal defect)

COLOR NUMBER	R-NODE STRESS RANGE	TOTAL ELEMENTS
1	0.1861797E+09 to 0.1785329E+09	1
2	0.1785329E+09 to 0.1708861E+09	0
3	0.1708861E+09 to 0.1632393E+09	0
4	0.1632393E+09 to 0.1555925E+09	0
5	0.1555925E+09 to 0.1479457E+09	0
6	0.1479457E+09 to 0.1402989E+09	0
7	0.1402989E+09 to 0.1326521E+09	0
8	0.1326521E+09 to 0.1250053E+09	1
9	0.1250053E+09 to 0.1173584E+09	2
10	0.1173584E+09 to 0.1097116E+09	4
11	0.1097116E+09 to 0.1020648E+09	1
12	0.1020648E+09 to 0.9441803E+08	3
13	0.9441803E+08 to 0.8677122E+08	1
14	0.8677122E+08 to 0.7912441E+08	301
15	0.7912441E+08 to 0.7147760E+08	1
16	0.7147760E+08 to 0.6383079E+08	5
17	0.6383079E+08 to 0.5618398E+08	0
18	0.5618398E+08 to 0.4853717E+08	0
19	0.4853717E+08 to 0.4089036E+08	0
20	0.4089036E+08 to 0.3324355E+08	1

Table C.5 - R-node stress ranges (Thick wall pipe model)

COLOR NUMBER	R-NODE STRESS RANGE	TOTAL ELEMENTS
1	0.7775798E+08 to 0.7529202E+08	1
2	0.7529202E+08 to 0.7282606E+08	0
3	0.7282606E+08 to 0.7036011E+08	0
4	0.7036011E+08 to 0.6789415E+08	0
5	0.6789415E+08 to 0.6542819E+08	0
6	0.6542819E+08 to 0.6296224E+08	0
7	0.6296224E+08 to 0.6049629E+08	0
8	0.6049629E+08 to 0.5803033E+08	1
9	0.5803033E+08 to 0.5556437E+08	1
10	0.5556437E+08 to 0.5309842E+08	1
11	0.5309842E+08 to 0.5063246E+08	1
12	0.5063246E+08 to 0.4816651E+08	2
13	0.4816651E+08 to 0.4570055E+08	1
14	0.4570055E+08 to 0.4323460E+08	0
15	0.4323460E+08 to 0.4076864E+08	4
16	0.4076864E+08 to 0.3830269E+08	286
17	0.3830269E+08 to 0.3583673E+08	8
18	0.3583673E+08 to 0.3337078E+08	4
19	0.3337078E+08 to 0.3090482E+08	1
20	0.3090482E+08 to 0.2843886E+08	1

ANSYS 5.2
NOV 21 1997
13:53:52
PLOT NO. 1
ELEMENTS
MAT NUM
F
M

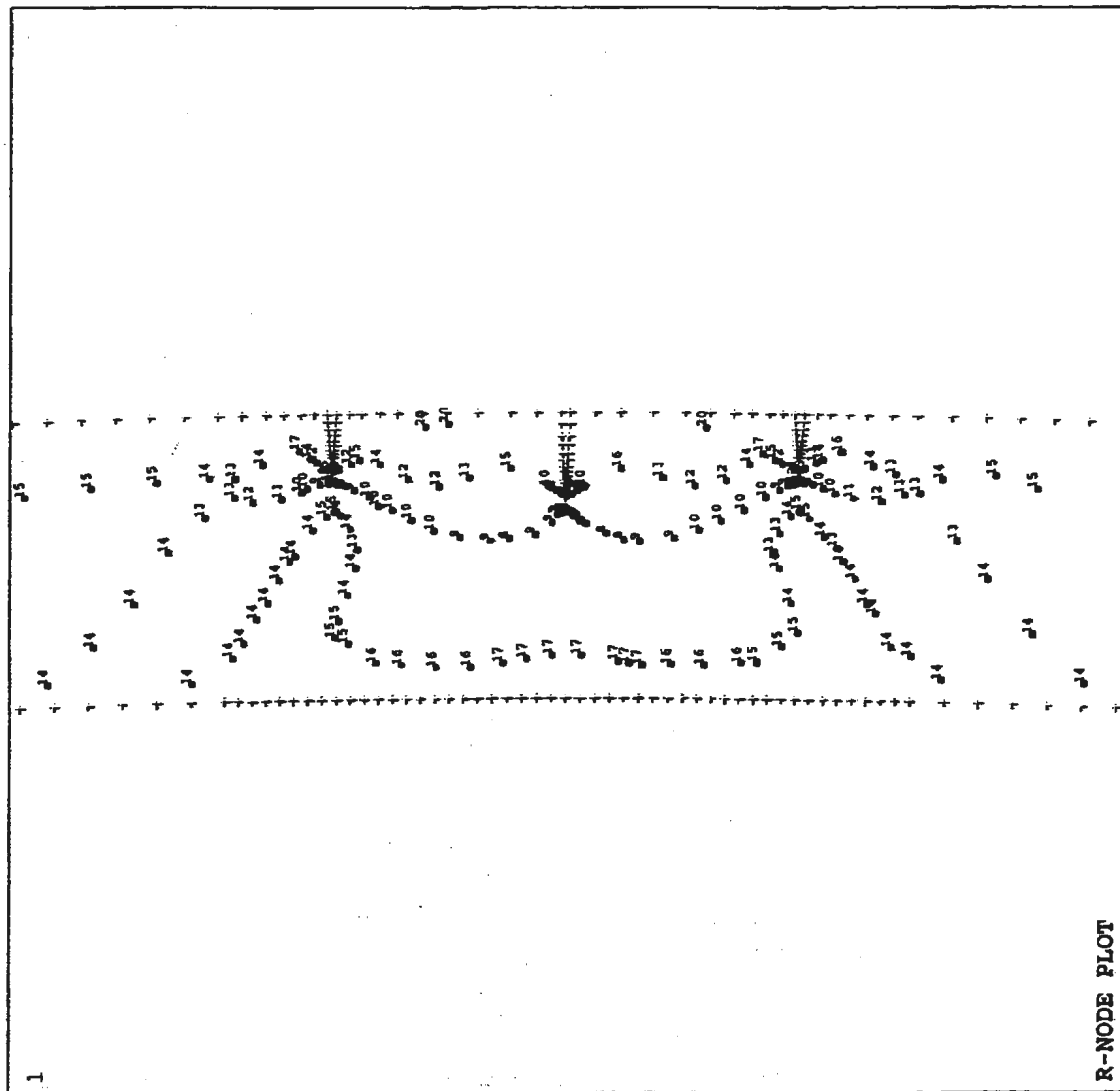


Figure C.16 - R-node plot (Multiple defects, Model 1)

Table C.6 - R-node stress ranges (Multiple defects, Model 1)

COLOR NUMBER	R-NODE STRESS RANGE	TOTAL ELEMENTS
1	0.2304945E+09 to 0.2197333E+09	2
2	0.2197333E+09 to 0.2089721E+09	0
3	0.2089721E+09 to 0.1982108E+09	0
4	0.1982108E+09 to 0.1874496E+09	2
5	0.1874496E+09 to 0.1766883E+09	2
6	0.1766883E+09 to 0.1659271E+09	2
7	0.1659271E+09 to 0.1551658E+09	4
8	0.1551658E+09 to 0.1444046E+09	4
9	0.1444046E+09 to 0.1336433E+09	19
10	0.1336433E+09 to 0.1228821E+09	17
11	0.1228821E+09 to 0.1121208E+09	2
12	0.1121208E+09 to 0.1013596E+09	13
13	0.1013596E+09 to 0.9059834E+08	14
14	0.9059834E+08 to 0.7983708E+08	622
15	0.7983708E+08 to 0.6907584E+08	63
16	0.6907584E+08 to 0.5831460E+08	9
17	0.5831460E+08 to 0.4755334E+08	9
18	0.4755334E+08 to 0.3679210E+08	0
19	0.3679210E+08 to 0.2603086E+08	0
20	0.2603086E+08 to 0.1526960E+08	3

ANSYS 5.2
NOV 21 1997
14:15:05
PLOT NO. 1
ELEMENTS
MAT NUM
F
N

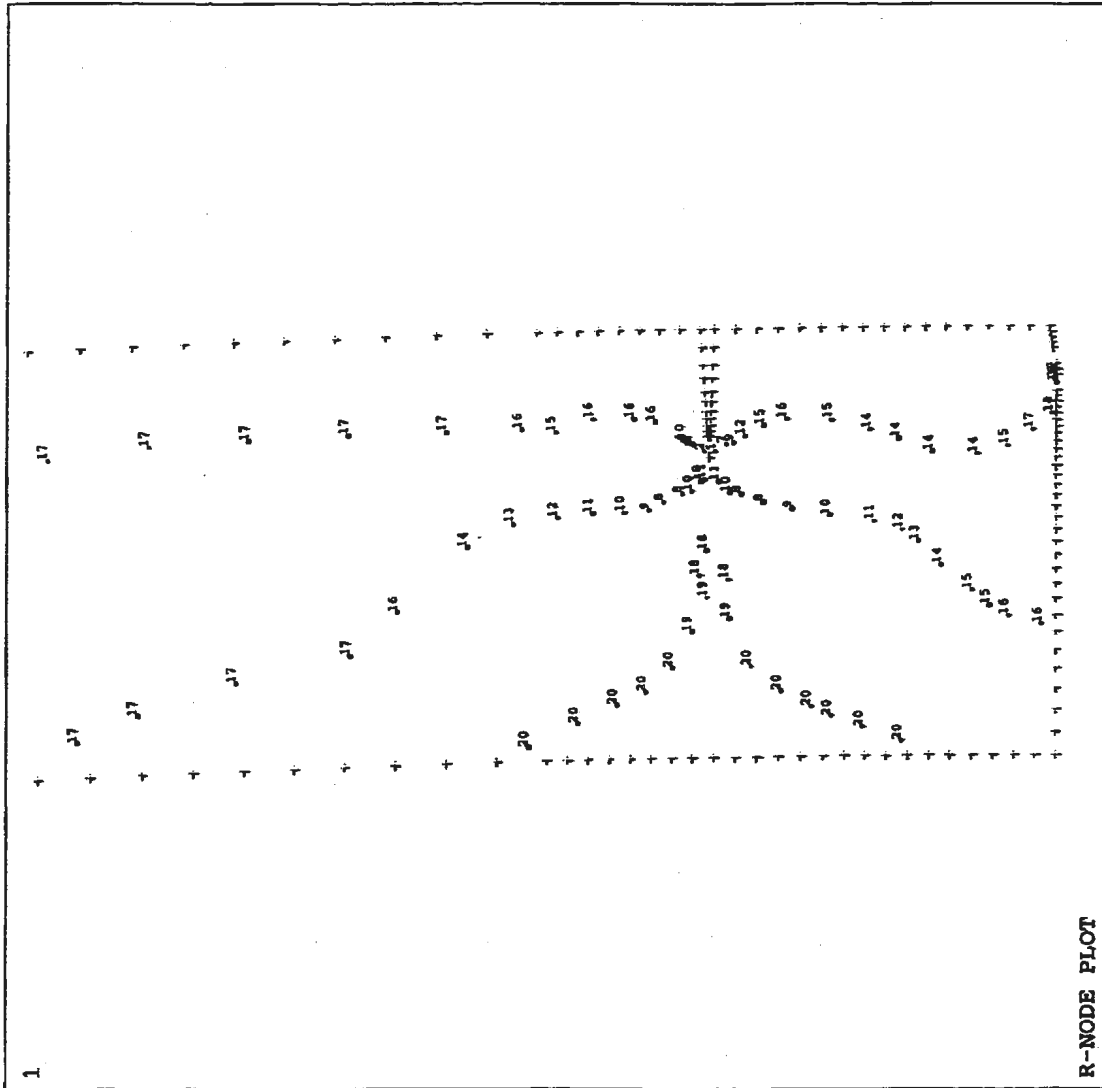


Figure C.17 - R-node plot (Multiple defects, Model 2)

Table C.7 - R-node stress ranges (Multiple defects, Model 2)

COLOR NUMBER	R-NODE STRESS RANGE	TOTAL ELEMENTS
1	0.2216399E+09 to 0.2131534E+09	1
2	0.2131534E+09 to 0.2046668E+09	1
3	0.2046668E+09 to 0.1961803E+09	0
4	0.1961803E+09 to 0.1876938E+09	0
5	0.1876938E+09 to 0.1792072E+09	0
6	0.1792072E+09 to 0.1707207E+09	0
7	0.1707207E+09 to 0.1622342E+09	1
8	0.1622342E+09 to 0.1537477E+09	5
9	0.1537477E+09 to 0.1452611E+09	4
10	0.1452611E+09 to 0.1367746E+09	6
11	0.1367746E+09 to 0.1282881E+09	4
12	0.1282881E+09 to 0.1198015E+09	3
13	0.1198015E+09 to 0.1113150E+09	2
14	0.1113150E+09 to 0.1028285E+09	6
15	0.1028285E+09 to 0.9434195E+08	6
16	0.9434195E+08 to 0.8585542E+08	8
17	0.8585542E+08 to 0.7736890E+08	330
18	0.7736890E+08 to 0.6888237E+08	5
19	0.6888237E+08 to 0.6039584E+08	3
20	0.6039584E+08 to 0.5190930E+08	11

BIBLIOGRAPHY

Al-Ansary, M.D. and Deiab, I.M. (1996). "Fracture Analysis For Pipes Containing a Finite Length Axial Part-through Crack," *International Journal of Pressure Vessels and Piping*, Vol. 68, pp. 127-133.

Brocks, W., Krafka, H., Künecke, G. and Wobst, K. (1992). "Stable Crack Growth of Axial Flaws in Pressure Vessels," *Nuclear Engineering and Design*, Vol. 135, pp. 151-160.

Brust, F.W. and Leis, B.N. (1992). "A Model For Predicting Primary Creep Damage in Axial Cracked Cylinders - I. Theory," *Engineering Fracture Mechanics*, Vol. 43, pp. 615-627.

Dong, Y.M., Yang, W. and Hwang, K.C. (1993). "Elastic-Plastic Defect Assessment Based on Ductile Fracture Process," *Nuclear Engineering and Design*, Vol. 142, pp. 27-41.

Kassir, M.A., Hofmayer, C.H. and Bandyopadhyay, K.K. (1992). "A Limit Load Criterion to Predict Crack Growth in Stainless Steel Pipes," *Engineering Fracture Mechanics*, Vol. 43, pp. 807-813.

Kobayashi, A.S., Polvanich, N., Emery, A.F. and Love, W.J. (1977). "Inner and Outer Cracks in Internally Pressurized Cylinders," *ASME Journal of Pressure Vessel Technology*, Vol. , pp. 83-89.

Leis, B.N. (1990). "Update on Stress-Corrosion-Crack Life Prediction Models For Pipelines," *International Pipeline Technology Conference*, Antwerp, Belgium, pp. 18.1-18.11.

Leis, B.N. and Mohan, R. (1995). "Coalescence Conditions for Stress-Corrosion Cracking Based on Interacting Crack Pairs," *International Pipeline Technology Conference*, Ostend, Belgium, Vol. 1, pp. 613-622.

Leis, B.N. and Parkins, R.N. (1993). "Modelling Stress-Corrosion Cracking of High-Pressure Gas Pipelines," Eighth Symposium on Line Pipe Research, Houston, Texas, pp. 19-1 to 19-24.

Miller, A.G. (1988). "Review of Limit Loads of Structures Containing Defects," *International Journal of Pressure Vessels and Piping*, Vol. 32, pp. 197-327.

Rahman, S., Wolkowski, G. and Brust, F. (1996). "Fracture Analysis of Full-Scale Pipe

Experiments on Stainless Steel Flux Welds," *Nuclear Engineering and Design*, Vol. 160, pp. 77-96.

Scott, P., Wilkowski, G., Sturm, D. and Stoppler, W. (1994). "Development of a Database of Pipe Fracture Experiments," *Nuclear Engineering and Design*, Vol. 151., pp. 359-371.

Smith, E. (1996). "K_r-L_r Failure Assessment Diagrams as Applied to a Flaw in the Vicinity of a Stress Concentration," *International Journal of Pressure Vessels and Piping*, Vol. 69, pp. 203-206.

Torop, V.M. and Orynyak, I.V. (1993). "The Evaluation of the Structural Strength of Pipes and Pressure Vessels With Axial Cracks," *International Journal of Pressure Vessels and Piping*, Vol. 53, pp. 159-179.



